CHAPTER 3

EXPERIMENTAL

The experimental work undertaken as a part of this research was conducted in both static laboratory and dynamic bench-scale settings. The intent of the laboratory testing was to screen candidate sorbents, collect rate data, and verify the reaction schemes proposed in Section 1.5. Initially, all of the laboratory screening was planned for the pTGA. However, because of limitations of the pTGA equipment, the bulk of the laboratory screening work was done at atmospheric pressures using the more conventional TGA. The purpose of the work on the bench-scale was to simulate real-world conditions and to determine the impacts of utilizing alkali sorbents on the overall performance of the entire system. The pressurized fluid-bed reactor (PFBR) was the main tool used for this portion of the work. Thermochemical equilibrium modeling was also utilized during all aspects of this research to verify and/or help explain phenomena seen during the laboratory and bench-scale experiments. SOLGASMIX and FACT were the two thermochemical equilibrium codes utilized.

The purpose of this chapter is to describe the equipment, explain the test protocols, and define the test matrices. Additionally, the information sought from each test sequence is presented to allow the reader to better understand the reasoning behind the choices made for this testing. Knowing this logic should make it easier to follow the data interpretation presented in Section 4 and understand the basis of the conclusions formulated as a result of this work.

3.1 Pressurized Thermogravimetric Analysis

The original experimental plan included the use of the pTGA for testing the use of candidate sorbents for capturing alkalies. It was hoped that this instrument could be utilized to measure rate constants from temperature versus weight gain curves, reaction orders from temperature versus weight gain at varying inlet NaCl concentrations, maximum uptake for each sorbent, reversibility of adsorption; determine whether

physical or chemical adsorption was the predominant mechanism; and identify the rate-limiting step. However, because of limitations of the equipment available at the EERC and the availability of resources to modify this equipment, these goals were not obtained using the pTGA. Some of the goals were obtained at atmospheric pressure using a regular TGA, as will be discussed in the Section 3.2. The experiments attempted in the pTGA will be described in the following section along with the failure of this equipment, to produce usable data.

3.1.1 Equipment Description

A pressurized TGA with the capability to characterize coal, char, sorbent, and catalyst materials is available at the EERC. The Spectrum Research and Engineering Corporation 900/600 "TG-Mini-Reactor" is reported to have a heatup rate of up to 100°C/min to >900°C (180°F/min to >1650°F) and can be operated at pressures from vacuum to 600 psig. The balance is capable of handling samples of up to 100 mg. Gas inlet and outlet ports enable the use of flowing inert and reactant gases while maintaining the preset pressure. The gas outlet from the sample chamber is readily interfaced to other instrumentation, i.e., FT-IR (Fourier transform infrared), GC–MS (gas chromatography–mass spectrometry), or impinger trains, for real-time gas analysis or gas effluent extraction. Control of the instrument and data collection is accomplished using manufacturer software on an IBM (or compatible) PC (personal computer). The raw data can be downloaded into ASCI files for import into commercial spreadsheets for data reduction and reporting.

3.1.2 pTGA Test Conditions

To meet the goals laid out in the introduction to this section, sodium needed to be introduced into the pTGA as a vapor at a controlled but variable concentration. Several different options were explored based partially on reports of previous researchers and partially on the experience of the operators of the pTGA at the EERC. The first avenue explored was to produce the sodium vapor in a separate "generator" and use a carrier gas to introduce the vapor into the pTGA. The desired concentrations ranged from 1 to 200 ppm. A review of the vapor pressures of various sodium salts indicated that sodium chloride has the highest vapor pressure and would, therefore, deliver these concentrations at the lowest temperature. However, because of the relatively high vapor pressure, high temperatures are required in the alkali

generator. At these temperatures, it is necessary to close-couple the generator and the pTGA and to heat all connecting lines between the two vessels to ensure that the sodium will not condense prior to reaching the pTGA. A pressure vessel capable of meeting these temperature/pressure conditions would be needed for the generator, as well as a heating source to heat this vessel to the required temperature. Because of the design of the inlet to the pTGA it was questioned whether the pTGA and alkali generator could be physically coupled because of the heating required to prevent condensation. In addition, even if possible, these system modifications far exceeded the resources available to this project. It should also be noted that sodium amide was considered as a source of alkali since it could potentially produce the desired sodium concentration at a lower system temperature; however, due to safety concerns (explosiveness), this option was not pursued.

A second option considered was to mix a water solution of sodium chloride and pump this solution into the pTGA. This would allow control of the sodium concentration by either varying the add rate of the solution to the pTGA or varying the concentration of the sodium in the solution. Previous researchers utilizing this technique noticed an accumulation of sodium chloride on the injection nozzle, implying that the water was evaporating leaving solid sodium chloride behind, eventually plugging the nozzle. Therefore, there was no guarantee that the sodium in the solution was making its way into the reactor; therefore, the vapor-phase concentration could not be controlled. A secondary concern was the injection of water vapor into the pTGA. The working components of the pTGA are exposed to the atmosphere within the pTGA and, therefore, are highly susceptible to corrosion. In the presence of water vapor, both HCl and H_2SO_4 would be present in relatively high concentrations, making corrosion a serious concern for the type of experiments being proposed.

The third idea for introducing the sodium to the pTGA was to put solid NaCl directly into the pTGA and let it vaporize in the pTGA. It would be necessary to place the NaCl in a location where the gas being introduced into the pTGA could pass across the NaCl and act as a carrier to move the alkali vapors across the sorbent. This method was chosen for testing on the pTGA. Figure 34 shows the pTGA schematically, with the NaCl located in a specially designed pan. This pan was made of a porous mesh to allow gases to

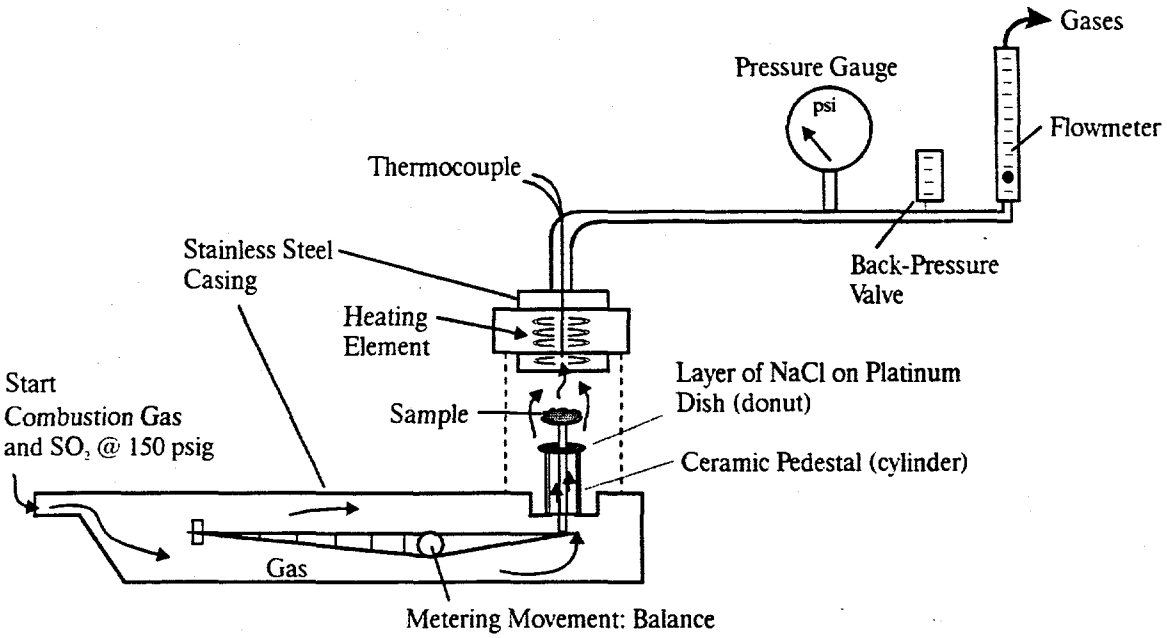

Figure 34. Configuration of the pTGA during attempted alkali generation/capture studies

pass through and located where the gas stream entering the pTGA should pass across it. The experimental trials performed under this configuration are described in the following subsection.

3.1.3 Failure of the pTGA

Testing on the pTGA was performed at 150 psig. The test protocol involved heating at a rate of 20°C/min (36°F/min) to the set point of 700°C (1292°F). The reactor was held at 700°C for 30 min and then ramped up to 775°C (1427°F) and held for another 30 min. Initially, baseline tests were performed with nepheline, albite, and sodalite in N_2 to establish a baseline without NaCl addition. These tests showed no weight change, indicating no decomposition was occurring. A test was then performed with nepheline in combustion gas. Again, no weight gain was noticed, indicating that SO_2 was not being absorbed by the nepheline. The next test was performed using albite and NaCl. No weight change was recorded. Because a gain in weight was expected, the next test utilized kaolin as the sorbent. Work by previous researchers (Uberoi et al., 1990) indicated that kaolinite should adsorb NaCl at these pressures and temperatures. The kaolinite showed a weight loss as the sample was being brought up to temperature. This is expected as it

releases water at approximately 550°C (950°F). No weight gain was noted for the kaolinite and NaCl at temperatures of 700°C (1292°F) and 775°C (1427°F).

The next step in evaluating the effectiveness of the pTGA as a screening tool for alkali sorbents was to perform a TGA at atmospheric pressure using the Dupont analyzer described in Section 3.2.1. The thermogram generated from albite plus NaCl showed a significant weight gain at 800°C (1472°F). The same test was repeated in the pTGA, with the pTGA operated at atmospheric pressure. No weight gain was observed. Although not conclusively determined, it was speculated that the flow of gas in the pTGA was such that the NaCl was not being transferred to the sorbent. As one final test, albite was mixed directly with NaCl at a ratio of 10:1 and put in the balance pan. No weight gain was noted when the sample was heated to 800°C (1472°F). At this point, it was decided that the pTGA could not be used for the sorbent-screening studies.

3.2 Atmospheric Thermogravimetric Analysis

Once it was determined that the EERC's pTGA was not suitable for investigating alkali sorbents, the emphasis was changed to the atmospheric TGA. This TGA was used 1) to investigate the original series of reactions proposed in Section 1.5 for capture of alkali using sodalites, 2) to gather rate data for candidate sorbents, and 3) to assist in the selection of sorbents for testing in the bench-scale reactor.

3.2.1 Equipment Description

The TGA equipment used in the research was a Dupont 951 TGA interfaced with a 1090 thermal analyzer control unit and data processor. The TGA consists of an electronic balance and a furnace capable of operating at temperatures up to 1200°C (2192°F). The instrument has a 100-mg sample capacity and a maximum heatup rate of 100°C/min. Typical sample sizes range from 10 to 40 mg of material.

Figure 35 is a diagram of the TGA as utilized for this work. Gas flows through the balance across the platinum sample pan, which is suspended by a horizontal quartz beam at the center of the furnace. The sample temperatures are determined by a chromel-alumel thermocouple located about 1 mm above the center of the sample pan. Weight, time, and temperature are computer-logged for later analysis.

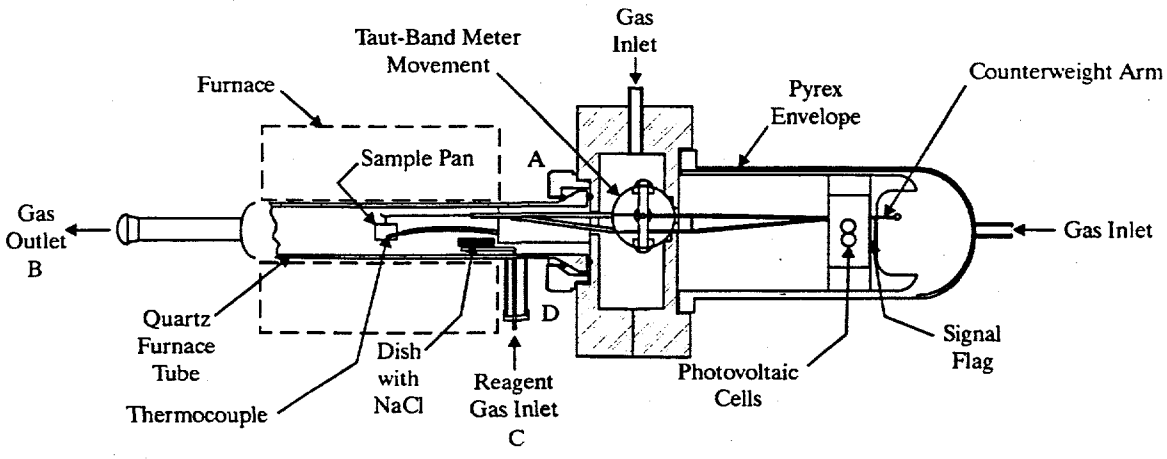

Figure 35. Schematic of the Dupont 951 TGA

For the experimental work performed, two different gas compositions were utilized. Some tests were performed using nitrogen. The intent of this selection was to expose the sorbents only to the sodium, chloride, and an inert gas. For other tests, a synthetic gas mixture of SO_2, CO_2, O_2, and N_2 was used to simulate the gas stream that the sorbent might see in a real combustion situation. It was thought that this gas composition would provide an evaluation of the sorbent's performance in a "true" environment. It was also felt that having SO_2 present in the system was critical, since the reaction scheme being proposed for simultaneous sodium and chlorine capture has reactions where SO_2 and Cl_2 compete. The concentrations of gases in the synthetic combustion mix are 2015 ppm SO_2, 14.29% CO_2, 4.95% O_2, and the balance N_2.

3.2.2 TGA Reaction Conditions

As discussed in the previous section, a method to add sodium to the sample gas that passes across the sorbent material was required for these experiments. For the same reasons as discussed for the pTGA, the approach taken for introducing vapor-phase sodium into the TGA was to place NaCl crystals in a pan upstream (to the gas inlet side as shown in Figure 35) of the sample pan that holds the sorbent. The intent of this configuration was to allow the sodium to vaporize in the heated chamber of the TGA and then have

the carrier gas sweep this sodium across the sorbent material. NaCl was chosen because it is the sodium salt that has the highest vapor pressure and, therefore, the highest sodium concentration over the range of interest. The temperatures utilized for the experiments and the corresponding sodium vapor-phase concentration are presented in Table 10. The concentrations presented in the table were determined from thermochemical equilibrium calculations and were not measured. The temperature required to reach these concentrations at 10.2 atm is also given. It can be seen from Table 10 that this range of sodium concentrations encompass the range expected for PFBC over the normal range of operation.

Table 10

Vapor-Phase Sodium Concentrations at the Various Temperatures Tested Using TGA

TGA Temperature, °C	NaCl Concentration, ppm	Equivalent Temperature at 10.2 atm, °C [1]
700	29	791
733	68	824
766	158	857
800	336	887

[1] Temperature that would result in the same concentration at 10.2 atm.

The sorbents tested in the TGA were all fine powders. In PFBC, the bed is granular in nature and would consist of a broad range of particles with a ⅛-in. topsize. The use of powders was preferred for the initial screening, however, since powders minimize sample variability and permit control of particle size (all samples were screened through a 30-mesh screen).

The general procedure for the TGA tests involved staged heating to quantify the adsorption rate at several different temperatures and NaCl concentrations during a single test sequence. The TGA was loaded with approximately 50 mg of the sorbent to be tested in the balance. If NaCl was to be used during the test, approximately 200 mg was placed in the pan at the inlet of the reactor, as shown in Figure 35. The TGA was heated up to 700°C and held at that temperature for ½ hr. The temperature in the TGA was then raised to 733°C and held for another 30 min. This was repeated for 766° and 800°C. After the 30-min exposure at 800°C, the reactant gas was changed and the TGA held at 800°C for another 30 min. For example, if the

main run was performed using a combustion gas mixture, the reactant gas was changed to inert (nitrogen) for the last 30 min. The intent was to provide an indication of the impact of carrier gas for the sample being tested.

This procedure generated thermograms similar to Figure 36. The time and weight gain at each condition are marked. A rate of adsorption was calculated as a fractional weight gain per unit time. This calculation yielded the amount of gas adsorbed (weight gained by sample) per weight of sorbent per unit time. The units chosen were mg gas adsorbed per gram sorbent per hour (mg/g/hr). The measured values ranged from 0 to 75.

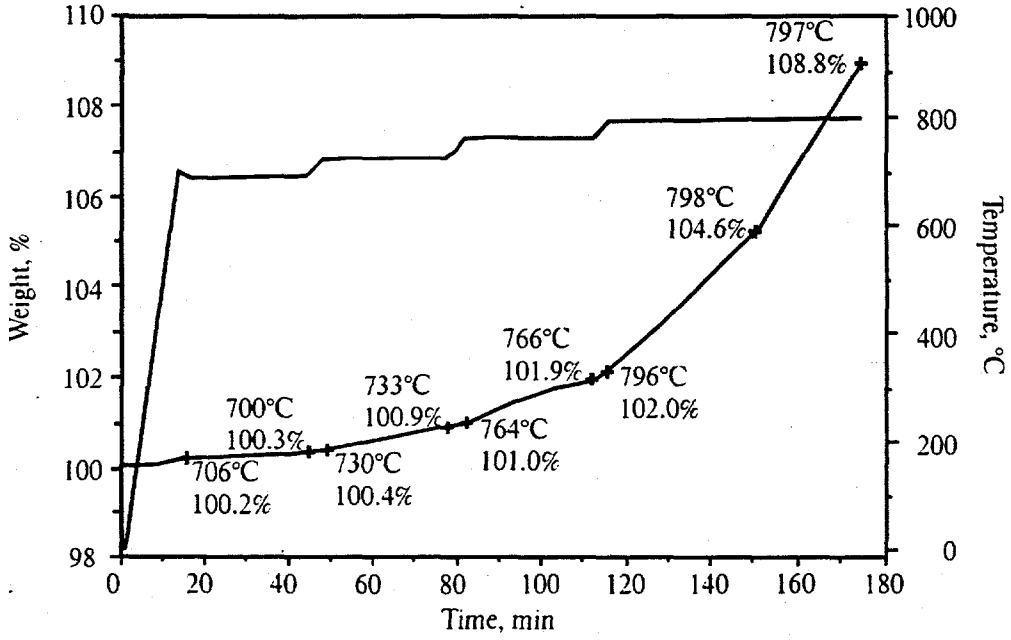

Figure 36. Thermogram from a stepwise TGA using albite as the sorbent with NaCl in combustion gas

3.2.3 Test Matrix for TGA Determinations

One objective of the TGA tests was to develop a better understanding of the rates and direction of the reactions proposed for simultaneously capturing alkali, sulfur, and chlorine. The reactions as presented in Section 1.6 are:

$$NaCl + 3\ NaAlSiO_4 \rightarrow Na_4Al_3Si_3O_{12}Cl \qquad [1]$$

(nepheline) (sodalite)

$$Na_4Al_3Si_3O_{12}Cl + 6\ SiO_2 \rightleftharpoons NaCl + 3\ NaAlSi_3O_8 \quad [2]$$

(sodalite) (albite)

$$Na_4Al_3Si_3O_{12}Cl + Na_2SO_4 \rightleftharpoons 2\ NaCl + Na_8Al_6Si_6O_{24}(SO_4) \quad [3]$$

(sodalite) (nosean)

$$Na_8Al_6Si_6O_{24}(SO_4) + 12\ SiO_2 \rightleftharpoons Na_2SO_4 + 6\ NaAlSi_3O_8 \quad [4]$$

(nosean) (albite)

$$2\ Na_4Al_3Si_3O_{12}Cl + SO_2 + O_2 \rightleftharpoons Na_8Al_6Si_6O_{24}(SO_4) + Cl_2 \quad [5]$$

(sodalite) (nosean)

The tests used to evaluate this series of reactions are presented in Table 11. Reaction 1 was investigated using nepheline with NaCl, with a weight gain indicating a forward reaction. The test with sodalite without NaCl, if accompanied by a weight loss, would indicate that the reverse of Reaction 1 was favored under the conditions tested. Albite was used both with and without NaCl and with combustion gas (SO_2) and without to study Reactions 2 and 4. To investigate the impact of SiO_2 on Reaction 2, two tests were performed with SiO_2 mixed with the sorbent. Tests with sodalite with a combustion gas and with and without NaCl were used to investigate Reactions 3 and 5.

Water was not included as a variable for this testing because of concerns of acid corrosion of the TGA equipment. While hydroxides are prevalent at higher operating temperatures typical of pc-fired systems, results of the modeling efforts reported in Section 2.2 indicate that the alkali sulfates and chlorides will be the primary gas phase species available for reaction. Some improvement in sorbent performance could be expected with water vapor due to the hydroxylation of inner layer reaction sites of the sorbents, and subsequent reaction of the hydroxylated sites with the vapor phase alkali. The inclusion of water vapor could also play a minor role in the above reactions through the formation of HCl and/or H_2SO_4, thereby changing the effective concentrations of Na_2SO_4, NaCl, SO_2, and Cl_2. Results from the PFBR testing which will be discussed in Section 5 substantiate the importance of the sulfates rather than hydroxides.

Several other conventional sorbents were also screened using the TGA. These sorbents and the test conditions used are presented in Table 12. The more conventional sorbents of kaolinite and activated bauxite were tested to serve as a comparison to the sorbents involved in Reactions 1 through 5 and to allow

comparison to work reported in the literature. A sample of zeolite that is used as a catalyst support surface was also tested to determine if its porous structure would serve as good sites for physical adsorption.

Table 11

Test Matrix for Evaluation of Sodalite Reactions Performed on the TGA

		Carrier Gas Used at Each Temperature					
Sorbent	NaCl	700°C	733°C	766°C	800°C	800°C	850°C
Albite	Yes	-	-	-	-	-	N_2
Albite	No	-	-	-	-	-	N_2
Albite	Yes	C[1]	C	C	C	N_2	-
Albite	No	C	C	C	C	N_2	-
Albite + Quartz	Yes	C	C	C	C	N_2	-
Albite + Quartz	Yes	N_2	N_2	N_2	N_2	-	-
Sodalite	Yes	C	C	C	C	N_2	-
Sodalite	No	C	C	C	C	N_2	-
Sodalite	Yes	N_2	N_2		N_2	C	-
Nepheline	Yes	C	C	C	C	N_2	-

[1] Combustion gas.

Table 12

Test Matrix for Screening of Conventional Sorbents in the TGA

		Carrier Gas Used at Each Temperature				
Sorbent	NaCl	700°C	733°C	767°C	800°C	800°C
$AlO(OH)_3$	Yes	C	C	C	C	N_2
Kaolinite	Yes	C	C	C	C	N_2
Bauxite	Yes	N_2	N_2	N_2	N_2	C
Bauxite	Yes	-	-	-	-	C
Zeolite	Yes	N_2	N_2	N_2	N_2	C

3.3 Bench-Scale Testing

The objective of this phase of testing was to perform dynamic tests under conditions that more closely simulate PFBC conditions to help define the effectiveness of selected sorbents under "real" conditions. The goal of these dynamic tests include an evaluation of 1) the impact of the sorbent on total gas-phase alkali concentration, 2) sintering or agglomeration in the bed, 3) deposition on heat-transfer surfaces, 4) bridging and blinding of hot-gas filter elements, and 5) the overall changes in the size distribution and quantity of the ash generated during the PFBC process. The equipment, the operational procedure, and the test matrix used to accomplish these goals are described in this section.

3.3.1 Equipment Description

The heart of the system used for this work is the PFBR. Flue gases generated in this system are collected in a hot-gas filter vessel. The flue gases are sampled for alkali using a specially designed alkali-sampling probe. Figure 37 shows this equipment schematically. Each of these components is described.

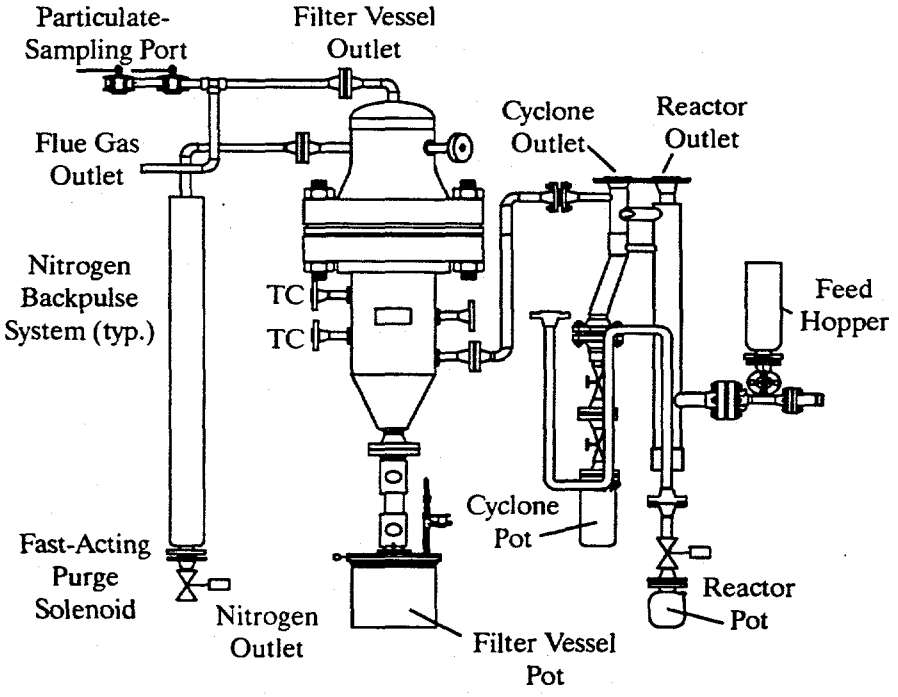

Figure 37. Schematic representation of the PFBR and hot-gas filter vessel test system

The PFBR is used at the EERC to simulate the bed chemistry, ash interactions, and emissions from a PFB under closely controlled conditions. This reactor is used for sorbent characterization, gaseous emissions including trace elements, agglomeration, and hot-gas cleanup testing over a wide range of operational conditions. The 140-cm (55-in)-tall reactor is constructed of 7.6-cm (3-in.) Schedule 80 pipe and is externally heated with three ceramic heaters. A hot cyclone collects the ash and bed material that is carried out of the reactor. Typical operating conditions for this reactor are shown in Table 13. The preheated fluidizing gas can be a mixture of air and nitrogen or just air; moreover, one additional gas such as carbon dioxide, carbon monoxide, sulfur dioxide, or a nitrogen oxide can be added to result in a flue gas similar to that generated in a full-scale FBC. Preheated gas at temperatures of up to 593°C (1100°F) and pressures of up to 200 psig are supplied at the bottom of the reactor through a 2.5-cm (1-in.) Schedule 40 pipe. The fluidizing gas is supplied at sufficiently high velocities to prevent the sized bed material from dropping out during operation. The use of both air and nitrogen as fluidizing gas allows excess air and gas velocity to be matched to any design condition.

Table 13

Typical PFBR Operating Conditions

Reactor Diameter	2.875-in. ID
Temperature	1400°–1700°F
Pressure	0–150 psig
Gas Flow Rate	1–30 scfm
Coal Feed Rates	1–8 lb/hr
Velocities	1–10 ft/sec
Cyclone Exit Temperature	Maximum 1600°F
Particulate Loading	200–9000 ppm

The fluidizing gas enters the 7.6-cm (3-in.) main section of the reactor through a conical transition. This conical section was designed without a distributor plate to allow quick removal and quench of the bed material after completion of a test. Bed material can be sampled or collected using a lock hopper system located at the bottom of the reactor. Ports for alkali-sampling probes or gas-/solid-sampling probes are

located at the top of the reactor and the top of the cyclone. An air-cooled deposition probe is located at the exit of the reactor. Alternatively, a sight port at the top of the reactor can be installed with a color videocamera for on-line observation of the bed during high-pressure operation. For this testing, the air-cooled deposition probe was installed at the top of the main reactor, and the alkali-sampling probe at the top of the cyclone. Figure 38 is a schematic of the PFBR showing the feed port, hot cyclone, fluidizing gas inlet, the deposition probe at the top of the reactor, and the sampling port on the top of the cyclone. Figure 39 is a photograph of the actual reactor vessel, cyclone, air preheater, reactor collection pot, and fuel feed hopper.

The use of external electric heaters around the reactor provides the capability to match the fuel feed rate to the amount of bed material in the reactor. The heaters can be used for maintaining the reactor and hot cyclone at temperatures of up to 1093°C (2000°F) for atmospheric operation and up to 925°C (1700°F) for operation at 10.2 atm (150 psi).

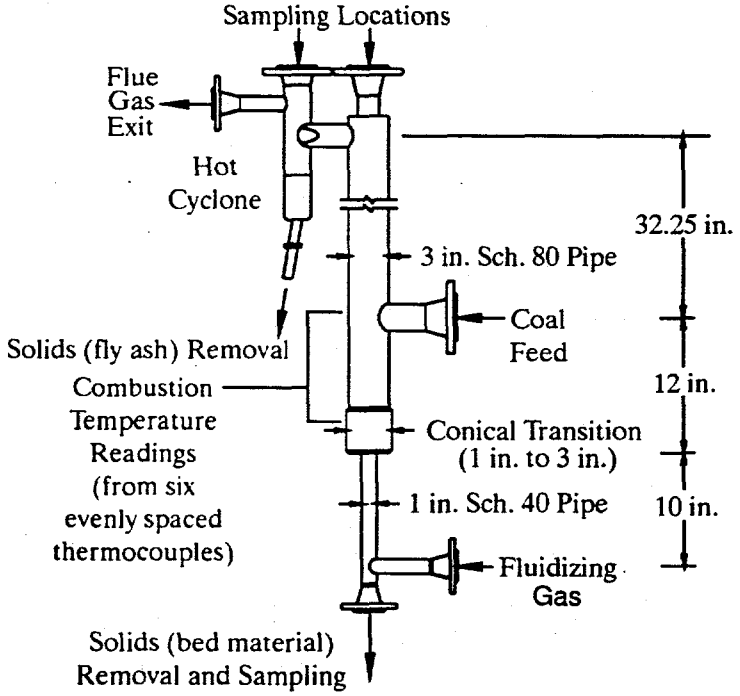

Figure 38. Schematic of PFBR pressure vessel

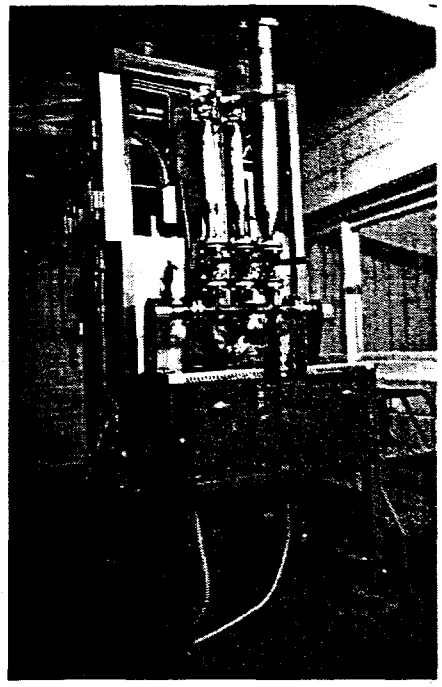

Figure 39. Photograph of PFBR pressure vessel

Dry coal and sorbent are premixed and metered into the reactor with a separate auger that feeds into a common water-cooled auger, which in turn carries the material into the reactor. A bed material hopper empties directly into the common auger, without flow control. Each hopper is maintained at a pressure slightly higher than that in the combustor during operation. The hoppers can be isolated from the pressurized system so that they can be refilled during a test. At the bottom of each hopper are sensors to alert the operator when the hoppers are empty and need to be refilled.

A data acquisition and control system is used to monitor and record all critical pressures, temperatures, flow rates, and emissions. These critical data include the gas flow rates, bed static pressure and differential pressures across the bed and cyclone, and eleven different internal reactor temperatures. These reactor temperatures are located at 0.25, 1.75, 3.5, 5, 7, 9, 11, 15, 23, 31, and 43.25 in. above the conical transition section. The air and nitrogen flow rates are controlled automatically to flow rate set points. The reactor pressure is automatically controlled to a pressure set point. Continuous emission sampling of the flue gas measured the levels of O_2, SO_2, NO_x, N_2O, CO, CO_2, and hydrocarbon. Solid

samples can include bottom ash, fly ash, and particulate samples from the stack to determine particulate loading leaving the cyclone.

3.3.1.2 Description of Hot-Gas Filter Vessel

Figure 40 illustrates the hot-gas cleanup (HGCU) vessel for the testing of ceramic candle filters on the 7.6-cm (3-in.) PFBR. This vessel was designed to handle all of the gas flow from the PFBR at its nominal design conditions. The vessel is approximately 25-cm (9.75-in.) ID and 152-cm (60-in.) long (including cone, vessel, and cap) and is designed to handle a gas flow up to 30 scfm at 843°C (1550°F) and 10.2 atm (150 psig). The tube sheet is interchangeable to handle different-sized filters. The filters can be sealed in the tube sheet with weighted metal donut rings or by metal clamps which counteract the upward force imparted across the candle filter by the filter's differential pressure. The vessel is sized such that it can handle three candle filters up to 45 cm (18 in.) long with a 6.0-cm (2.375-in.) OD. This provides candle spacing of 9.8-cm (3.85-in.) center line to center line and enables filter face velocities as low as 0.76 m/min (2.5 ft/min) to be tested in the PFBR. Higher face velocities can be achieved by using shorter candles or higher gas flow rates. Operating conditions for the filter vessel are shown in Table 14.

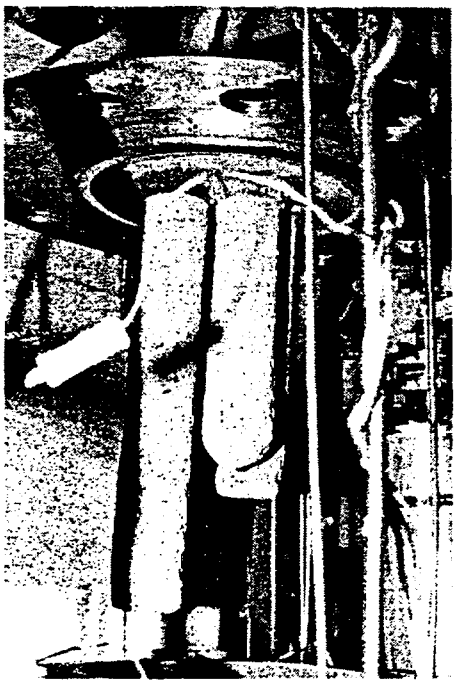

Figure 40. Photograph of the inside of the bench-scale hot-gas filter vessel on the PFBR

Table 14

High-Temperature High-Pressure (HTHP) Filter Vessel Operating Capabilities

Vessel Diameter	9.75-in. ID
Temperature	up to 1550°F
Pressure	up to 150 psig
Gas Flow Rate	up to 30 scfm
Filter Sizes	2.375 in. OD by 18 in. long
Number of Candles	Up to 3
Filter Face Velocities	2.5–12 ft/min
N_2 Backpulse System	up to 1550°F inlet; both short, high-pressure and long, low-pressure pulses

Ports in the filter vessel allow temperature and pressure measurements to be obtained. These same ports can be utilized to insert a water-cooled borescope probe for visually inspecting the filter elements. The ash letdown station consists of two high-temperature valves to act as lock hoppers to isolate the ash hopper from the filter vessel.

The nitrogen backpulse system is designed to supply a minimum of three candle volumes per pulse for the longest candle filters and even higher for the shorter candle filters. The nitrogen is capable of being heated up to 815°C (1500°F) before it enters the filter vessel. The length and volume of nitrogen displaced into the vessel are controlled by the regulated pressure (up to 20 atm [300 psig]) of the cold nitrogen reservoir and the solenoid valves used to control the timing of the cold-gas pulse which displaces the hot nitrogen into the filter vessel. Because of a height limitation, a heated 2.5-cm (1-in.) pipe is used to connect the 7.6-cm (3-in.) PFBR to the hot-gas filter vessel.

3.3.1.3 EERC Alkali-Sampling Probe Equipment Description

An alkali condensation sampling train was used to monitor the vapor-phase alkali concentrations in the PFBR tests. The condensation sampling train was chosen over the other techniques discussed in Section 2.6 because of its relatively low cost to build and operate and its relative simplicity to operate. Disadvantages are the difficulty in collecting a representative sample, especially samples which might be collected under reducing conditions, and the delay in obtaining the analytical results. The alkali-sampling train typically extracts a representative sample from the cyclone outlet of the PFBR.

The PFBR alkali-sampling probe consists of a 3.34-cm (1.3-in.) OD stainless steel pipe which has been fitted with a small ceramic filter provided by the CeraMem Corporation. The principle behind the sampling probe is to extract a hot-gas sample through a ceramic filter that is representative of the hot-gas filters currently being developed for advanced coal-fired power generation systems. After passing through the ceramic filter maintained at full system temperature, the gases and any vapor-phase alkali species which passed through the filter are cooled and allowed to condense on a high surface area "cold finger." The gas then passes through a final filter to collect any remaining aerosol particles and then through a series of water bubblers for the trapping of any additional alkali vapors and the removal of water vapor. This gas finally passes through pressure and flow measurement and control devices. Figure 41 is a diagram illustrating the alkali-sampling probe and heat exchanger with the bubbler train. The high surface area cold finger and the final filter are removed at the end of a test and washed with deionized water to dissolve the alkali species. The washings and the bubbler solutions are analyzed to determine the amount of alkali collected from the flue gas sampled. Measuring the volume of rinse solution and the concentration of alkali species in rinse solution and monitoring the total volume of gas sampled allow the vapor-phase alkali concentration to be calculated in the gas stream.

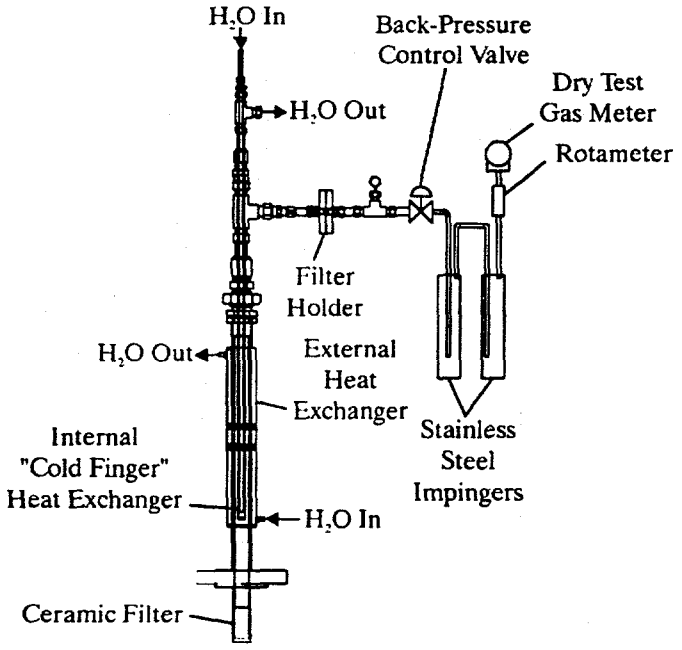

Figure 41. Schematic of EERC extractive alkali-sampling probe

3.3.2 PFBR Operations Protocol

All tests performed on the PFBR followed the same operating procedures. The system was heated up to 840°C (1550°F) using the electrical heaters and was brought up to system pressure prior to the introduction of coal. The air and nitrogen flows to the system were balanced to a calculated ratio that would yield approximately 25% excess air once full coal feed was established. The total flow rate of these two gases was established to provide the desired gas velocity within the reactor. Once the system was at temperature and pressure, 1700 g of bed material was introduced into the reactor. This would lower the reactor temperature to about 480°C (900°F). Once all of the bed material was added, coal feed was initiated. The reactor temperature would climb back to the desired temperature over about a 10-min time period. The flow rates of air and nitrogen were adjusted to provide 25% excess air and a superficial gas velocity of 0.91 m/sec (3.0 ft/sec). The reactor was allowed to stabilize at the selected conditions prior to starting the alkali sampling. This typically took about 30 min. Alkali sampling was initiated by opening the valves to the sampling probe and establishing a flow rate of approximately 50 L/min through the sampling probe. After 4 hr of alkali sampling, the alkali probe was brought off-line by closing the valves. The remaining coal in the hoppers was allowed to run out, and the run was terminated. The total time on coal was typically 5 hr.

Once the coal supply was exhausted, the reactor temperature was allowed to cool to approximately 700°C (1300°F). The bed material was drained into the bottom hopper. The system was depressurized and the gas flows stopped. The filter vessel was pulsed once while the system was still hot. The system was allowed to cool overnight. The bed material, cyclone ash, and filter vessel hopper ash were retrieved, weighed, and put in sample containers for future analyses. The top of the reactor and the cyclone and the bottom of the filter vessel were removed, and any ash that was held up in the system was removed, weighed, and saved for future analysis. The deposition probe was removed and photographed. The alkali probe was removed, and washed into a 2-l flask for subsequent analysis of Na, Cl, and SQ. The run data logged during the test were retrieved on diskette, with the data reduction performed off-line.

Typical run conditions are shown in the following figures. Figure 42 shows the measured temperatures from one of the tests performed on the PFBR. The higher temperatures in the upper zones of the PFBR are indicative of fines burning in the freeboard. This is typical for FBCs which feed coal at a location high in the bed or over bed. The set point for this work was the average temperature in Zone 1. The reactor pressure held constant for all runs. The cyclone pressure drop remained constant all runs, indicating that the cyclone was not plugging during any of the tests. Some increase in bed pressure drop was noted, especially for those tests utilizing high sorbent add rates because of a buildup of solids in the bed.

Typical gas concentrations are shown in Figure 43. The concentration (partial pressure) of oxygen was held at a value comparable to a full-scale unit. The CO_2 partial pressure, however, was lower. As explained in the equipment description, it is necessary to use a combination of nitrogen and air as the combustion gas for the PFBR. This helps balance the heat load to the combustor and allows the heat input per volume bed to approximate that of an operating PFBC. To maintain the correct excess air level without the addition of nitrogen, the coal feed rate would need to be unrealistically high as compared to

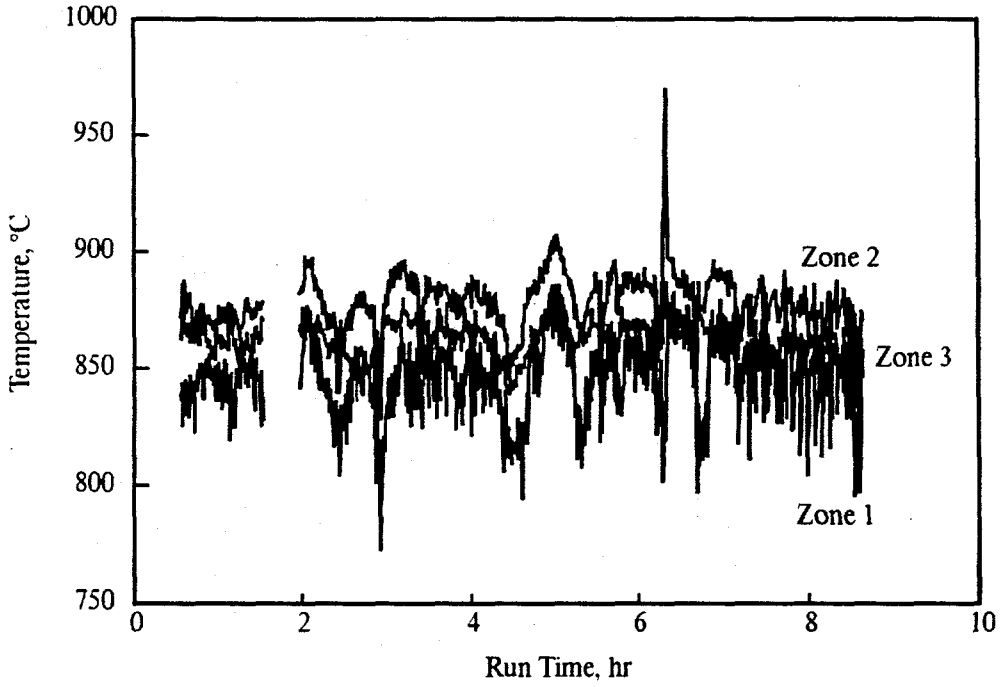

Figure 42. Characteristic measured temperatures for the PFBR

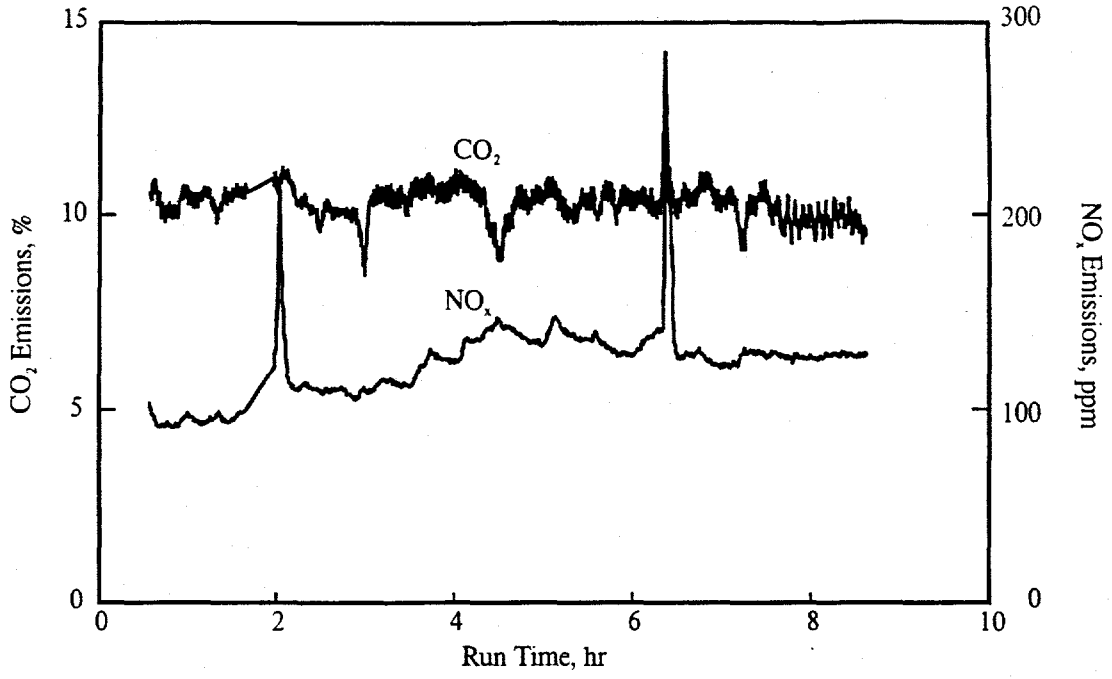

Figure 43. Characteristic gas compositions from the PFBR

commercial units and would make it difficult to maintain the proper temperature, excess air, and velocity balance within the reactor. One concern with this lower-than-normal partial pressure for CO_2 is the potential for calcination of the carbonates to oxides in the PFBR, while in commercial units, the higher partial pressure would preclude any calcination. Figure 44 indicates that at the temperature and pressures utilized for these runs, the CO_2 partial pressure may have been high enough to preclude calcination.

The typical temperature profiles for the hot-gas filter vessel are shown in Figure 45. The filter vessel reaches temperature at a slower rate than the PFBR; however, this figure shows that the vessel was at steady state for most of the test. Pressures within the filter vessel are also shown (Figure 46). The effect of backpulsing on the filter pressure drop can be seen from this figure. Ideally, the pressure drop should return to its baseline value after pulsing. A rapid increase in pressure drop accompanied by an increase in the baseline pressure drop (clean value) is indicative of blinding and/or bridging in the filter vessel.

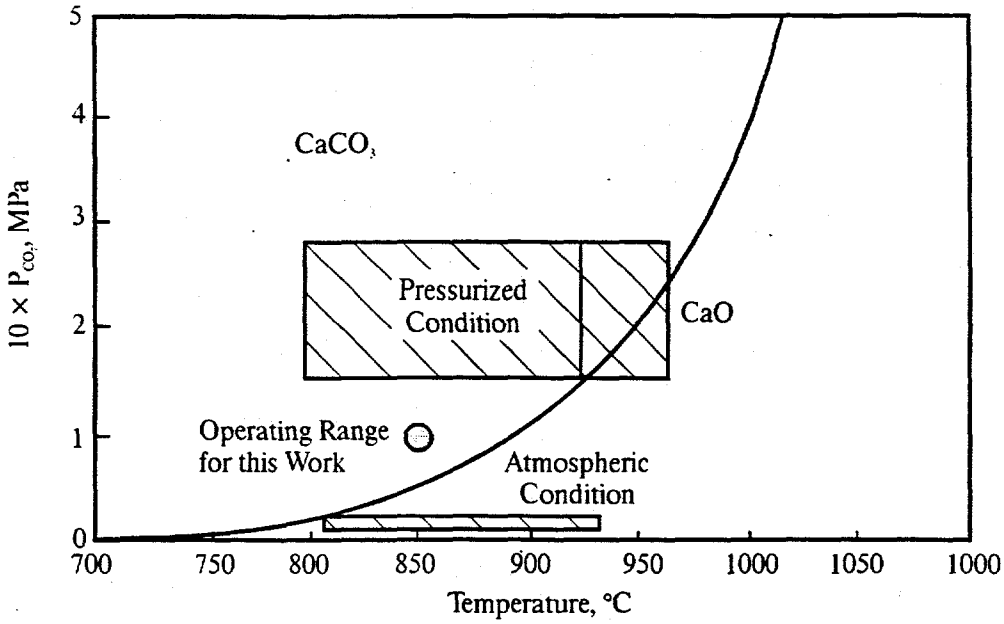

Figure 44. Pressure–temperature equilibrium of $CaCO_3$ and CaO

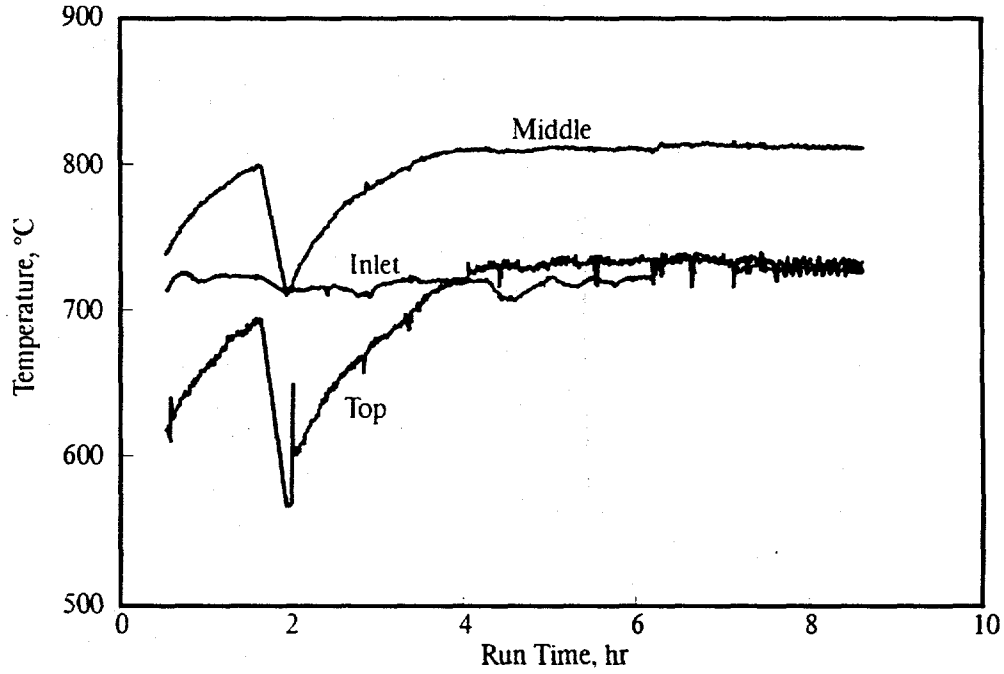

Figure 45. Characteristic temperature profile from the hot-gas filter vessel

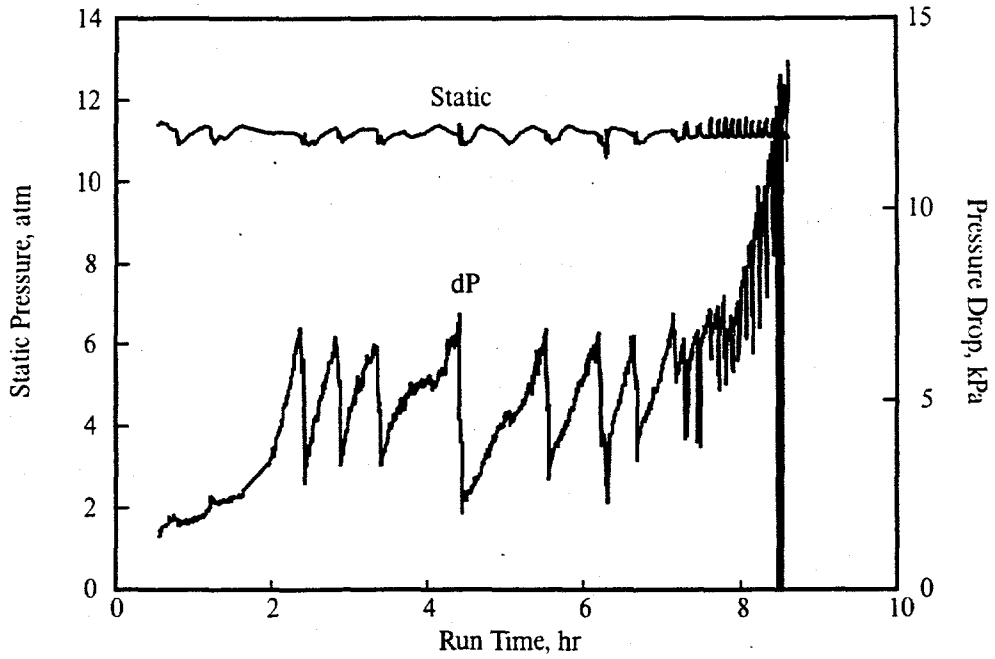

Figure 46. Characteristic pressure profile from the hot-gas filter vessel

3.3.3 Test Matrix for PFBC Testing

The matrix of tests used for this work is presented in Table 15. The first five tests were performed prior to the start of this work and were utilized as baseline tests. Test 1296, the first test performed under this work, was to establish the effectiveness of albite as an alkali sorbent. The original test matrix included several additional tests utilizing albite to determine operational effects such as sorbent add rate and size, sodium concentration in the feed, and system operating temperature. The poor performance of albite in the first test resulted in a change in the test matrix.

The coal choice for the next series of tests (1496–1896) was changed from Beulah, North Dakota, lignite to Belle Ayr, Wyoming, subbituminous. Compositions of these fuels are presented in Table 16. The reason for this change was that during Runs 1296 and 1396, the pressure drop in the filter vessel rose very quickly. Repeated pulsing could not drop the pressure drop to a safe operating range. Both Runs 1296 and 1396 had to be terminated prior to the scheduled 4 hr of alkali sampling. Belle Ayr was chosen as a substitute coal because it had been extensively characterized during previous research and it had a relatively

low inherent sodium content, thereby allowing the sodium content to be artificially established through the addition of sodium acetate.

Table 15

Test Matrix for Bench-Scale Testing Utilizing the PFBC

Test Number	Fuel	Sorbent	Sorbent Size	Sorbent/Na, wt/wt	Fuel Additive
PR01A	Blacksville	Dolomite	-⅛ in.	-	None
B13-0894	Beulah	Dolomite	-⅛ in.	-	None
B14-1294	Beulah	None	-	-	None
B15-1294	Beulah	Kaolinite	-⅛ in.	30:1	None
B17-1294	Beulah	Kaolinite	-30 mesh	30:1	None
B1-1296	Beulah	Albite	-30 mesh	30:1	None
B1-1396	Beulah	None	-	-	None
BEL-1496	Belle Ayr	None	-	-	None
BEL-1596	Belle Ayr	None	-	-	NaAc,[1] S
BEL-1696	Belle Ayr	Kaolinite	-⅛ in.	10:1	NaAc, S
BEL-1796	Belle Ayr	Kaolinite	-30 mesh	10:1	NaAc, S
BEL-1896	Belle Ayr	Bauxite	-⅛ in.	10:1	NaAc, S
B1-1996	Beulah	Bauxite	-⅛ in.	10:1	None
B1-2096	Beulah	Bauxite	-⅛ in.	3:1	None
B1-2196	Beulah	Bauxite	-⅛ in.	5:1	None

[1] Sodium acetate and sulfur were added to the fuel.

The second change to the originally planned matrix was a switch from sodalite-forming sorbents such as albite to the more conventional sorbents of kaolinite and bauxite. This change was made since the albite was ineffective in capturing vapor-phase sodium and did not resolve the ash deposition and filter-blinding issues. Kaolinite and bauxite were chosen since these two sorbents have been shown to be effective sorbents when utilized in either packed beds or entrained in the flue gas. It was suspected that they would be effective in the application being studied as a part of this research.

Table 16

Properties of Fuels Used for Bench-Scale Testing on the PFBR

Mine Name:	Blacksville	Beulah	Belle Ayr
Type:	Bituminous	Lignite	Subbituminous
Proximate, mf, wt%			
Volatile Matter	37.7	45.6	49.1
Fixed Carbon	49.6	37	41.6
Ash	12.7	17..4	9.3
Moisture	2.9	19.9	23.3
Ultimate, mf, wt%			
Carbon	70.1	56.8	65.8
Hydrogen	5	3.5	4.8
Nitrogen	1.4	0.7	1
Sulfur	2.8	3.1	0.4
Oxygen	8	18.5	18.7
Ash	12.7	17.4	9.3
Heating Value, Btu/lb	12,388	9203	11,230
Ash Composition, % as oxides, SO_3-free basis			
SiO_2	48.2	31.3	27.5
Al_2O_3	21.6	14.5	13
Fe_2O_3	23.8	24.4	3.9
TiO_2	0.8	0.8	1.1
P_2O_5	0.2	0.4	0.7
CaO	1.8	15.3	38
MgO	1.8	8.8	3.2
Na_2O	0.3	4.3	1.2
K_2O	1.5	0.1	0.3
SO_3	2.6	21.7	11.2

Test 1496 was, therefore, performed to establish a baseline on the Belle Ayr coal. Test 1596 established a baseline for the Belle Ayr at a higher sodium content. For Tests 1596 through 1896, sodium acetate was added at a rate of 3.76 g per kg coal, resulting in a final sodium concentration of 0.164 wt%.

The intent was to add sodium to the Belle Ayr at a level to duplicate the percentage of Na_2O in the ash of the Beulah lignite. Sulfur was added to the Belle Ayr to a level comparable to the Beulah lignite. The sodium acetate and sulfur were premixed with the coal.

Tests 1696 and 1796 were designed to determine the impact of utilizing kaolinite as a sorbent and the impact of particle size. Test 1896 tested the effectiveness of bauxite. Results from these three tests showed bauxite to be a better sorbent than kaolinite and the coarse material favorable to the fine with regard to alkali capture and reducing deposition. Therefore, Tests 1996 through 2196 were designed using the coarse bauxite for the sorbent. The fuel was switched back to Beulah to 1) demonstrate that bauxite could mitigate the filter blinding, capture a high percentage of vapor-phase alkali, and control depositional problems encountered during tests 1296 and 1396 and 2) determine the add rate required for the bauxite to be effective.

CHAPTER 4

RESULTS OF TGA SCREENING TESTS

The results of the work performed on the TGA will be presented in this chapter along with its interpretation. First, the data from the tests will be tabulated to provide an overall view of the work performed. Since one purpose of this work was to investigate the reaction scheme for sodalite formation, results will first be applied to those reactions. Following this discussion, the data will be represented in various forms to show reaction mechanisms for the different sorbents tested and to present the reasoning used in selecting sorbents for testing in the bench-scale reactor.

4.1 Rate Data from TGA Testing

Seventeen different TGA tests were performed. A typical thermogram is shown in Figure 47. Thermograms from all seventeen tests are given in Appendix C. For each temperature, the rate of adsorption was calculated as follows:

$$(wt\%_t - wt\%_i)/(t - t_i) \qquad [61]$$

where $wt\%_i$ is the weight % at the beginning of the test period, wt is the weight percent at the end of the test period, and t_i and t are the corresponding initial and ending times. The calculated values are adjusted to obtain units of mg/g/hr. For example, for the 733 °C condition, the rate of 18 mg/g/hr is calculated as follows:

$$(101.9\% - 101.0\%)/(110 \text{ min} - 81 \text{ min}) \times (1000 \text{ mg/g}) \times (60 \text{ min/hr}) \qquad [62]$$

Table 17 presents the results for each TGA condition. A rate of 2 mg/g/hr represents a weight gain of only 0.1 wt%. Although this represents only a small weight change over each test condition, weight changes of

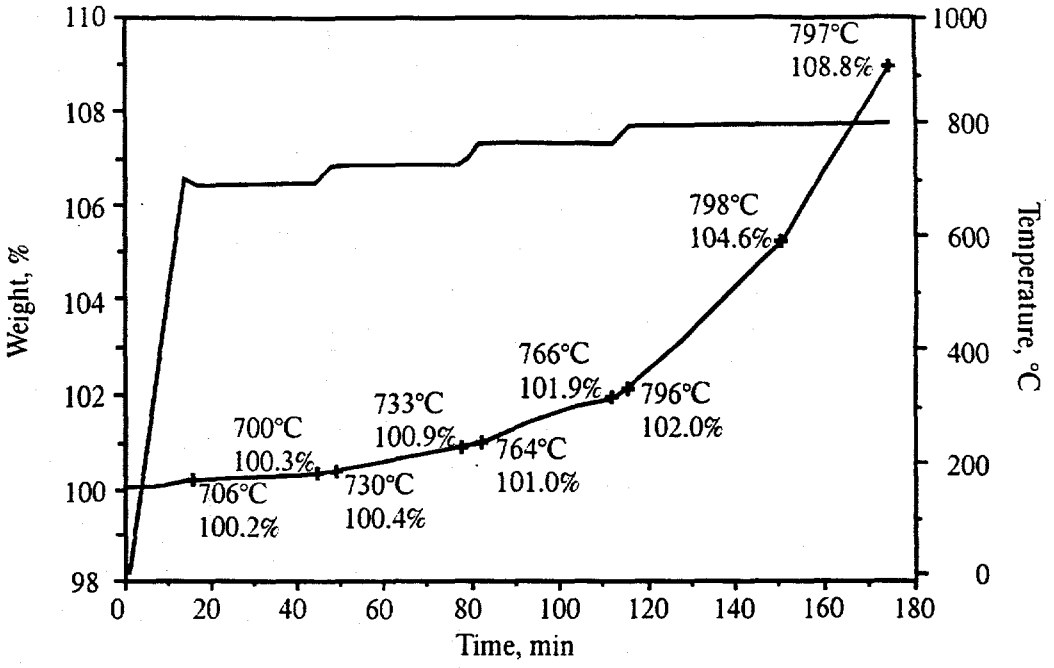

Figure 47. Thermogram of albite exposed to NaCl with a combustion carrier gas

this magnitude are within the sensitivity of the instrument. It is important to note that for Tests 3, 5, and 10 the NaCl melted at the last condition. For those tests, the rate change prior to the melting was taken and is recorded in Table 17.

4.2 Sodalite Reactions

As proposed in Section 1.6, a series of five reactions were viewed as important in the use of sodalites for capture of alkali, chlorine, and sulfur. This reaction scheme is again presented here to facilitate discussion of the relevant TGA tests.

$$NaCl + 3\ NaAlSiO_4 \rightarrow Na_4Al_3Si_3O_{12}Cl \qquad [1]$$

(nepheline) (sodalite)

$$Na_4Al_3Si_3O_{12}Cl + 6\ SiO_2 \rightarrow NaCl + 3\ NaAlSi_3O_8 \qquad [2]$$

(sodalite) (albite)

$$Na_4Al_3Si_3O_{12}Cl + Na_2SO_4 \rightarrow 2\ NaCl + Na_8Al_6Si_6O_{24}(SO_4) \qquad [3]$$

(sodalite) (nosean)

$$Na_8Al_6Si_6O_{24}(SO_4) + 12\ SiO_2 \rightleftharpoons Na_2SO_4 + 6\ NaAlSi_3O_8 \quad [4]$$

(nosean) (albite)

$$2\ Na_4Al_3Si_3O_{12}Cl + SO_2 + O_2 \rightleftharpoons Na_8Al_6Si_6O_{24}(SO_4) + Cl_2 \quad [5]$$

(sodalite) (nosean)

Table 17

Rates of Adsorption Calculated from TGA Experiments

Test No.	Sorbent	NaCl	Initial Gas	29 ppm 700°C	68 ppm 733°C	158 ppm 766°C	336 ppm 800°C	336 ppm 800°C	850°C[1]
1	Albite	Yes	Nitrogen	-	-	-	-	-	9.3
2	Albite	No	Nitrogen	-	-	-	-	-	-1.6
3	Albite	Yes	Combustion	2	20	18	72	72	-
4	Albite	No	Combustion	2	1	1	1	0	-
5	Albite + Quartz	Yes	Combustion	2	14	28	60	58	-
6	Albite + Quartz	Yes	Nitrogen	0	2.4	2.3	2.3	-	-
7	Sodalite	Yes	Combustion	11	7	18	35	20	-
8	Sodalite	No	Combustion	8.1	4.1	2.7	1.2	-2.4	-
9	Sodalite	Yes	Nitrogen	0	3.2	3	3.8	-	-
10	Nepheline	Yes	Combustion	5.4	9.4	16	18	16	-
11	$AlO(OH)_3$	Yes	Combustion	32	19	28	24	15	-
12	Kaolinite	Yes	Combustion	1	6	15	24	28	-
13	Activated Bauxite	Yes	Nitrogen	-6	0	0.7	1.8	36	-
14	Activated Bauxite	Yes	Combustion	-	-	-	-	55	-
15	Zeolite	Yes	Nitrogen	-10	-6	-5	-9	4.3	-
16	Sodalite	No	Nitrogen	0	0	0	0	-	-
17	Albite	Yes	Combustion	5.9	6.2	13	19	-	-

[1] Switch from combustion gas to nitrogen, or nitrogen to combustion gas for Tests 13, 15, and 16.

Several tests were performed with albite and sodalite, since they participate in several of the reactions listed above. Tests 8 and 10 was designed to determine whether nepheline would react with NaCl under the expected conditions in the PFBC to form sodalite under Reaction 1, or if the temperatures were such that sodalite would decompose and release the NaCl from its structure. Results from Test 10 indicate a weight gain over the concentration and temperature range tested, with that rate increasing with concentration/temperature, indicating that Reaction 1 was proceeding to the right. The results from this test showed a definite weight gain at the lower temperatures when sodalite was exposed to combustion gas with no NaCl. This indicates that the sodalite was probably adsorbing SO_2. It cannot be determined directly from these data if the sodalite would decompose in the presence of an inert gas and force Reaction 1 to the left at the temperatures of interest for this study. Test 16 was, therefore, performed using sodalite in nitrogen. The lack of weight gain or loss indicates that decomposition is not occurring over the range of temperatures from 700° to 800°C.

A rate decrease in Test 10 using nepheline, from 18 to 16 mg/g/hr, was measured as the gas was switched from a combustion gas to inert. This indicates that the SO_2 and Cl_2 may be competing for the same reaction sites. Reactions 3 and 5 show this reaction, with the sodalite that was formed from Reaction 1 reacting with the SO_2 to form nosean and releasing Cl_2. The weight gains observed during Test 8 give clues to this reaction. Since SO_4 is heavier than the Cl_2 that it replaces, a weight gain is expected if Reaction 5 (or 3) is to proceed to the right. A moderate weight gain was noted during Test 8 at the lower temperatures. This rate decreased from 8.1 to 1.4 mg/g/hr at the temperature increased from 700°C to 800°C. Furthermore, when the gas was changed from a combustion gas to an inert gas, the rate became negative. This indicates that the replacement of the chlorine with sulfate is preferred at the lower temperatures and that in the absence of gas phase SO_2, desorption of the SO_4 from the sodalite is likely to occur. Test 16 confirmed that the weight loss was not from decomposition of the sodalite.

While Test 8 examined Reactions 3 and 5 to determine whether sodalite would preferentially replace the chlorine with SO_4, Test 7 examined these reactions with both SO_2 and NaCl present in the gas phase to

determine which direction the reaction would proceed over a range of SO_2-to-chlorine partial pressures. These results show a weight gain for the sodalite, with this weight gain increasing with increasing NaCl content. It is important to remember that the concentration of NaCl is over one order of magnitude greater at 800° than at 700°C. This indicates that over the range of partial pressures of SO_2-to-Cl tested, Reactions 3 and 5 would be expected to proceed to the right and that the SO_4 would replace Cl. Since the adsorption rates were decreasing with temperature during Test 8 showing an inverse temperature dependence of SO_2 sorption by sodalite, the results of Test 7 indicate that Reaction 3, rather than Reaction 5, is responsible for the change in weight. Therefore, the Na_2SO_4 obviously plays a very important role in this reaction scheme, much more so than just the SO_2. This may be due to kinetic or diffusion limitations; however, a more probable explanation is the importance of gas condensation on the sorbent particle resulting in "wetting" of the solid. This changes the reaction from one of gas–solid to liquid–solid, with the rate of the liquid–solid reaction expected to be much higher than its gas–solid counterpart. There is evidence of these liquid–solid reactions from tests using the albite that will be presented later.

The thermoequilibrium modeling reported in Section 2.2 also confirms this conclusion. As can be seen by Figure 14, as the amount of sodium or sulfur changes (indicated by a change in the (K + Na)/S ratio), the vapor-phase concentration of the Na_2SO_4 remains constant due to changes in the amount of Na_2SO_4 that condenses. The amount of condensation that occurs to maintain this equilibrium will increase as either the sodium or sulfur vapor content increases at a given condition.

Since both temperature and NaCl concentrations are changing simultaneously in these TGA tests, SOLGASMIX was used to indicate the change of liquid Na_2SO_4 over the range of conditions tested. For the simple system C, O, S, Na, and Cl SOLGASMIX shows the liquid Na_2SO_4 concentration to be 0.145×10^{-4} at 700°C and 29 ppm NaCl, and 1.68×10^{-4} at 800°C and 336 ppm NaCl. This shows that as the concentration of NaCl increases, the condensed Na_2SO_4 will increase, even though the temperature has increased. Test 17 verified the importance of SO_2 concentration in the overall reaction scheme. Keeping everything else constant, reducing the gas-phase SO_2 concentration by 4 (2015 to 500 ppm), the rate of

adsorption decreased dramatically. It is speculated that this difference is caused by the reduction in condensable Na_2SO_4.

Tests 3 through 6 were designed to look specifically at Reactions 2 and 4. Test 3 utilized albite as the sorbent with NaCl addition to examine Reactions 2 and 4 moving to the left. These are the favored reactions for alkali capture with this system with the alkali being either NaCl or Na_2SO_4. High rates of adsorption showed that albite has promise as an alkali sorbent. It is known in solutions saturated in silica that Reactions 2 and 4 will proceed to the right. Stormer and Carmichael (1971) discuss the impact of silica saturation on sodalite formation in an albite system as shown in Figure 48. The calculated stability field of sodalite at 727°C (1340°F) and 1127°C (2060°F) is shown. Sodalite will be stable at silica and NaCl activities below both curves; the upper curve is for pure albite, the lower for an activity of 0.5 albite in coexisting feldspar. The lower boundary of the shaded area labeled "Quartz Bearing" is defined by the activity of silica glass in equilibrium with crystallizing quartz. Below this line, quartz will not be stable. The upper boundary of the shaded area labeled "Nepheline Bearing" is defined by the activity of silica in equilibrium with nepheline and albite. Above this line, nepheline will not be stable; below it an albite-rich feldspar will not be stable.

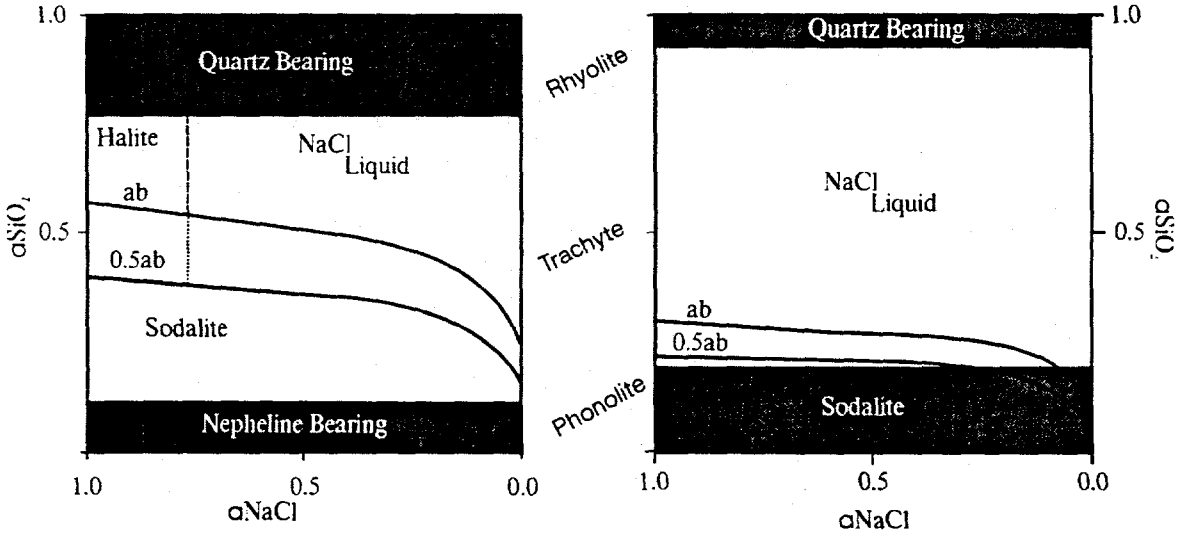

Figure 48. Stability field of sodalite at 727° and 1127°C

Because many coal ashes contain relatively large amounts of silica, it was important to determine the impact of the silica on alkali adsorption at the conditions found in the PFBC. Test 5 addressed this issue. The addition of the silica in a 50:50 weight ratio of silica to albite did not impact the rate of adsorption. It was interesting to note that when the carrier gas was switched to inert, the adsorption rate further increased. However, in Test 6, where nitrogen was used as the carrier gas, no significant adsorption was seen at any temperature. Apparently, as discussed above, the SO_2 or Na_2SO_4 is necessary to initially wet the sorbent and initiate the adsorption reactions. Once a wetted surface exists, then the albite and/or silica is able to adsorb the NaCl in addition to the Na_2SO_4. Test 4, performed with SO_2 but without NaCl, and Test 6, performed with NaCl but no SO_2, confirm that the Na_2SO_4 is the initiating (wetting) agent.

Evidence of this can be seen in Figures 49 and 50. After completion of Tests 3 and 5, the reacted sorbents were mixed and examined using the scanning electron microscope (SEM). These samples were combined to provide a sample large enough for SEM characterization. In Figure 49, the large quartz particle can be seen to be wetted by sodium and sulfur. The elemental map shows this wetting as localized areas high in sodium and sulfur. Particle analysis indicates little penetration (reaction) of the sodium or

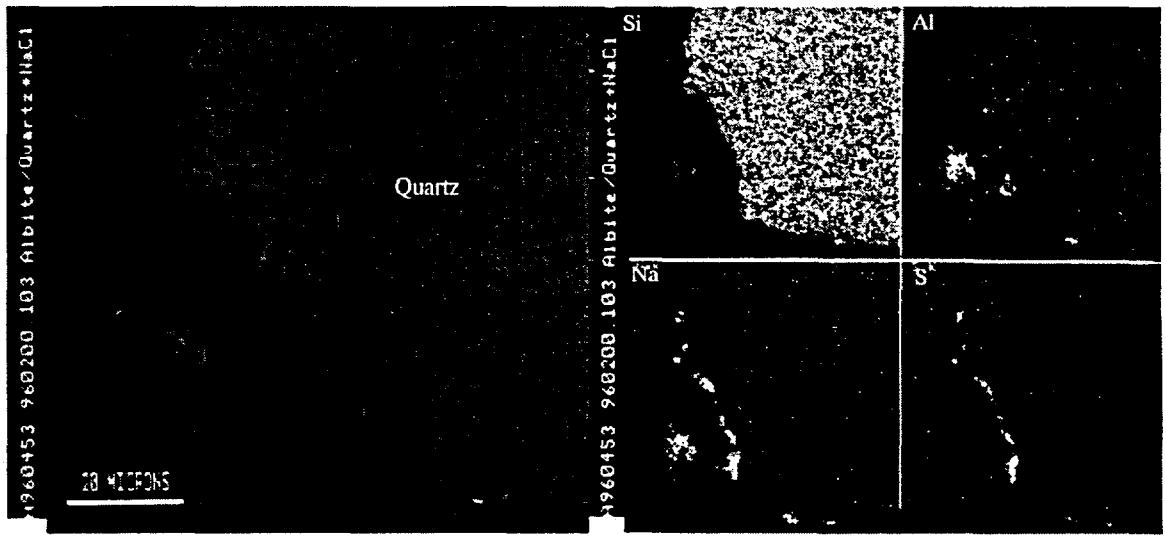

Figure 49. SEM photograph of albite and quartz sample from TGA using NaCl and combustion gas

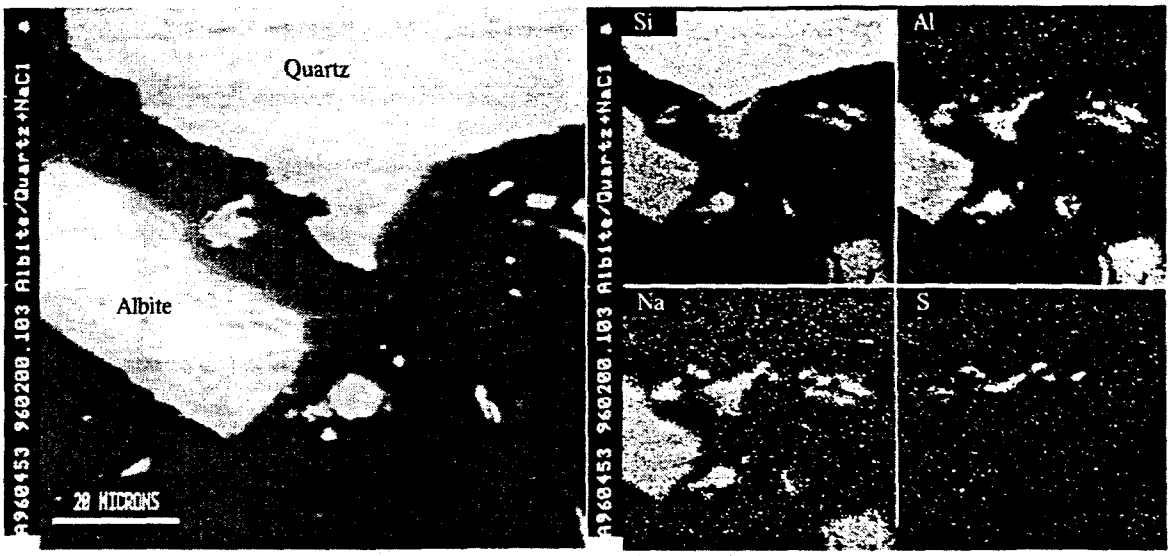

Figure 50. SEM photograph of albite and quartz sample from TGA using NaCl and combustion gas

sulfur into the quartz particle. Some reaction of sodium and sulfur with the small albite particle is seen. The silica particle can be easily differentiated from the albite particle by comparing areas with silicon only (quartz) to those with silicon, aluminum, and sodium (albite).

Figure 50 shows a similar trend. Again, sodium and sulfur are seen to be wetting the surface of the quartz particle, with no evidence or reaction with the quartz. It should be noted that surface reactions are likely occurring but are not detectable under the SEM. An albite particle is seen in the vicinity of the quartz particle in the area of the sodium sulfate. It is uncertain if this albite particle plays a role in the wetting and subsequent reaction of the sodium sulfate with quartz.

Figure 51 further examines the mechanism of alkali capture with albite. An analysis of several points were performed, with the results shown in Table 18. Some variation in the albite is noted from Point 1 to Point 3. At Point 4, a sharp increase in sodium and sulfur is noted, indicating a reaction with sodium sulfate. Points 5 and 6 show a similar trend. Point 6 marks the transition back to the unreacted albite identified as Point 7. It is interesting to note that at the interface between the albite of Point 7 and the

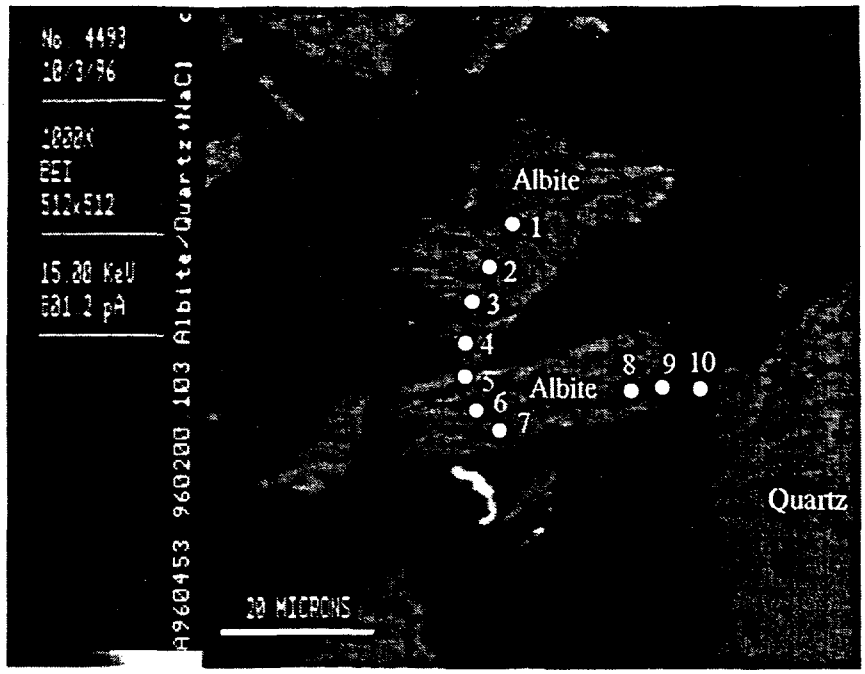

Figure 51. SEM point analysis of albite and silica exposed to NaCl in combustion gas in TGA

Table 18

Point Analysis of SEM of Albite and Quartz Particles from SEM Using NaCl and Combustion Gas

Point	1	2	3	4	5	6	7	8	9	10
Elemental Analysis, mole %										
Na	7.3	7.7	7.5	15	12.6	9.6	7.4	8.3	8.4	0.4
Al	8	8.3	9.4	5	6.8	7.9	9.1	8.7	17.2	0
Si	23.6	24.5	29.1	14.5	20.6	22.7	27.6	25.8	21.7	35.6
S	0	0	0	8.5	5.7	1.6	0	0.9	1.8	0.2
Cl	0.1	0	0	0	0.1	0	0	0.8	1.1	0.1
O	60.9	59.5	54	56.9	54.2	58.1	55.8	49.8	49.8	63.7
Stoichiometry										
Na	1.9	2.1	2.2	4.2	3.7	2.7	2.1	2.4	2.7	0.1
Al	2.1	2.2	2.8	1.4	2	2.2	2.6	2.5	5.5	0
Si	6.2	6.6	8.6	4.1	6.1	6.2	7.9	7.4	7	9
S	0	0	0	2.4	1.7	0.5	0	0.2	0.6	0
Cl	0	0	0	0	0	0	0	0.2	0.4	0
O	16	16	16	16	16	16	16	16	16	16

quartz of Point 10 both sulfur and chlorine are detected along with a comparable amount of sodium. It is speculated that the reaction was initiated by the sodium sulfate during the first part of the TGA test, while the chlorine may have been incorporated into the melt during the last part of the test, when high adsorption rates were seen using nitrogen as the carrier gas. This also provides evidence that both the sulfur and chlorine can coexist in the sorbent particle and that depending upon the ratio of SO_2-to-Cl_2 partial pressure, simultaneous capture of alkali, chlorine, and sulfur may be possible.

Figure 52 is taken from Stormer and Carmichael (1971) and shows the relationship between chlorine and sulfur in the sodalite system. According to Reactions 3 and 5, an equilibrium exists between nosean (sulfur-bearing) and sodalite (chlorine-bearing). The weight gain in Test 8 indicates that Reaction 5 may be proceeding to the right. When exposed to both SO_2 and Cl as in Test 7, the reaction still proceeds to the right. Assuming an ideal gas, the log f_{SO2}/f_{Cl2} is approximated by log C_{SO2}/C_{Cl2} where f and C are the fugacities and concentrations of SO_2 and Cl_2. At 700°C, the log f_{SO2}/f_{Cl2} is approximately 2.5; assuming all of the Cl released by vaporizing the NaCl is present as Cl_2. At 800°C, this value is approximately 1.1. The corresponding f_{O2} is approximately 5×10^{-2}, again assuming ideal gas. This indicates that nosean is indeed

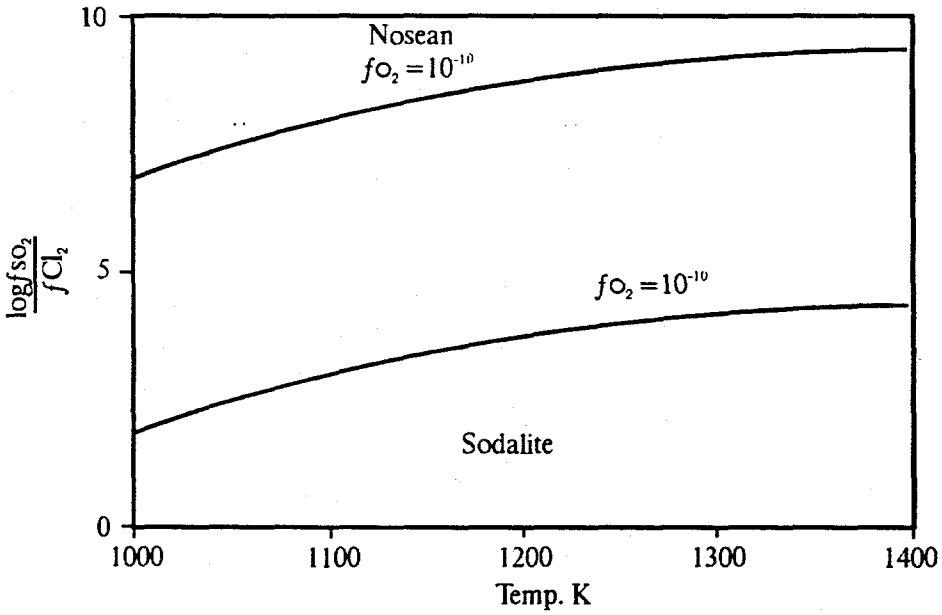

Figure 52. Equilibrium between nosean and sodalite at constant oxygen fugacity (Stormer and Carmichael, 1971)

thermodynamically preferred for the low-temperature conditions. Extrapolating the f_{O_2} to 5×10^{-2} indicates that nosean may also be thermodynamically preferred at the higher-temperature case. Sodalite would be the preferred species for a higher chlorine concentration.

The results from this screening exercise indicate that over the range of temperature and sodium, chlorine, and SO_2 concentrations tested that nosean is the preferred product. Using albite as the starting material, there may be a number of intermediate reactions occurring including sodalite formation, but these reactions, in the presence of SO_2, will proceed to nosean formation. Sodalite could be formed at relatively low SO_2 concentrations and high Cl concentrations. Low SO_2 concentrations may be favored in the PFBC because of dolomite addition for control of sulfur emissions; however, for most coals, the chlorine content will also be low. Simultaneous alkali and chlorine capture, to any significant degree, are, therefore, not expected.

4.3 Adsorption Rates and Mechanisms

Section 4.2 focused primarily on the reaction scheme presented for the capture of alkali, sulfur, and chlorine using sodalites. This section looks at the eight different materials tested to compare the overall adsorption rates and mechanism of adsorption. The data taken for each test were reduced to generate rate vs. NaCl concentration and ln k vs. 1/T curves where k is the rate/concentration and T is the temperature. An example of the type of curves generated is given as Figure 53. The following background discussion is added to justify the approach taken and the conclusions reached.

The rate expression for adsorption at equilibrium conditions, assuming both adsorption and desorption are occurring, can be written as the rate of adsorption of the gas species A onto the surface minus the rate at which A is desorbed (Fogler, 1974), or:

$$R_{ads} = k_a(P_a C_v - C_{as}/K_a) \qquad [63]$$

where R_{ads} is the rate of adsorption, k_a is the rate constant, P_a is the partial pressure of the adsorbent (alkali in this case), C_v is the number of vacant sites of the absorber (sorbent), C_{as} is the number of active sites on the sorbent, and K_a is the ratio of the rate constant for adsorption divided by the rate constant for desorption. The work on the TGA measured the initial rates of adsorption for the system and not the equilibrium.

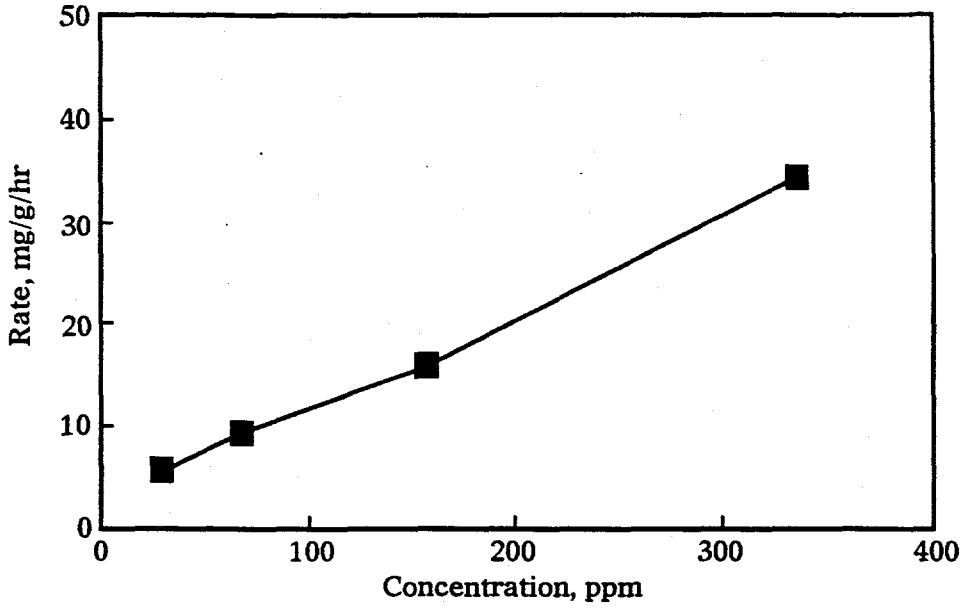

Rate of weight gain as a function of NaCl vapor-phase concentration

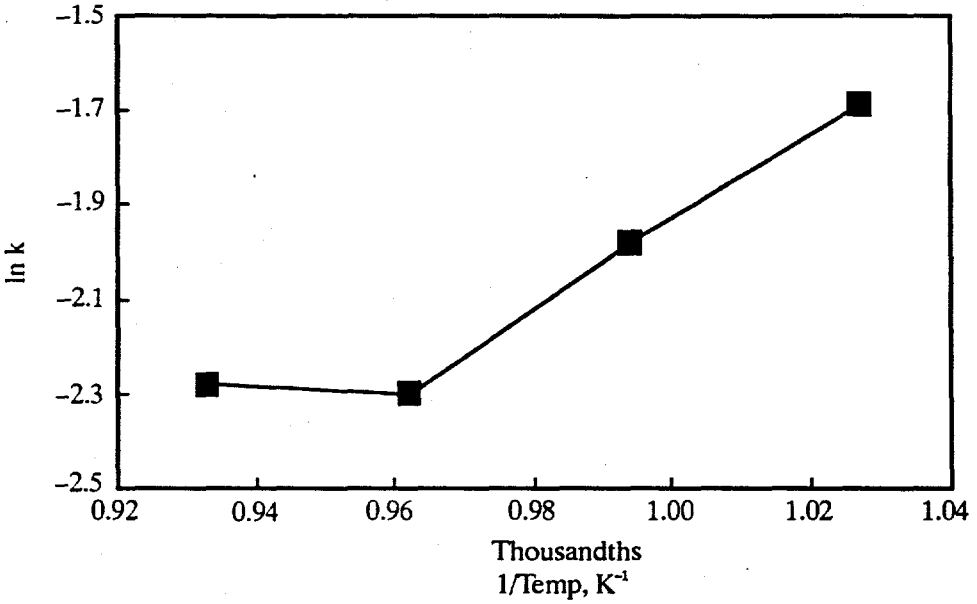

ln k (rate/concentration) as a function of 1/temperature

Figure 53. Graphical presentation of TGA data utilized for extracting kinetic information

Therefore, there is little or no alkali to be desorbed, and term C_{as}/K_a can be ignored. One can also assume that until a significant amount of the alkali has been adsorbed, the number of vacant sites will remain relatively constant. One can also substitute C_aP_T for P_a where C_a is the concentration of the alkali and P_T is the total pressure. The rate expression can then be expressed simply as:

$$R_{adsi} = KC_a \quad [64]$$

or:

$$K = R_{adsi}/C_a \quad [65]$$

where $K = k_aP_aC_v$ and R_{adsi} is the initial rate of adsorption. K may be a function of temperature. If so, the Arrhenius equation is assumed to be valid, and K can also be expressed as:

$$K = Ae(-E/RT) \quad [66]$$

In the FBC, Uberoi and others (1990) have developed the rate expression specifically for fluid beds. In this case, the rate equation becomes:

$$R_{ads} = (1 - \epsilon_o)KC_a(1 - C_{sf}/C_s) \quad [67]$$

where ϵ_o is the porosity of the bed and C_{sf}/C_s is the ratio of used sites to total sites available on the sorbent. Initially, C_{sf}/C_s is zero since no sites are taken. For a defined system, $(1-\epsilon_o)$ is a constant, so the initial rate of adsorption can be again written as

$$R_{adsi}=KC_a \quad [68]$$

If K varies with temperature, it can be expressed as the same Arrhenius expression used above.

The TGA data were plotted as rate vs. concentration and ln K vs. 1/T where K is rate/concentration. In addition, a linear regression was performed about ln K and 1/T, with the intercept of the regression being equal to ln A and the slope equal to -E/R in accordance to Eq. 66. Results from this analysis are presented in Table 19.

Table 19

Rate Data Collected During TGA Experiments

	NaCl	Initial Gas	E, kcal/mole
Positive Rate vs. Concentration Negative ln k vs. 1/T			
Albite	Yes	Combustion	20
Albite	Yes	Combustion (500 ppm)	25
Albite + Quartz	Yes	Combustion	17
Kaolinite	Yes	Combustion	19
Positive Rate vs. Concentration Positive Ln K vs 1/t			
Sodalite	Yes	Combustion	-0.5
Nepheline	Yes	Combustion	-13
$AlO(OH)_3$	Yes	Combustion	-54
Flat Rate vs. Concentration			
Albite	No	Combustion	NA[1]
Albite + Quartz	Yes	Nitrogen	NA
Sodalite	No	Combustion	NA
Sodalite	Yes	Nitrogen	NA
Activated Bauxite	Yes	Nitrogen	NA
Zeolite	Yes	Nitrogen	NA

[1] Analogy not applicable to nonadsorbing cases.

The data are grouped into three categories. The first category showed a positive slope on the rate vs. concentration curve, indicating that these materials are potentially good sorbents. This group also has a negative slope of ln K vs. 1/T. The negative slope (positive E/R) for these materials is indicative of chemical reaction being the primary mechanism of adsorption. As an example, the characteristic plots for albite are shown in Figure 47. This is consistent with the observed reaction of the sodium sulfate with the

albite and silica as discussed previously and work by previous researchers using kaolinite (Uberoi et al., 1990). For comparison, the activation energy for kaolinite as calculated from this work, 19 kcal/mole is in fair agreement with the value of 31 kcal/mole calculated by Uberoi and others (1990).

The second category had a positive rate vs. concentration curve, again indicating that these materials have the propensity to adsorb the alkali, but have a positive slope for the ln K vs. 1/T. The positive E/R (negative activation energy) indicates that the mechanism for adsorption for these materials is physical. These curves are shown in Figure 53 for sodalite as an example. This result is somewhat surprising, since it was expected that the sodalite and nepheline would react chemically according to Eqs. 1 through 5 as discussed above. The open structure of the sodalite, as discussed in Section 2.4.1, does provide space within the crystalline structure necessary for physical adsorption. The structure of nepheline is not as open as the sodalite and would be expected to have more difficulty physically adsorbing material. The synthetic bauxite ($AlO[OH]_3$) also has a porous structure.

The third category is for those materials with a flat rate vs. concentration curve. This would indicate that the rate of adsorption is independent of alkali concentration and, therefore, probably limited by diffusion of the gas into the sorbent particle. All of these materials showed very low adsorption rates, and their independence of alkali concentration most likely means that these materials are not effective sorbents. It is interesting to note that all of the materials in this category were tested under the conditions of either no NaCl addition or with nitrogen as the carrier gas. All materials tested with both NaCl and combustion gas (SO_2) showed a significant amount of adsorption. It is also noted that for the bauxite, switching from nitrogen to combustion gas at the end of the test resulted in a high rate of adsorption (36 mg/g/hr), while the rate in nitrogen was less than 2 mg/g/hr.

SEM photographs were taken of the bauxite after exposure to NaCl in a combustion gas and an elemental map generated (Figure 54). In addition, several point analyses were performed. The SEM map shows that the sodium and sulfur are dispersed fairly evenly throughout the bauxite particle. This indicates that the vapor-phase alkali and sulfur are diffusing into the bauxite and being physically adsorbed followed

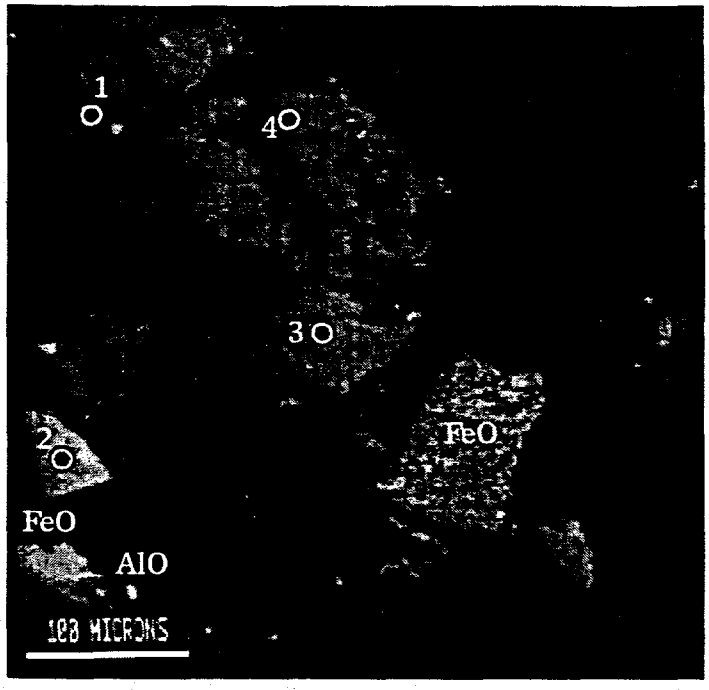

SEM photograph showing locations of particles on elemental map and of point analysis

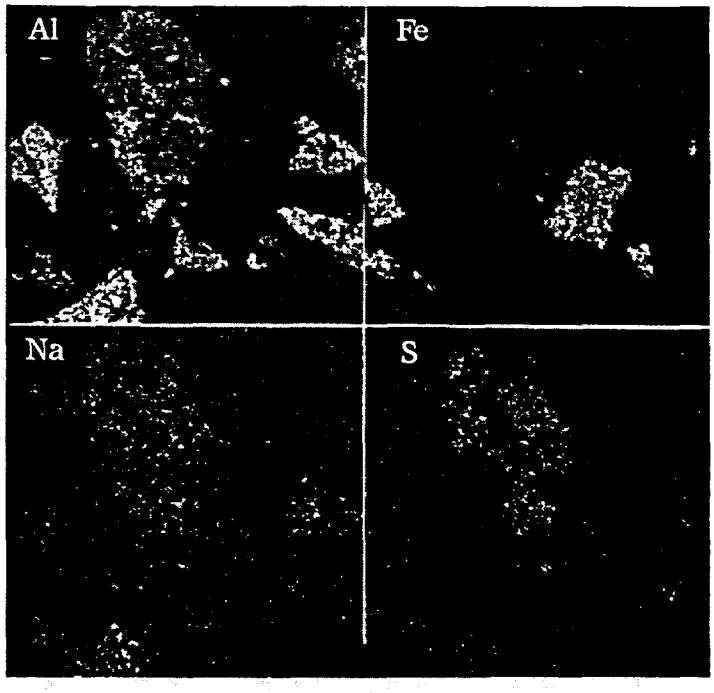

Elemental mapping

Figure 54. Morphology of bauxite after 6-hr exposure to combustion gas and NaCl in the TGA

by a chemical reaction. There is no evidence of wetting of the surface with Na_2SO_4 as was the case with the albite, representing a completely different adsorption mechanism. The SEM point analysis (Table 20) shows a portion of the bauxite with some adsorption occurring at Point 1. Point 2 is an iron oxide particle from impurities in the bauxite. No adsorption is noted on the iron particle. Points 3 and 4 in the interior of the bauxite particles show sodium and sulfur even in the deep interior of the particle.

4.4 Selection of Sorbents

Albite was chosen as the most likely candidate for a commercial sorbent from the sodalite-based compounds because it is more available and less costly than the other minerals. Nepheline and sodalite are more rare than albite, more costly and, therefore, less applicable as a commercial sorbent. Albite is commercially mined for use in refractory manufacture. There is no reference of the use of albite in bench- or pilot-scale systems of any kind to make a judgment on its expected performance based on previous research.

Table 20

Point Analyses of Bauxite after 6 hr of Exposure to Combustion Gas and NaCl in the TGA

Point	1	2	3	4
Elemental Analysis, mole %				
Sodium	0.8	0.3	1.4	1.4
Aluminum	40.9	0.1	21.2	21.6
Silicon	0.2	0	4	3.58
Sulfur	0.7	0.3	3.85	3.1
Chlorine	0.2	0.1	0.1	0
Iron	0.7	37.5	3.2	0.3
Oxygen	56.5	61.6	66.3	67.1
Stoichiometry				
Sodium	0.2	0.1	0.3	0.3
Aluminum	11.6	0	5.1	5.2
Silicon	0.1	0	1	0.9
Sulfur	0.2	0.1	0.9	0.7
Chlorine	0.1	0	0	0
Iron	0.2	9.7	0.8	0.7
Oxygen	16	16	16	16

Of the other sorbents tested, kaolinite and bauxite appeared to be the best candidates based on their rate of adsorption. The initial adsorption rate for kaolinite as measured by the TGA experiments using NaCl in a combustion gas was 24 mg/g/hr, while that for bauxite ranged from 36 to 55 mg/g/hr. The corresponding rate for albite is 72 mg/g/hr. Both bauxite and kaolinite are commercially available and have been tested in granular and packed-bed filters with success in removing up to 99% of the incoming vapor-phase alkali.

The candidates selected for testing on the bench-scale PFBR, therefore, were albite, kaolinite, and bauxite.

CHAPTER 5

BENCH-SCALE TESTING OF ALKALI SORBENTS

Results from the TGA testing indicated that several materials could make good sorbents for capturing alkali. The purpose of the bench-scale testing was to determine how effective these sorbents could be in capturing alkali in a dynamic system that more closely approximates the conditions in a commercial PFBC. Factors used to evaluate the sorbent's effectiveness included the gas-phase alkali concentration, impacts on ash deposition and agglomeration, and changes in hot-gas filter performance. The 7.6-cm (3-in.) PFBR described in Section 3.3 was utilized for this work. This chapter discusses the results of the testing on the PFBR. A summary of the run conditions and general operating performance will be presented first, followed by results showing the distribution of ash and sorbent. These two sections will serve as background for discussing the phenomenon that is occurring with regard to vapor-phase alkali (Section 5.3), ash deposition (Section 5.4), and hot-gas filter performance (Section 5.5).

5.1 Summary of Operating Data from PFBR Testing

Eleven tests were performed on the PFBR as part of this research. These tests are designated as B1-1296 through B1-2296. The tests were performed with the hot-gas filter vessel on-line and with the ash deposition probe in place. Vapor-phase alkali sampling was performed for all of these tests. Five other tests were performed previously, but only vapor-phase alkali sampling was performed. Results from these five tests are included in the results of Section 5.3, Capture of Vapor-Phase Alkali, but are not included elsewhere.

The matrix of tests for the PFBR testing was discussed in Section 3.3 and is repeated in Table 21 for convenience. All tests were designed to operate at the same temperature, excess air, and velocity to eliminate operating conditions as variables, allowing the work to focus on differences in fuel and additives.

Variables included in this test matrix include fuel type, sodium content, sorbent type, sorbent add rate, and sorbent size.

Table 21

Test Matrix for PFBR Testing

Test Number	Fuel	Sorbent	Sorbent Size	Sorbent/Na, wt/wt	Fuel Additive
B1-1296	Beulah	Albite	-30 mesh	30:1	None
B1-1396	Beulah	None	-	-	None
BEL-1496	Belle Ayr	None	-	-	None
BEL-1596	Belle Ayr	None	-	-	NaAc,[1] S
BEL-1696	Belle Ayr	Kaolinite	-⅛ in.	10:1	NaAc, S
BEL-1796	Belle Ayr	Kaolinite	-30 mesh	10:1	NaAc, S
BEL-1896	Belle Ayr	Bauxite	-⅛ in.	10:1	NaAc, S
B1-1996	Beulah	Bauxite	-⅛ in.	10:1	None
B1-2096	Beulah	Bauxite	-⅛ in.	3:1	None
B1-2196	Beulah	Bauxite	-⅛ in.	5:1	None
B1-2296[2]	Beulah	Bauxite	-⅛ in.	5:1	None

[1] Sodium acetate and sulfur added to the fuel.
[2] Repeat of Test B1-2196.

The two fuels utilized for the testing were Beulah Standard North Dakota lignite and Belle Ayr, Wyoming, subbituminous coal. The Beulah lignite is characterized by a relatively high sodium content in the ash and was, therefore, chosen as a good baseline coal for testing the effectiveness of the alkali sorbents. The ash content of this coal is approximately 11 wt% on an as-received basis. Most of the alkaline and alkaline earth elements of the ash are present as organically bound cations, while the iron is present as relatively small pyrite. The Belle Ayr is low in sodium and has a relatively high calcium content which is also primarily organically bound as is the case with the lignite. The Belle Ayr is also low in sulfur. This coal was chosen because its low sodium and sulfur allowed it to be spiked to allow control of the final levels of these elements without changing the rest of the makeup of the coal.

Prior to each test, the fuel feed was premixed to match the specified test conditions. All of the additives, including the sodium acetate to adjust the sodium content, the elemental sulfur to adjust the sulfur

content, and the sorbents (albite, kaolinite, bauxite, and dolomite) to capture the alkali and sulfur were weighed and mixed with the coal. This mixture was then added to the coal hopper to be used for the testing. The addition of these materials altered the makeup of the ash material being fed into the combustor. Table 22 presents an analysis of the additives used in the PFBR testing. A new fuel composition was calculated for each run to take into account the added sodium and sulfur and to establish a baseline for comparing the results of the tests. Table 23 presents the calculated analysis of the fuels and ashes, including the sodium, sulfur, and the additives. Test B1-1396 was the baseline (no additives) for the Beulah lignite, and BEL-1496 was the baseline for the Belle Ayr subbituminous.

Table 22

Analysis of Additives Used During PFBR Testing

	Bauxite	Kaolinite	Albite	Dolomite
SiO_2	11.0%	52.1%	62.3%	0.0%
Al_2O_3	84.2%	44.9%	26.3%	0.0%
Fe_2O_3	4.8%	0.8%	0.0%	0.0%
NaO_2	0.0%	0.0%	11.4%	0.0%
CaO	0.0%	0.0%	0.0%	36.6%
MgO	0.0%	0.0%	0.0%	15.2%

A summary of selected run conditions is presented in Tables 24 and 25. Appendix A includes the average and standard deviations for all measured points. For all of the tests, the reactor ran very smoothly as indicated by the curves for temperature, pressure, and emissions (Figures 42–46) similar to those presented in Section 5.3 and the low standard deviations for each measured point. Although each test was designed to run at exactly the same conditions, some discrepancies exist. Each test was planned for approximately 4.5 hr at steady state to allow a 4-hr alkali sample to be taken. Test B1-1296 utilizing the Beulah with albite as the alkali sorbent was stopped after 2.6 hr because of blinding of the hot-gas filter. As will be shown in Section 5.3.3, the pressure drop rose at a rapid rate and could not be reduced by backpulsing the filter elements. Therefore, the run was terminated to protect the hot-gas filter vessel and

Table 23

Analysis of the Fuels Used for PFBR Testing Including Added Sodium, Sulfur, and Sorbents

	B1-1296	B1-1396	BEL-1496	BEL-1596	BEL-1696	BEL-1796	BEL-1896	B1-1996	B1-2096	B1-2196	B1-2296
Proximate Analysis, as received, wt%											
Moisture	19.90	19.90	16.70	16.70	16.70	16.70	16.70	19.90	19.90	19.90	19.90
Volatile Matter	37.29	37.29	37.87	37.87	37.87	37.87	37.87	37.29	37.29	37.29	37.29
Fixed Carbon	31.86	31.86	40.56	40.56	40.56	40.56	40.56	31.86	31.86	31.86	31.86
Ash	10.95	10.95	4.87	4.87	4.87	4.87	4.87	10.95	10.95	10.95	10.9
Higher Heating Value, Btu/lb	7,693	7,693	9,750	9,802	9,802	9,802	9,802	7,693	7,693	7,693	7,693
Ultimate Analysis, as received, wt%											
Carbon	48.21	48.21	57.50	55.97	55.97	55.97	55.97	48.21	48.21	48.21	48.21
Hydrogen	3.12	3.12	4.32	4.21	4.21	4.21	4.21	3.12	3.12	3.12	3.12
Nitrogen	0.74	0.74	0.70	0.68	0.68	0.68	0.68	0.74	0.74	0.74	0.74
Sulfur	1.32	1.32	0.36	3.01	3.01	3.01	3.01	1.32	1.32	1.32	1.32
Oxygen	15.76	15.76	15.56	15.14	15.14	15.14	15.14	15.76	15.76	15.76	15.76
Ash	10.95	10.95	4.87	4.74	4.74	4.74	4.74	10.95	10.95	10.95	10.95
Moisture	19.90	19.90	16.70	16.25	16.25	16.25	16.25	19.90	19.90	19.90	19.90
Ash Composition, % as oxides											
Calcium, CaO	12.00	12.00	26.60	22.10	21.20	21.10	21.10	12.00	12.00	12.00	12.00
Magnesium, MgO	6.90	6.90	7.00	5.80	5.60	5.60	5.60	6.90	6.90	6.90	6.90
Sodium, Na_2O	3.40	3.40	1.30	1.80	1.70	1.70	1.70	1.70	3.40	3.40	3.40
Silica, SiO_2	24.50	24.50	27.80	23.10	24.30	22.60	22.60	24.50	24.50	24.50	24.50
Aluminum, Al_2O_3	11.40	11.40	13.10	10.90	12.30	13.90	13.90	11.40	11.40	11.40	11.40
Ferric, Fe_2O_3	19.10	19.10	5.50	4.60	4.40	4.60	4.60	19.10	19.10	19.10	19.10
Titanium, TiO_2	0.60	0.60	1.30	1.10	1.10	1.10	1.10	0.60	0.60	0.60	0.60
Phosphorus, P_2O_5	0.30	0.30	1.00	0.80	0.80	0.80	0.80	0.30	0.30	0.30	0.30
Potassium, K_2O	0.10	0.10	0.30	0.30	0.20	0.20	0.20	0.10	0.10	0.10	0.10
Sulfur, SO_3	21.70	21.70	16.00	29.60	28.40	28.40	28.40	21.70	21.70	21.70	21.70

Table 24

Summary of Process Data from PFBR Testing of the Beulah Lignite

Test No.	B1-1296	B1-1396	B1-1996	B1-2096	B1-2196	B1-2296
Coal Feed Rate, kg/hr	2.59	2.59	2.54	2.41	2.71	2.54
Dolomite Feed Rate, kg/hr	0.00	0.00	0.29	0.15	0.17	0.16
Additive	Albite	None	Bauxite	Bauxite	Bauxite	Bauxite
Additive Feed Rate, kg/hr	0.26	0	0.27	0.08	0.15	0.14
Cyclone Pressure Drop, kPa	1.78	2.54	1.23	1.74	1.31	1.69
Reactor Pressure, MPa absolute	1.13	1.20	1.13	1.13	1.14	1.14
Fluidizing Gas, lpm						
Air	348	328	354	339	362	346
Nitrogen	295	326	297	296	288	289
Total	644	655	652	636	650	636
Flue Gas						
Oxygen, %	4.85	4.56	4.795	4.62	4.88	4.94
Excess Air, %	25.0	23.4	24.1	23.8	26.0	25.1
FG SGV,[1] m/sec	0.94	0.87	0.97	0.93	0.96	0.94
Reactor Temperatures, °C						
Preheater Exit	326	314	319	323	319	324
Plenum	413	439	393	406	397	412
Zone 1 Average	848	776	846	834	836	845
Zone 2 Average	856	816	880	868	881	878
Zone 3 Average	861	863	858	856	872	862
Reactor Average	838	806	859	848	857	859
Cyclone Exit Temperature	821	805	799	801	732	722
Filter Vessel Temperatures, °C						
Inlet	821	805	799	800	732	722
Low	826	791	797	805	800	798
Middle	813	775	791	795	789	785
Top	757	716	715	736	NA[2]	706

[1] Flue gas superficial gas velocity.
[2] Not available.

Table 25

Summary of Process Data from PFBR Testing of the Belle Ayr Coal

Test No.	BEL-1496	BEL-1596	BEL-1696	BEL-1796	BEL-1896
Coal Feed Rate, kg/hr	1.98	2.21	2.06	2.10	2.00
Dolomite Feed Rate, kg/hr	0.00	0.00	0 0.0	0.00	0.00
Additive	None	None	Kaolinite	Kaolinite	Bauxite
Additive Feed Rate, kg/hr	0	0	0.08	0.08	0.08
Cyclone Pressure Drop, kPa	1.79	1.52	1.71	1.98	1.62
Reactor Pressure, MPa absolute	1.13	1.13	1.13	1.13	1.13
Fluidizing Gas, lpm					
Air	368	368	354	361	347
Nitrogen	283	283	282	269	291
Total	651	651	636	630	637
Flue Gas					
Oxygen, %	4.86	4.70	4.80	4.02	4.75
Excess Air, %	25.5	23.9	25.2	25.9	24.6
FG SGV, m/sec	0.96	0.97	0.95	0.94	0.93
Reactor Temperatures, °C					
Preheater Exit	321	318	324	328	323
Plenum	427	414	424	415	395
Zone 1 Average	830	842	850	844	846
Zone 2 Average	877	888	875	884	868
Zone 3 Average	923	912	889	904	869
Reactor Average	863	869	866	868	857
Cyclone Exit Temperature	821	805	799	801	732
Filter Vessel Temperatures, °C					
Inlet	846	854	837	831	807
Low	830	832	811	821	815
Middle	816	821	799	806	806
Top	762	763	737	738	738

tube sheet. Test B1-1396 was also stopped prematurely, after 0.8 hr, also due to uncontrollably high pressure drops across the ceramic filters in the hot-gas filter vessel. Test B1-2196 was stopped after only 1 hour due to computer problems. The data from this test are included, although their quality is somewhat suspect because of the short test duration and computer problems. Test B1-2296 was an 8-hr test.

The reactor pressure was held constant at the 1.13 MPa (150 psig) for all tests. A rise in pressure in the PFBR is noted when the filter vessel is being backpulsed with high-pressure air 1.8 to 2.3 MPa (240 to 300 psig). Therefore, for those tests where it was necessary to backpulse the filters, a higher average reactor pressure is noted. For Test 1396, the filter was backpulsed repeatedly, which accounts for its significantly higher reactor pressure. Excess air was consistently around 25% and the SGV at its set point of 0.91 m/s (3 ft/s).

The set point for the temperature was an average bed (Zone 1) temperature of 843°C (1550°F). Tests 1296 and 1396 were performed at lower temperatures (818°C [1504°F] and 776°C [1429°F], respectively) because of miscommunication with the PFBR operator. For these two tests, the control point used was the Zone 3 temperature rather than Zone 1. The remainder of the reactor temperatures are within 20°C of the set point. A second difference to note in temperatures is the higher Zone 3 temperature for the Belle Ayr tests versus those with the Beulah. This indicates that more of the Belle Ayr was burning in the freeboard region of the bed. This impacts the alkali and sulfur capture efficiencies since the fuel burning in the freeboard does not contact the in-bed sorbents.

Tables 26 and 27 summarize the emission data from these tests. Test 1396 showed high CO and low CO_2 emissions. This is probably due to the shortness of the test. Carbon monoxide is typically high at the beginning of the testing as coal is first introduced. For a longer duration run, these high CO values for the short time period for conversion to coal would not have a noticeable effect on the run averages. The other emission to note is the apparent reduction in NO_x with the addition of bauxite and kaolinite. Since NO_x emissions are very sensitive to temperature, the NO_x was plotted versus temperature in Figure 55. The lowered emissions are clearly not temperature-dependent. Limestone has been demonstrated to have a catalytic effect on NO_x emissions, and a similar phenomena may be occurring here. Albite did not appear to affect the NO_x emissions.

Table 26

Emissions Data from PFBR Tests Performed Using Beulah Lignite

	B1-1296	B1-1396	B1-1996	B1-2096	B1-2196	B1-2296
O_2, %	4.85	4.56	4.80	4.62	4.88	4.94
Excess Air, %	25.48	23.13	25.30	23.96	25.80	26.25
CO Content, ppm	11	290	11	16	25	5
CO Content,[1] ppm	12	318	12	18	28	6
CO Emission, lb/MMBtu	0.034	1.121	0.031	0.048	0.073	0.014
CO Content, corrected ppm	23	633	22	33	50	10
CO_2 Content, %	4.7	3.8	5.3	4.9	5.0	5.1
CO_2 Content,[1] %	5.2	4.1	5.8	5.3	5.6	5.7
CO_2 Content, corrected %	9.7	8.2	10.7	10.0	10.1	10.4
NO_x Content, ppm	69	67	76	58	108	61
NO_x Content,[1] ppm	77	73	84	64	121	68
NO_x Emission, lb/MMBtu	0.353	0.426	0.347	0.286	0.516	0.289
NO_x Content, corrected ppm	142	146	155	119	217	125
SO_2 Content, ppm	55	75	4	8	25	25
SO_2 Content,[1] ppm	61	82	4	9	28	28
SO_2 Emission, lb/MMBtu	0.392	0.663	0.025	0.055	0.166	0.165
SO_2 Retention,[2] %	85.7	75.8	99.1	98.0	93.9	94.0
SO_2 Content, corrected ppm	113	164	8	16	50	51
Avg. Comb. Temp., °C	821	805	799	800	732	722
Moisture in FG, vol%	5.0	5.0	5.0	5.0	5.0	5.0

[1] Corrected to 3% O_2.

[2] Moisture-free fuel carbon and sulfur values used in the sulfur retention calculation.

Table 27

Emissions Data from PFBR Tests Performed Using Belle Ayr Coal

	BEL-1496	BEL-1596	BEL-1696	BEL-1796	BEL-1896
O_2, %	4.86	4.70	4.80	5.02	4.75
Excess Air, %	25.67	24.51	25.18	26.76	24.82
CO Content, ppm	0	0	8	31	18
CO Content,[1] ppm	0	0	9	35	20
CO Emission, lb/MMBtu	0.000	0.000	0.022	0.082	0.050
CO Content, corrected ppm	0	0	16	61	37
CO_2 Content, %	5.0	4.9	4.8	5.0	4.8
CO_2 Content,[1] %	5.6	5.4	5.3	5.7	5.3
CO_2 Content, corrected %	9.9	9.5	9.6	9.9	9.7
NO_x Content, ppm	77	172	61	41	54
NO_x Content,[1] ppm	86	190	68	46	60
NO_x Emission, lb/MMBtu	0.347	0.775	0.277	0.178	0.247
NO_x Content, corrected ppm	152	336	122	81	110
SO_2 Content, ppm	16	470	348	441	381
SO_2 Content,[1] ppm	18	519	387	497	422
SO_2 Emission, lb/MMBtu	0.100	2.949	2.201	2.672	2.430
SO_2 Retention,[2] %	86.3	51.8	64.0	56.4	60.3
SO_2 Content, corrected ppm	32	918	694	866	776
Avg. Comb. Temp., °F	1585	1597	1590	1594	1575
Moisture in FG, vol%	5.0	5.0	5.0	5.0	5.0

[1] Corrected to 3% O_2.

[2] Moisture-free fuel carbon and sulfur values used in the sulfur retention calculation.

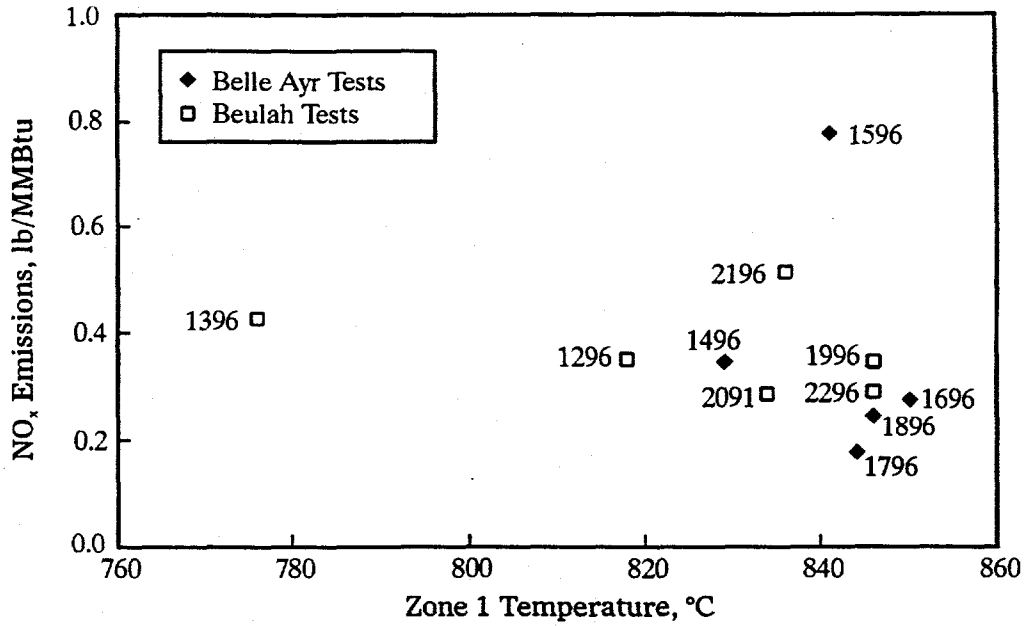

Figure 55. NO_x emissions as a function of temperature for PFBR tests

5.2 Distribution and Chemistry of the Ash Generated from Capture Tests

At the conclusion of each test, ash in the bed, cyclone, and filter vessel drain pots were collected, weighed, and submitted for analysis. During maintenance, material that was deposited on the reactor or cyclone walls and the deposition probe was removed and weighed. The filters were pulsed cold at 50 psig, and this material was also collected and weighed. Material balances were performed for each of the tests with the results presented here. Knowing how each of the sorbents will affect the solids loadings going into the primary cyclone and the filter vessel is important in evaluating the overall impacts of the sorbent on performance.

Figure 56 presents graphically the material balances for each of the tests performed as the percentage of ash removed in the cyclone, filter vessel, and bed based on the total percent of ash and bed material fed into the system. A miscellaneous category accounts for ash that built up in the crossover from the reactor to the cyclone or the cyclone to the filter vessel. Closures were near 100% for most tests. If one first looks at the base case for the test for the Beulah coal, Test B1-1396, the following observations can be made. Only a

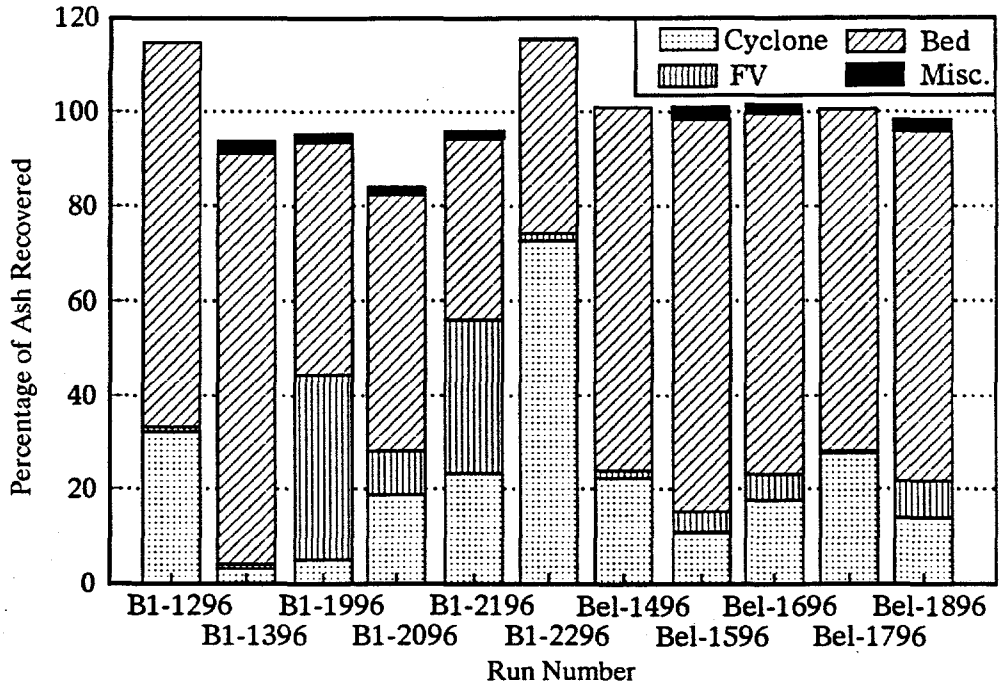

Figure 56. Material balance for PFBR testing expressed as percent of ash removed based on total solid material added

small percentage of the ash left the bed and entered into the cyclone and filter vessel. Also, a significant amount of material was found hung up in the reactor. Observation of the bed material at the conclusion of the test indicated the onset of agglomeration. Agglomeration is the build up of ash on the bed particles and has been shown to be caused by the organically bound sodium in the coal fluxing with calcium and forming sodium calcium sulfates (Mann et al., 1995). The generation of this sticky ash kept a large percentage of the ash in the bed, rather than releasing it from the bed as fly ash.

The test using albite as the sorbent (B1-1296) as compared to the baseline test (B1-1396) shows a significant increase in the percentage of cyclone ash generated. It is speculated that this increase is due to carryover of the albite into the cyclone. Table 28 presents an analysis of the material collected from the cyclone for each test. It is obvious from the high silica levels that some of the quartz bed material is breaking up and being carried out of the bed. The quartz bed material is more prevalent in the coarser cyclone ash (d_{50} approximately 100 microns) compared to the fine filter vessel ash (d_{50} approximately 30 microns). Figure 57 shows the size distribution for the major ash streams from Test 1296.

Table 28

Elemental Analysis of Cyclone and Filter Vessel Ash from PFBR Testing on Sulfur-Free Basis, mole %

Run	1296	1396	1496	1596	1696	1796	1896	1996	2096	2296
Coal	B1	B1	BEL	BEL	BEL	BEL	BEL	B1	B1	B1
Filter Vessel										
Si	30.9	31.7	34.8	42.7	40.3	39.5	39.6	25.8	28.6	25.4
Al	11.6	12.8	15.8	16.9	17.3	17.6	25.5	13.3	15.7	9.6
Fe	8.3	14.3	7	7.6	7.9	6.6	10.2	7	10.5	13.2
Ca	29.2	18.5	31.9	23.9	25.7	21.2	12.8	31.8	26.2	20.5
Mg	16.4	4	6.5	3.5	3.3	6.2	4.5	18.5	11.7	8.4
Na	1.3	17.1	1.7	2.9	2.9	6.2	4.9	2.6	6.2	20.9
S	15.2	18	4	10.8	20.1	11.8	8.5	4.4	11.2	27.2
Cyclone Ash										
Si	41.7	51.8	43.5	47.9	60.7	44.2	48.1	48.9	29.5	27.4
Al	14.5	12.1	14.5	14.9	14.2	21.4	20.6	11.8	14.7	14.8
Fe	121.4	12.2	6.7	6.7	5.4	6.7	9.9	8.9	9.9	13.3
Ca	16.9	14.8	26.4	22.4	12.7	18.6	15.6	18.8	27.4	26.7
Mg	5.8	4.2	5.6	4	3.8	4.3	2.7	8.3	14.5	13
Na	7.5	4.4	1	1.8	1.5	2.5	1.2	2.9	3.3	3.6
S	6.3	7.6	2.9	8.9	3.5	4.5	4.6	5.6	6.7	8.5

Continuing with the comparison of Tests 1296 and 1396, the higher aluminum and sodium contents for Test 1296 are indicative of enrichment of albite in the cyclone ash. The percentage of ash collected in the filter vessel appears to be similar for both cases. However, by comparing the rates of ash collected in the cyclone and filter vessel as is done in Figure 58, it can be seen that fine fly ash was being generated at a higher rate for the base test than for the test with albite. The albite may be limiting the amount of fine Na_2SO_4 that either forms by reaction or by serving as a site for heterogeneous condensation. TGA tests (Section 4.2) showed condensation of Na_2SO_4 on the albite particle followed by chemical reaction.

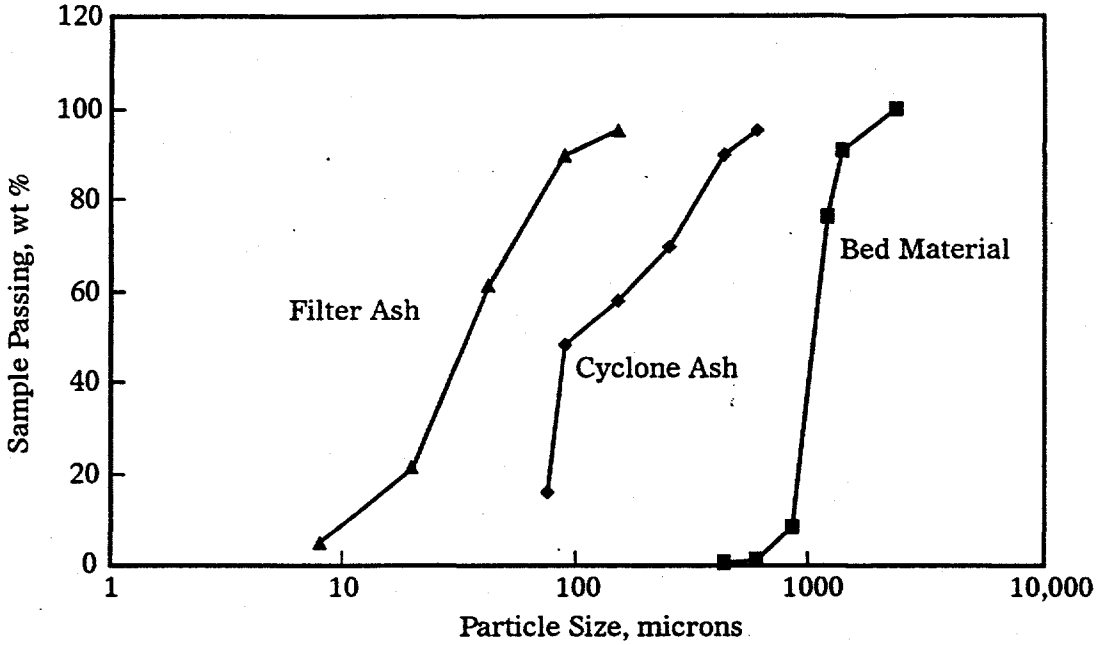

Figure 57. Distribution of size of bed material, cyclone, and filter ash for Test B1-1296

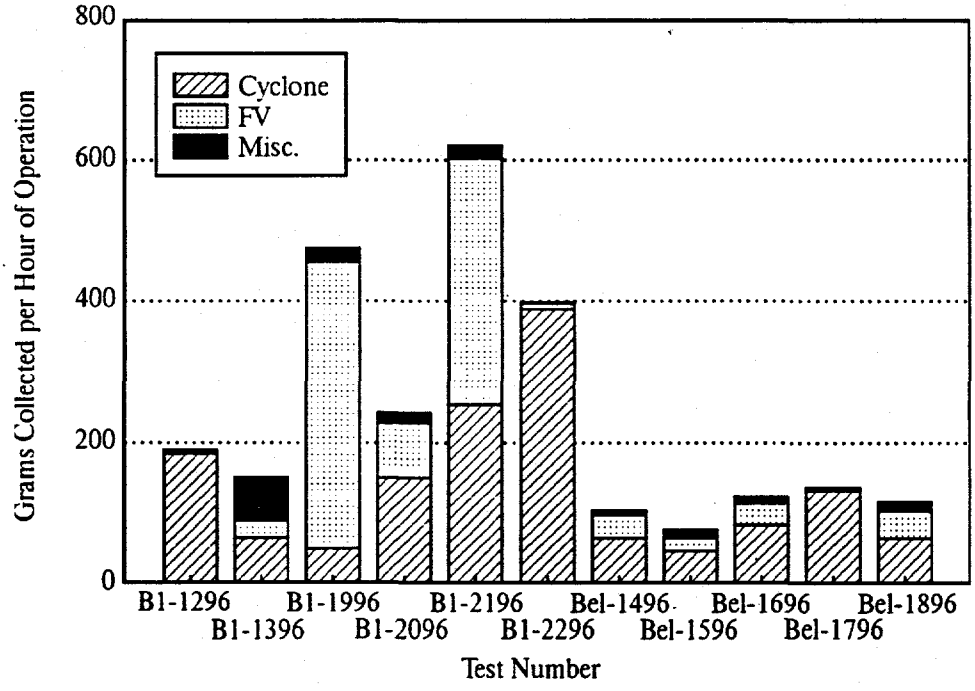

Figure 58. Mass flow of cyclone and filter vessel ash from PFBR tests

The impact of using the bauxite additive for alkali capture on the distribution of ash from the Beulah tests is shown by the bars for B1-1996 (10:1 bauxite:sodium), B1-2096 (3:1 bauxite:sodium), and B1-2196 and B1-2296 (5:1 bauxite:sodium). The percentage of ash ending up in the filter vessel increases with increasing amounts of added bauxite as shown in Figure 56. The loading to the filter vessel, as shown in Figure 58, is about three times as high as the base case for the 3:1 add rate of bauxite and an order of magnitude higher for the 10:1 add rate. The potential impact of these changes on filter vessel performance will be discussed in more detail in Section 5.5. It should be noted that for Test B1-2296, the filters were not backpulsed after the test; therefore, the mass balance does not reflect the real amount of filter ash collected during the test. A difference is also noted in the amount of cyclone catch between Tests B1-2096 (3:1) and B1-2196 and 2296 (5:1). The increase in cyclone ash corresponds with the increases noted in the filter vessel ash, indicating that the bauxite was generating fines that were leaving the bed. The difference between these two tests and B1-1996 (10:1) is that two different samples of bauxite were used, with that used in B1-1996 being coarser than the second batch that was used for the last three tests. The coarser bauxite seemed to remain in the bed more than the fine bauxite. The fact that the fines generation, as indicated by the filter vessel collection, more closely followed the add rate indicates that these fines are probably generated by relatively small pieces of the bauxite being flaked off larger bauxite particles by the mechanical action of the bed, rather than the larger bauxite particles fragmenting into several smaller pieces. Analyses of the ash streams tend to confirm these trends. The cyclone ash catch from B1-1996 has lower aluminum than the base case of B1-1396, indicating that bauxite was not building up in the cyclone. This can be more easily seen from Table 29 which shows the deviation of the cyclone and filter vessel ashes from the original fuel mix used for the test. The numbers for each element presented in the table are calculated by dividing the percent in the cyclone or filter vessel ash by the percent in the fuel. Therefore, a number greater than one represents an enrichment of that element in the ash while a number less than one represents a depletion. Focusing on aluminum, a number greater than one would indicate that the ash contains a greater percentage of the sorbent than originally mixed in the fuel while a number less than one represents a disproportionately higher quantity of ash from the original coal. Tests B1-2096 and 2296 show an enrichment in aluminum presumably due to elutriation of the bauxite from the bed. In the filter vessel,

both Tests B1-1996 and 2096 show an enrichment in aluminum (bauxite). Test 2196 may not show this enrichment since the filters were not pulsed after the test, with the finer bauxite remaining on the filters.

Table 29

Comparison of the Ash Chemistry of the Cyclone and Filter Vessel Ash to the Parent Fuel Mix[1]

Test	1296	1396	1496	1596	1696	1796	1896	1996	2096	2296
Filter Vessel										
Si	0.92	1.26	1.43	1.89	1.51	1.63	1.86	1.37	1.32	0.97
Al	0.68	0.96	1.23	1.4	1.13	1.27	1.65	0.89	1.19	0.55
Fe	0.37	0.48	0.97	1.13	1.09	1	1.55	0.32	0.42	0.43
Ca	2.05	0.98	0.9	0.72	0.73	0.67	0.41	1.51	1.25	0.81
Mg	20.6	0.44	0.83	0.48	0.41	0.87	0.65	2.01	1.24	0.73
Na	0.15	3.04	0.94	1.04	0.96	2.29	1.88	0.64	1.31	3.62
S	1.24	1.15	0.34	0.49	0.94	0.55	0.4	0.33	0.77	1.9
Cyclone										
Si	1.37	2.31	1.81	2.16	2.75	1.98	2.35	2.57	1.42	1.31
Al	0.94	1.03	1.14	1.26	1.12	1.67	1.4	0.78	1.17	1.06
Fe	0.61	0.47	0.94	1.02	0.9	1.1	1.57	0.4	0.41	0.55
Ca	1.31	0.88	0.75	0.69	0.44	0.64	0.53	0.88	1.38	1.33
Mg	0.92	0.52	0.72	0.55	0.59	0.65	0.41	0.89	1.61	1.43
Na	0.99	0.89	0.59	0.64	0.58	1	0.46	0.69	0.74	0.79
S	0.51	0.48	0.25	0.4	0.16	0.21	0.22	0.42	0.46	0.59

[1] Numbers in table are the cyclone or filter ash concentrations divided by the fuel ash.

The results of the tests with the Belle Ayr coal show similar trends as the tests with the Beulah, with some differences due mainly to differing sodium levels between the two fuels. A comparison of B1-1396 and BEL-1496 in Figure 57, both fuels without any additives, show a higher rate of ash production for the Beulah coal as expected because of the higher ash content of the Beulah. While significant amounts of the Beulah ash remained in the bed or hung up in the reactor piping, very little of the Belle Ayr ash remained in the bed, and the piping was clean after the test. These differences are due to the low sodium in the Belle

Ayr as compared to the Beulah. When the Belle Ayr was spiked with sodium for Test BEL-1596, more ash was retained in the bed, and some holdup in the reactor was noted, indicating that this additional sodium was promoting bed agglomeration and ash deposition.

With regard to the additives used for the Belle Ayr tests, increases in the amount of fly ash generated were noted when the additives were used similar to the Beulah case. The add rates for the Belle Ayr were less than for the Beulah cases; therefore, much smaller increases in mass flow rates were noted. For the two tests with coarse and fine kaolinite, Tests BEL-1696 and BEL-1796 in Figure 57, respectively, a change in the distribution between cyclone and filter ash was noted. For the coarse kaolinite, a lower percentage of the cyclone ash and a higher percentage of the filter vessel was noted as compared to the fine kaolinite test. The probable reason for this is similar to that noted for the coarse and fine bauxite from the tests with the Beulah coal. For the coarse kaolinite, the fines are generated from small pieces breaking off of the larger kaolinite particles, creating a very fine ash fraction. The fine kaolinite was small enough that much of it could elutriate from the reactor without any breakage. Therefore, the fly ash generated from the fine kaolinite feed is coarser than that generated from the coarse kaolinite feed. The chemical analysis of both the cyclone and filter vessel ash (Table 29) shows an enrichment in kaolinite as noted by the higher aluminum content for these tests. Test BEL-1896 utilized bauxite as the alkali sorbent. The quantity and distribution of the ash is similar to Test BEL-1696, which used kaolinite of the same size and add rate.

5.3 Capture of Vapor-Phase Alkali

One of the initial goals of this project was to determine if alkali could be reduced to accepted levels by using in-bed sorbents for protecting the gas turbine. There is some discrepancy as to what level of vapor-phase alkali is acceptable, but it typically ranges from 24 to 125 ppb, as discussed in Section 1.1. The alkali, chlorine, and sulfur vapor concentrations measured as a part of this work are presented in Table 30. In addition, six tests that had been previously performed and are included to expand the basis for discussion. Results from these additional tests are not presented in the other subsections of Section 5 because no material balances or analytical work were performed for the tests.

Table 30

Measured Vapor Concentrations of Sodium and Chlorine from the PFBR Tests

Test	Na in Fuel, ppm	Fuel	Sorbent	Sorbent/ Na	Na in Gas, ppb	Na Capture, %	Cl, ppb	Zone 1 Temp., °C
PR01A	381	Blacksville	Dolomite	-	640	-	11000	862
B13-0894	2745	Beulah	Dolomite	-	3000	17	2970	808
B13-1294	2745	Beulah	None	0	3616	-	3000	798
B14-1294	2745	Beulah	Kaolin	30:1	840	77	560	831
B17-1294	2745	Beulah	Kaolin	30:1	270	93	680	831
B1-1296	2745	Beulah	Albite	18:1	4771	-	137	818
BEL-1496	468	Belle Ayr	None	0	940	-	373	829
BEL-1596	865	Belle Ayr	None	0	3327	-	2062	841
BEL-1696	865	Belle Ayr	Kaolin	10:1	742	57	1468	850
BEL-1796	865	Belle Ayr	Bauxite	10:1	673	62	2674	844
BEL-1896	865	Belle Ayr	Bauxite	10:1	587	67	1706	846
B1-1996	2745	Beulah	Bauxite	10:1	506	90	1462	846
B1-2096	2745	Beulah	Bauxite	3:1	2185	54	1846	834
B1-2296	2745	Beulah	Bauxite	5:1	1850	61	2260	846

Tests B13-0894 and B14-1294 were performed under similar operating conditions and provide an indication of reproducibility. The slightly lower sodium concentration for B13-0894 may be due to some physical adsorption of the sodium on the dolomite. The test with albite as the sorbent, 1296, showed the highest vapor-phase sodium content. This indicates that the albite was ineffective at capturing sodium in the bed. The temperature for this test was higher than that for Test B13-1294, and the higher alkali concentration could also be a function of this higher temperature.

Tests 1496 and 1596 were both performed with the Belle Ayr coal, with the difference being that the feed for 1596 was spiked with sodium acetate and sulfur. The impact of doubling the sodium concentration in the fuel essentially doubled the vapor-phase alkali concentration. The higher alkali content in the vapor phase also appeared to increase the vapor-phase chlorine concentration. This is reasonable based on the modeling results presented in Figure 13 which show an increased level of NaCl as the (Na+K)/Cl ratio increases.

The impact of the sorbent size on alkali capture was investigated for kaolinite during Tests B14-1294 and B17-1294 and for bauxite during Tests 1796 and 1896. As discussed in the previous subsection, the coarser material has more of a tendency to stay in the bed and will result in a longer residence time to react with the alkali. The finer sorbents have significantly more surface area than the coarser material. For both the kaolinite and bauxite, the alkali sorbents were more effective for the finer size, indicating the higher surface area of the fine material more than offset the shorter bed residence time.

Tests 1696 and 1796 provide a direct comparison of the effectiveness of kaolinite versus bauxite for capturing alkali. As can be seen by Table 30, the bauxite showed a slight improvement in collection efficiency over the kaolinite (62% versus 57%) This may be within the experimental error for these tests and indicates that if considering vapor-phase alkali capture alone, both would serve equally well.

The impact of add rate on the efficiency of alkali capture for bauxite was determined during Tests 1996, 2096, and 2296. As expected, the higher the sorbent add rate, the lower the vapor-phase alkali. These results also show that extremely high add rates of sorbents would be required to meet turbine specifications. However, as will be discussed in the next two subsections, other improvements in operating performance are noted at the lower add rates.

Chlorine and sulfur concentrations were also determined for each test. The chlorine values shown in Table 30 do not appear to exhibit any clear trends. The sulfur, not shown here, followed the expected trends of lower sulfur emissions for those tests using dolomite as a sorbent. The other sorbents (kaolinite, bauxite, and albite had no effect on SO_2 emissions. The values of sulfur measured corresponded reasonably well with the SO_2 emission data presented in Tables 26 and 27.

5.4 Ash Deposition

It has been demonstrated in other work (Mann et al., 1995) that coals high in alkali have a tendency to form deposits on heat-transfer tubes and other surfaces within the fluid bed. Depending upon the amount of alkali in the fuel and the nature of the other constituents of the ash, these deposits may or may not be troublesome to the overall operation of the fluid bed. Therefore, as a part of these studies, the impact of reducing the vapor-phase alkali content on ash deposition was studied. One of the primary methods was the use of a deposition probe that was inserted into the top of the reactor. Figure 59 shows the location of this probe relative to the reactor exit and the upper flange. It is important to note that a portion of the probe resides in a stagnant zone at the top of the reactor and only the bottom portion is exposed to the flow of flue gases as they leave the reactor. This results in two distinct types of deposits on the probe. As can be seen in Figure 60, the deposit on the bottom potion of the probe is what one would expect to see in the convective pass of an FBC. The deposit on the upper part of the probe is not representative of a real system and appears to be formed when larger particles are entrained into the freeboard. Burning coal particles in this upper stagnant region provide the temperature required to fuse these entrained ash/bed particles.

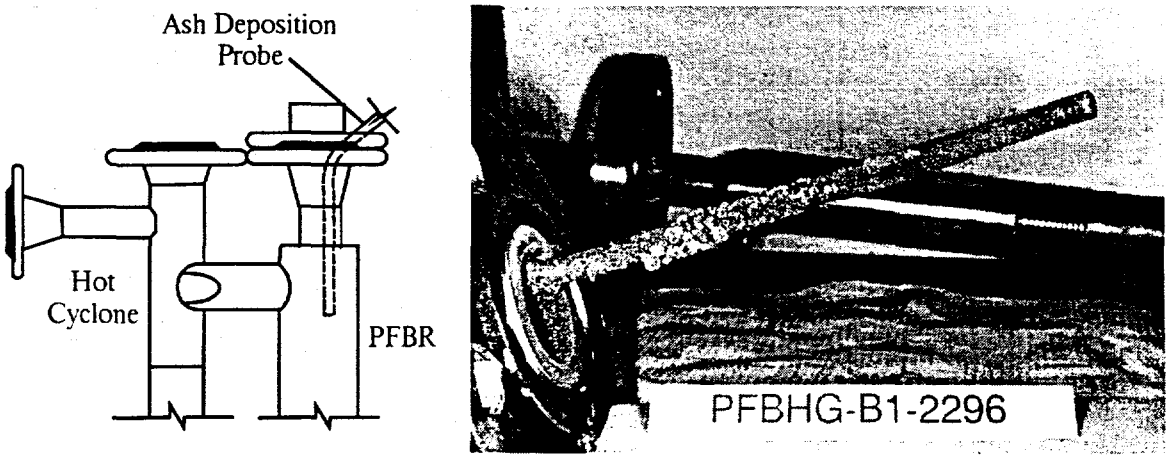

Figure 59. Schematic of the top of the PFBR showing the location of the ash deposition probe

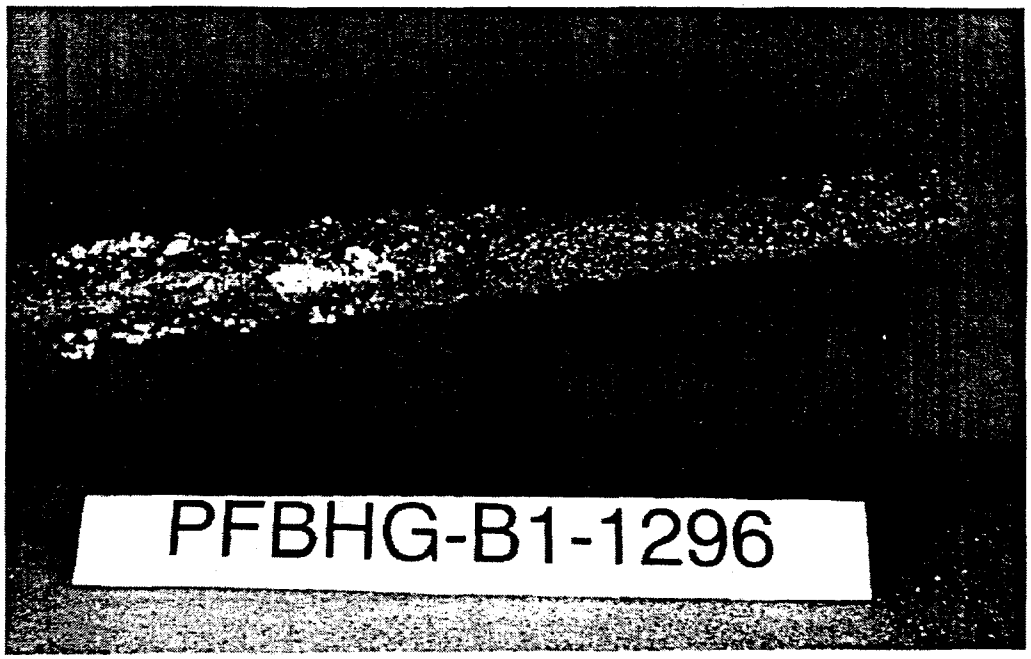

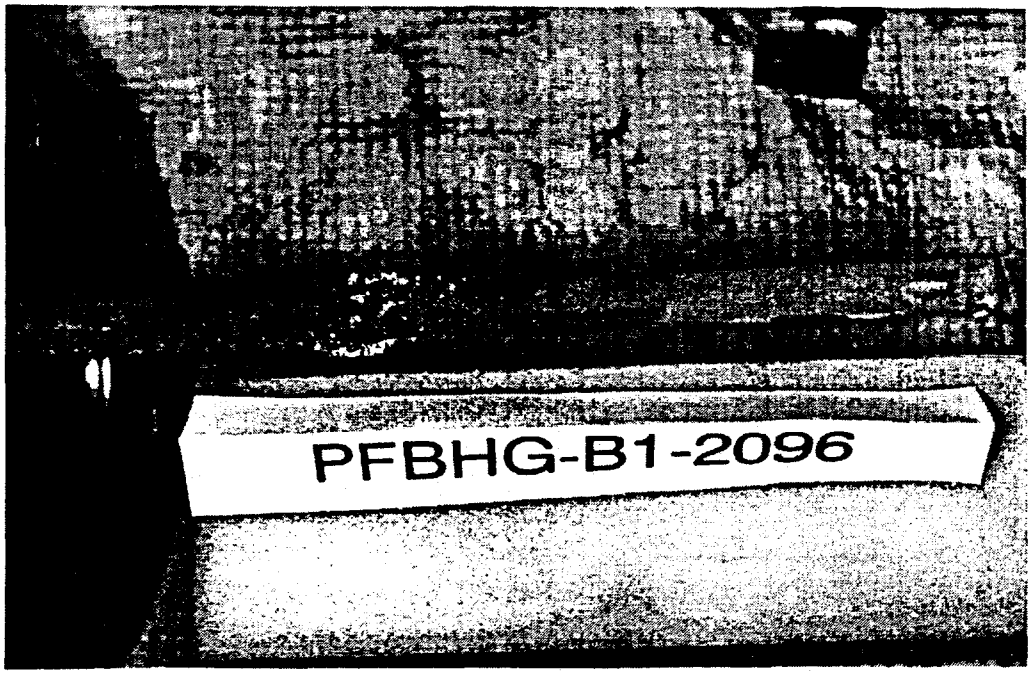

Figure 60. Photographs of ash deposition probe from the PFBR after alkali capture tests

To allow a comparison between each test condition, photographs of the deposition probe were taken after every test. A qualitative assessment of the severity of deposition was made for each test based on visual inspection of the probes after the tests and through the use of the photographs. Results of this qualitative assessment are given in Table 31. For comparison, the deposition was rated from 1 to 10, with 10 representing the level of deposition for the baseline Beulah test (B1-1396). The baseline test with the Belle Ayr (1496) represents the least amount of deposition and was assigned a value of 1. The test with the albite as a sorbent showed no improvement in the nature of the ash deposited on the probe. Adding sodium and sulfur to the Belle Ayr coal increased its propensity for deposition as expected. When kaolinite was added as an alkali sorbent, the amount of material deposited seemed to increase. The nature of the deposit also changed from a sintered deposit for the baseline cases, with the kaolinite-based deposit appearing to be a less compact, cohesive powder and more loosely bonded to the probe surface. The use of the fine kaolinite as sorbent resulted in more deposition than did the case with the coarse kaolinite. For the tests with the Belle Ayr, the test with bauxite resulted in very little evidence of deposition. When used with the Beulah coal, the bauxite caused a significant improvement in deposition over the baseline case.

Table 31

Weights of Material Collected after Each Test Used to Qualify Deposition Rates

Run Number	Sorbent	Reactor, g	Cyclone, g	Probe, g	Probe Deposit Ranking
B1-1296	Albite	50	551	NA	10
B1-1396	None	312	81	NA	10
BEL-1496	None	NA	NA	NA	1
BEL-1596	None	25	65	0.2	3
BEL-1696	Kaolinite	18	53	1.2	3
BEL-1796	Kaolinite	57	625	2.5	6
BEL-1896	Bauxite	10	84	1.4	1
B1-1996	Bauxite	14	74	0.2	2
B1-2096	Bauxite	1	78	0.4	4
B1-2196	Bauxite	26	22	1.9	3
B1-2296	Bauxite	25	58	1.6	3

Another indication of the propensity of the ash to deposit at various locations in the PFBC is the quantity of material that would be found sticking to the walls of the reactor and cyclone after the completion of a test. These values are recorded in Table 31. Significant quantities of material hung up in the reactor and/or cyclone for the baseline test with the Beulah coal as expected based on its relatively high sodium content. The test with albite also displayed an ash with a strong tendency to stick. Since the albite was ineffective in capturing the vapor-phase sodium, it is not surprising that similar deposition rates are seen for this case. The only other test with substantial hang up of material is the test using fine kaolinite and the Belle Ayr coal. This type of deposition would pose a problem for a commercial PFBC and would preclude using the fine kaolinite as a sorbent.

To provide an indication of the potential source of this deposition, an analysis was performed on the material hanging up in the reactor from three tests. The tests chosen, B1-1296, BEL-1696, and BEL-1896 represent the three sorbents tested: albite, kaolinite, and bauxite. The analyses in Table 32 show that for the case of the albite and the Beulah coal, the deposited material was enriched in sodium, calcium, and sulfur. These components are common in low-temperature deposition phenomena, with the sticky material being sodium calcium sulfate. Table 33 compares materials from the test using the -⅛-in. kaolinite as sorbent. The analysis of the material collected from the top of the reactor after the test shows a buildup of silica from the bed and kaolinite-derived material. Sodium, calcium, and sulfur are depleted in this sample, indicating that this phase was not the cause of the deposition as was the case with the Beulah coal and albite. It is speculated that the fines generated from the kaolinite are acting as the material to stick to the surfaces of the reactor. The case with the bauxite, Test BEL-1896, was similar to that with kaolinite and showed an enrichment in silica, aluminum, and iron, indicating that the deposited material was primarily sorbent based (Table 34). In a real system, it is expected that the type of deposition from the kaolinite and bauxite would be easier to control through the use of soot blowers than the more tenacious deposits that are typical of sodium calcium sulfates.

Table 32

Elemental Analysis of Material from Run B1-1296: Sulfur-Free Basis

	Fuel Mix Ash	Bed Material	Top of Reactor	Cyclone Ash	Filter Vessel Ash	Candle Deposit
Expressed as Mole Fraction						
Si	32.5	83.3	38.8	41.7	30.9	41
Al	16.4	4.2	15.4	14.5	11.4	10.1
Fe	21.6	3.8	12.9	12.4	7.3	5.8
Ca	13.8	2.2	17.2	16.9	29.7	16.4
Mg	6.7	3	5.2	5.8	17.2	5.2
Na	8.1	3.1	9.6	7.5	1.3	18.7
S	12.3	2.9	7.5	6.3	9.9	15.9
Expressed as a Percent of Feed						
Si	1	2.56	1.19	1.28	0.95	1.26
Al	1	0.26	0.93	0.88	0.7	0.62
Fe	1	0.18	0.6	0.57	0.34	0.27
Ca	1	0.16	1.25	1.22	2.16	1.19
Mg	1	0.44	0.77	0.86	2.56	0.78
Na	1	0.38	1.19	0.92	0.16	2.31
S	1	0.24	0.61	0.51	0.8	1.29

5.5 Filter Performance

The place where in-bed alkali sorbents may have the greatest impact on performance is in the hot-gas filter vessel. As the filters remove the ash from the gas stream, ash builds up on the candles, and the pressure drop across the filter increases. The candles are periodically backpulsed with high-pressure gas to remove the material from the filters. Once the ash is removed from the filters by the backpulse, the

Table 33

Elemental Analysis of Material from Run BEL-1696: Sulfur-Free Basis

	Fuel Mix Ash	Bed Material	Top of Reactor	Cyclone Ash	Filter Vessel Ash	Candle Deposit
Expressed as Mole Fraction						
Si	27.1	37.9	60.7	40.3	37.2	28.9
Al	15.5	18	14.2	17.3	16.9	15.8
Fe	7.4	8.3	5.4	7.9	7.7	9.4
Ca	36.1	26.1	12.7	25.7	23	30.9
Mg	8	4.1	3.8	3.3	4.1	4.3
Na	3	2.1	1.5	2.9	8.4	7.3
S	21.3	14.8	3.5	20.1	19.4	24.8
Expressed as a Percent of Feed						
Si	1	1.4	2.24	1.49	1.38	1.07
Al	1	1.22	0.96	1.17	1.14	1.07
Fe	1	1.13	0.73	1.07	1.04	1.28
Ca	1	0.73	0.36	0.72	0.65	0.87
Mg	1	0.91	0.46	0.41	0.51	0.53
Na	1	0.69	0.48	0.94	2.77	2.4
S	1	0.69	0.16	0.94	0.91	1.16

pressure drop will return to a baseline value and then build up again as it starts its next cleaning cycle. The ash that is pulsed off of the filters falls into an ash hopper where it is removed. Two primary concerns in hot-gas filtration are bridging and blinding. Bridging is the phenomenon where ash builds up on the candles to the point where an ash "bridge" forms between two or more candles. These bridges can eventually block flows and result in failure of the filtering system. Bridging is not usually accompanied by sharp and

Table 34

Elemental Analysis of Material from Run BEL-1896: Sulfur-Free Basis

	Fuel Mix Ash	Bed Material	Top of Reactor	Cyclone Ash	Filter Vessel Ash	Candle Deposit
Expressed as Mole Fraction						
Si	25	39.4	48.1	39.6	24.9	31.3
Al	17.9	19.3	20.6	25.5	14.6	21.2
Fe	7.6	11.5	9.9	10.2	7.8	12.1
Ca	36	20	15.6	12.8	42.6	22.3
Mg	8	4.9	2.7	4.5	7.6	3
Na	3	2.4	1.2	4.9	1.1	6.9
S	21.3	9.9	4.6	8.5	16.2	20.7
Expressed as a Percent of Feed						
Si	1	1.59	1.94	1.6	1.01	1.26
Al	1	1.08	1.15	1.42	0.81	1.18
Fe	1	1.51	1.29	1.33	1.02	1.59
Ca	1	0.56	0.43	0.36	1.18	0.62
Mg	1	0.61	0.034	0.56	0.95	0.38
Na	1	0.8	0.38	1.61	0.35	2.27
S	1	0.46	0.22	0.4	0.76	0.97

uncontrollable rises in pressure drop. Filter blinding, on the other hand, does result in high pressure drops across the filter. These pressure drops sometimes may be controlled by frequent backpulsing. In the case of severe blinding, the filter vessel must be shut down and brought off-line for cleaning.

Both blinding and bridging were noted for the tests performed as a part of this project. Figure 61 presents the pressure drop curves for the tests performed with the Beulah lignite. A rise in pressure drop can be seen in these curves as an ash layer builds up on the filters. An instantaneous decrease in pressure drop (over a 3-min backpulse sequence) is seen as this ash layer is removed during backpulsing followed by an increase in pressure drop as the ash cake builds up again during the next cleaning cycle. Ideally, the pressure drop would rise to a predetermined value and would return to a constant baseline value after each cleaning cycle. The length of time between cleaning would also be consistent and of a relatively long duration.

With this as background, the data presented in Figure 61 can be interpreted. The baseline test with Beulah coal, 1396, had to be terminated after approximately 45 min because the pressure drop rose so fast and could not be reduced by backpulsing. The pressure drop for that test approached 200 in. of water before the reactor could be shut down. Pressure drops of this magnitude can potentially cause mechanical failure of the tube sheet supporting the system or to the filter themselves. Test 1296 using the Beulah

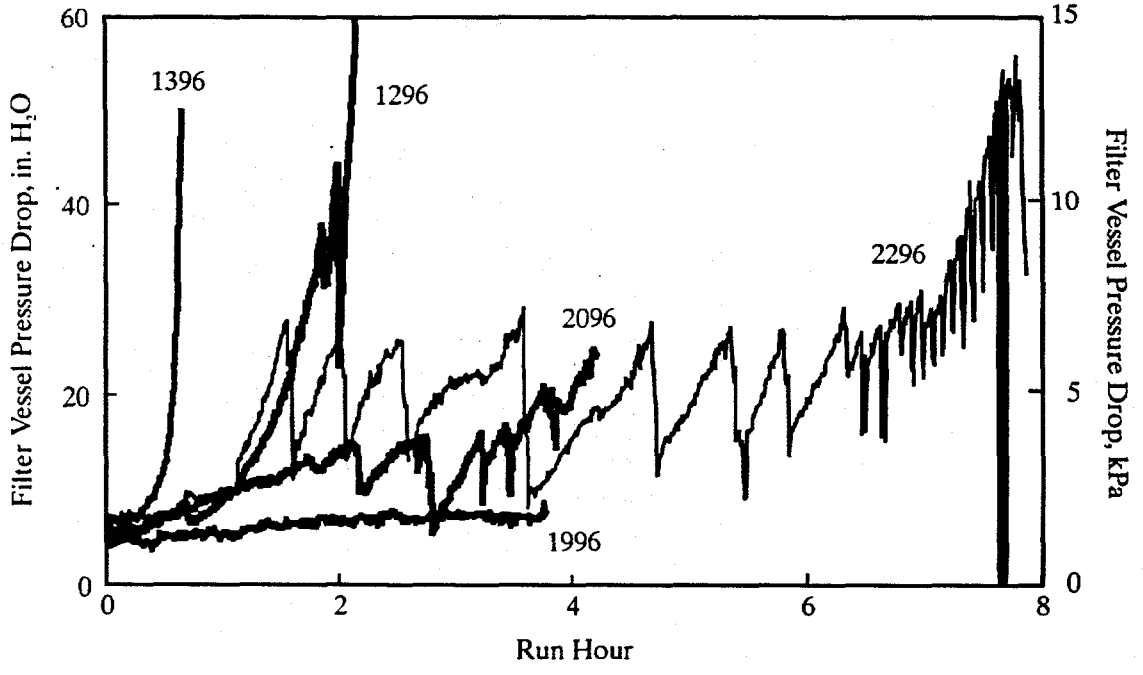

Figure 61. Filter pressure drop for PFBR tests using Beulah lignite

lignite with albite had to be terminated after 2 hr. Again, the pressure drop rose very fast and could not be returned to a safe baseline value after several successive attempts to backpulse. Test 1996 at a 10:1 bauxite-to-sodium feed ratio showed complete control over the blinding problems noted in Tests 1296 and 1396. During this test, the pressure drop showed very little rise over the 4-hr test duration. The success of this test was the basis for performing Test 2096 at the 3:1 bauxite add rate. The pressure drop rose much faster for this test, but appeared to be controllable by backpulsing for the first several cleaning cycles. At the end of the test, the backpulsing was becoming less effective at reducing the pressure drop, and given more time, the filter may have become blinded. This test was terminated because the supply of feed material for the test was exhausted (each test was planned for 4 hr). Test 2296 utilized the bauxite at a 5:1 feed rate and was planned for 8 hr in duration to provide longer-term trends. For the first 6 hr of this test, the pressure drop appeared to be under control. However, starting at Run Hour 6, the backpulse time interval had to be shortened to several minutes, and it was not effective at returning the pressure drop to the baseline value. This test was terminated before the scheduled 8 hr because of the blinding of the filters.

The results from the tests with the Belle Ayr are less dramatic. As can be seen in Figure 62, the addition of sodium and sulfur in 1596 resulted in a higher rate of increase in pressure drop as compared to 1496, which was the test with the as-received Belle Ayr. The pressure drops for Tests 1696 through 1896 show that both the kaolinite and bauxite were effective in reducing the pressure drop across the filters. This improved performance is directly attributable to the reduction in vapor-phase sodium. The difference in filter performance between the Belle Ayr and Beulah is also directly related to the sodium content of the flue gas. Figure 63 shows the condition of the filters after tests performed on Belle Ayr coal (part of a separate program and not the same filters used in this work) and from the tests with the Beulah coal. The Belle Ayr ash did not cause a noticeable buildup of material on the filters. However, the filters removed after Test 2296 with the Beulah coal and 5:1 bauxite addition show a substantial buildup on all three of the filters.

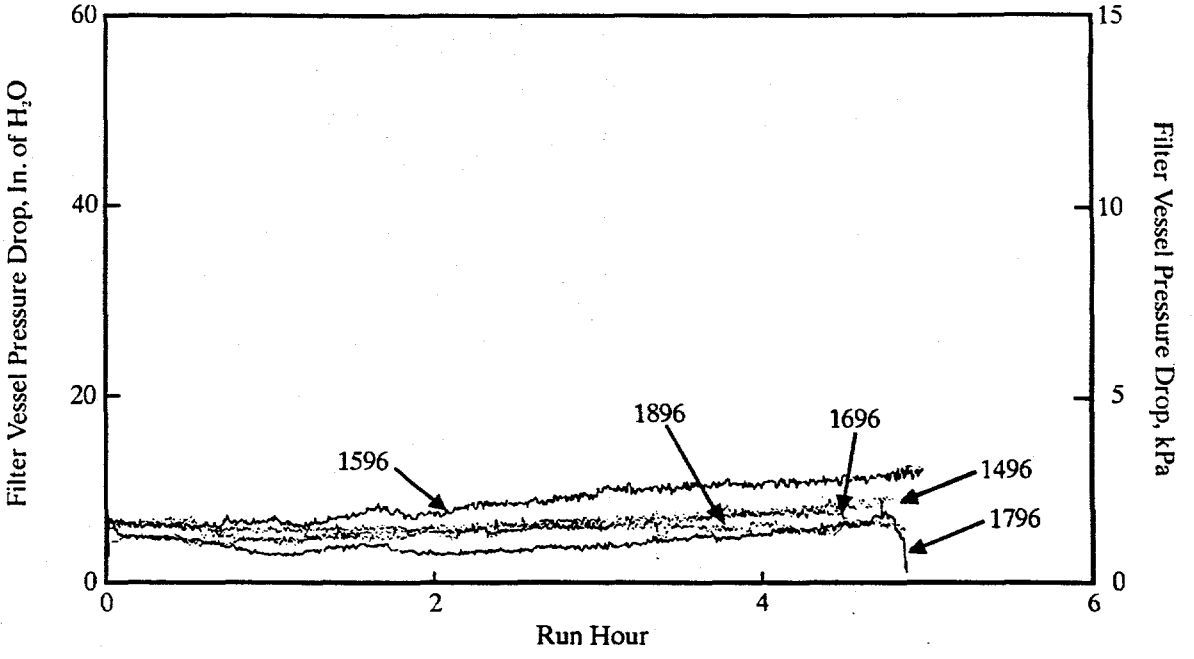

Figure 62. Filter vessel pressure drop for the Belle Ayr tests on the PFBR

Detailed analyses were performed on a number of samples to obtain a better grasp of the physical observations made. Figure 64 shows an SEM image of a cross section of deposit removed from a filter after the test with the albite. This test caused filter blinding and a forced shutdown after 2 hr of operation. This photograph shows that the interface between the deposit and the filter was an almost continuous layer of fused material. It is easy to visualize how this type of deposit would blind a candle filter. This deposit was analyzed using the SEM with an elemental map, also shown in Figure 64. This map shows that the interface between the deposit and filter is sodium sulfate. This material appears to have formed from condensation of sodium sulfate on the surface of the candle filters. The filter cake that was built up on top of this sodium sulfate layer is a mix of fly ash with sodium and calcium sulfates coating some of the particles and producing necks that are holding the particles together. The SEM photo and map of Figure 65 show this. Discrete ash and albite particles can be seen and identified as discrete particles from the elemental maps of silicon and aluminum. The sulfate layers and necks can be seen in the photograph, with the composition of the coatings shown as sodium and/or calcium based from the elemental map. The map of sulfur (not shown)

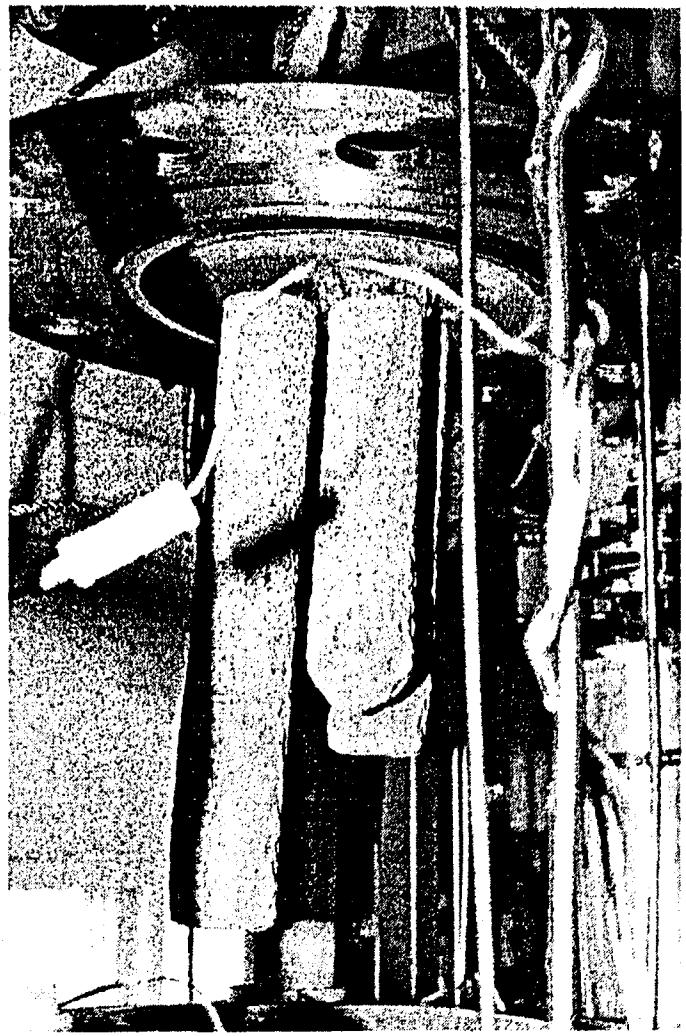

Filters after testing with Belle Ayr coal

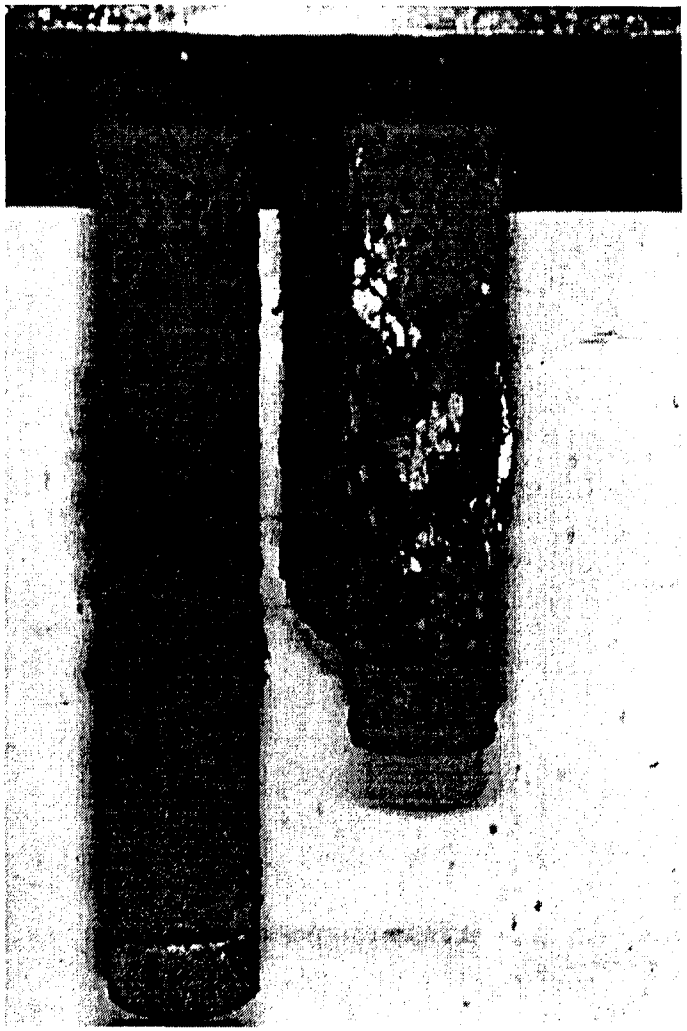

Filters after testing with Beulah Lignite

Figure 63. Photograph of candles after PFBR testing.

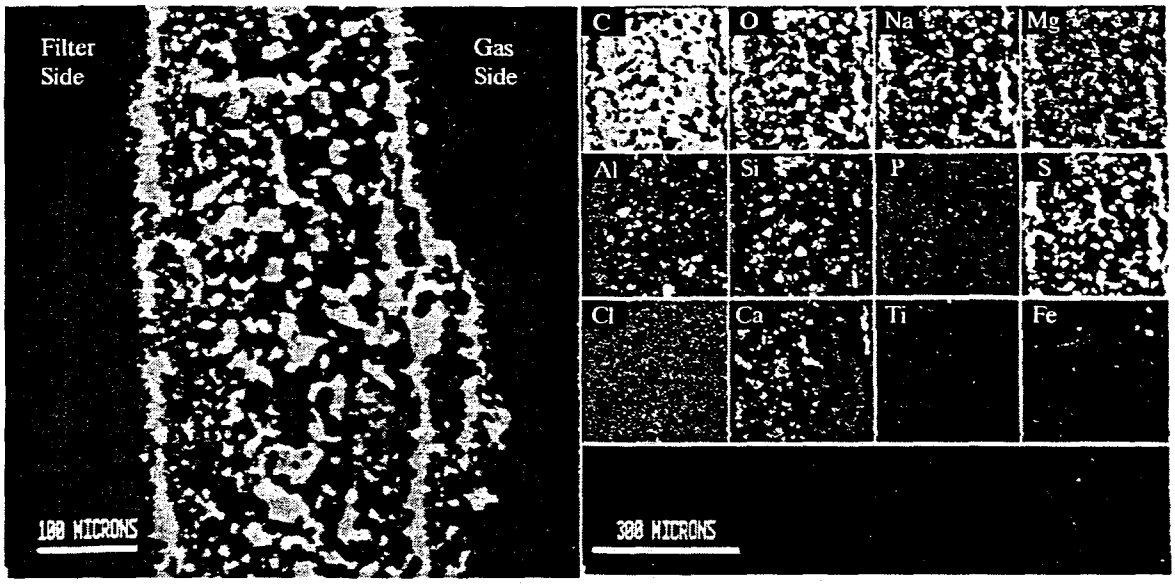

Figure 64. SEM photograph and elemental map of candle deposit from Test 1296

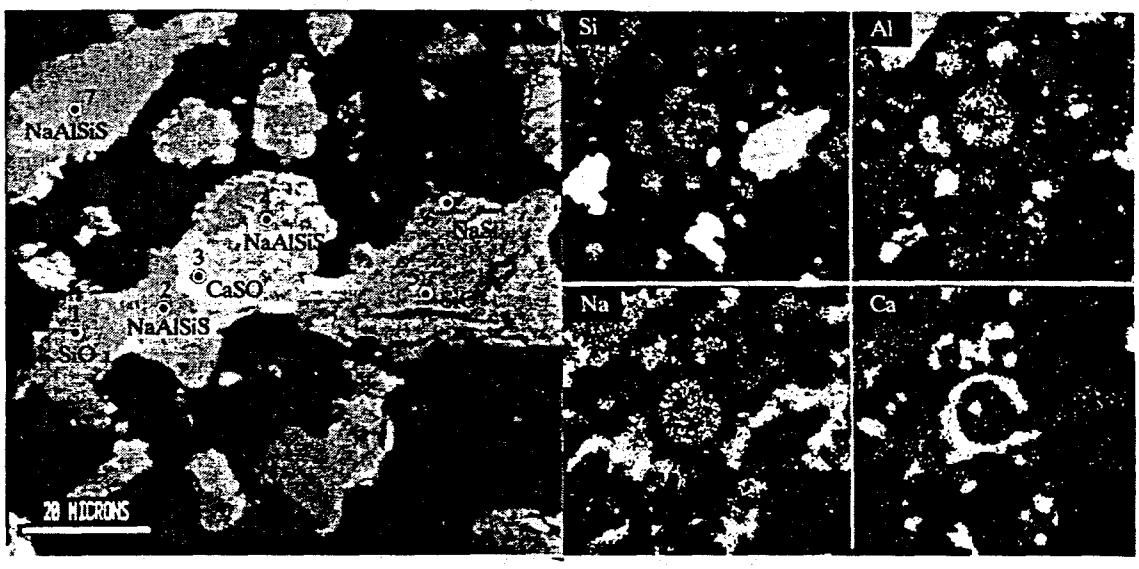

Figure 65. Close-up SEM photograph and elemental map of filter deposit from Test B1-1296

corresponds to the sodium and calcium verifying that this is the material binding the ash particles together. Specific points within this mix were analyzed with the point analysis given in Table 35. The quartz grains can be easily identified at Points 1 and 5. Points 2, 4, and 7 appear to be albite-derived. These particles have interacted with the sodium, calcium, and sulfur. Points 3 and 6 show the calcium and sodium calcium sulfates. A look at the stoichiometry suggests that this material is fully sulfated. It is speculated that they condensed as sulfates on the surface of the candle filters and on the ash particles that were building up the filter cake. This condensation was probably occurring continuously since the beginning of the test, and material had been condensed quickly enough to form a continuous layer on the filters and cause the blinding.

Table 35

Point Analysis of the Filter Deposit from Test B1-1296 and Shown in Figure 65

	1	2	3	4	5	6	7
Elemental Analysis, mole %							
Na	0	8.8	0	8.3	0	20.1	4
Al	0	11.4	5.7	10.1	0	3.9	13.8
Si	36.5	12.3	0	15.5	36.7	0.9	13.7
S	0	7.1	19.4	5.7	0	28.5	6.7
Ca	0.1	2.1	18.8	1.3	0	5.2	0.9
Fe	0.1	0.2	0	0.8	0	0.5	0
O	63.3	58	56.1	58.3	63.3	40.9	61

At the completion of Test BEL-1896, small flakes of filter were noted in the ash material collected from the filter vessel. Apparently, one of the filters installed was starting to lose its integrity, and it was shedding its outside layer. The inside of the filter maintained its integrity, as indicated by the filter's ability to maintain a pressure drop; no visible particulates in an outlet gas sample; and a clean, white filter interior noted at the end of this test campaign. The presence of these pieces of filter provided the opportunity to examine the ash–filter interface. Figure 66 is an SEM photograph of an unexposed section of the filter. An

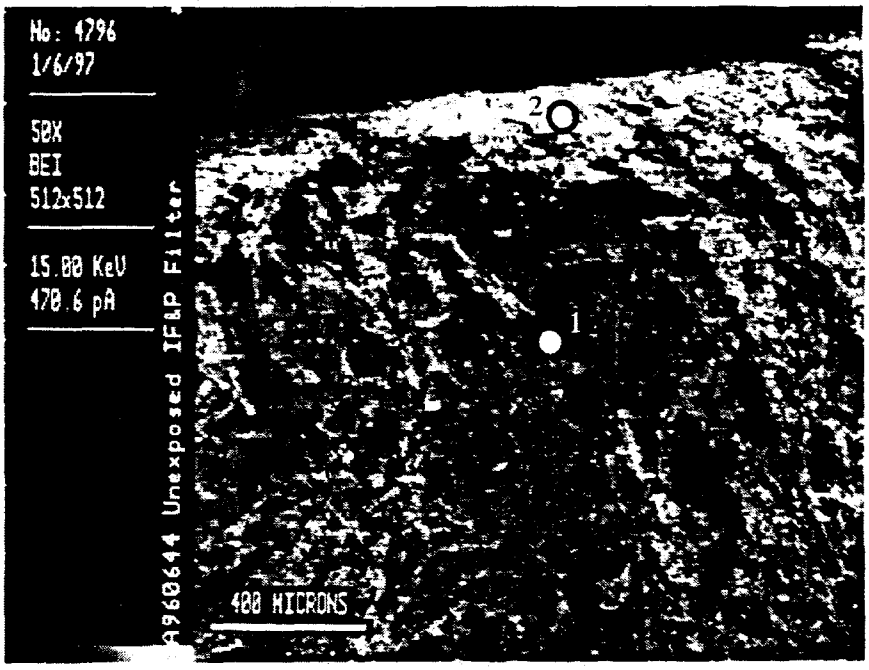

Figure 66. SEM photograph of an unexposed section of the filter that failed during the PFBR tests

analysis of the outer coating and the inner filter material is presented in Table 36. Figure 67 presents SEM photographs of a piece of filter removed after Test 1896. The porous nature of the filter can be seen from these figures. The thin coating of ash is also seen. There was very low pressure drop buildup during this test. A point analysis (Table 36) taken at the edge of the filter yields some interesting results that help explain the failure of the filter. This particulate filter is made up of silica and alumina and is coated with yttrium to provide a protective coating. Point 5 is an analysis of a point within the actual filter, showing the relative composition of silica and aluminum. The other four points taken at the ash–filter interface show high concentrations of yttrium that was utilized for the coating. These analyses indicate that sulfur was attacking the yttrium coating and forming a yttrium sulfate. Calcium and sodium appear to associated with the yttrium coating also and may be partially responsible for the destruction of the protective layer of yttrium.

Figure 68 shows SEM photos of a piece of the same filter removed after Test B1-1996. This piece shows a much thicker ash layer. This is logical, since this fuel resulted in a much higher pressure drop than that observed in the previous test. Again, the porous nature of the filter is seen. The filter cake from this

Table 36

Analysis of Selected Points from an Unexposed Filter and the Filter after Test 1896 and Shown in Figures 66 and 67

	1	2	3	4	5	6	7
Elemental Analysis, mole %							
Na	0.8	0	4.8	0.3	0.4	0	4.5
Al	24.7	1.4	0	0.3	19.7	0	0
Si	20.4	0	0	0	16.1	0	0
S	0	0	18.4	14.8	1.1	15.8	18.6
Ca	0	0	2.5	0	0.1	0	0.1
Y	0	93.2	13.8	22.3	0	15.4	19.3
O	54.8	2.4	60.5	62.4	62.6	68.9	57.6

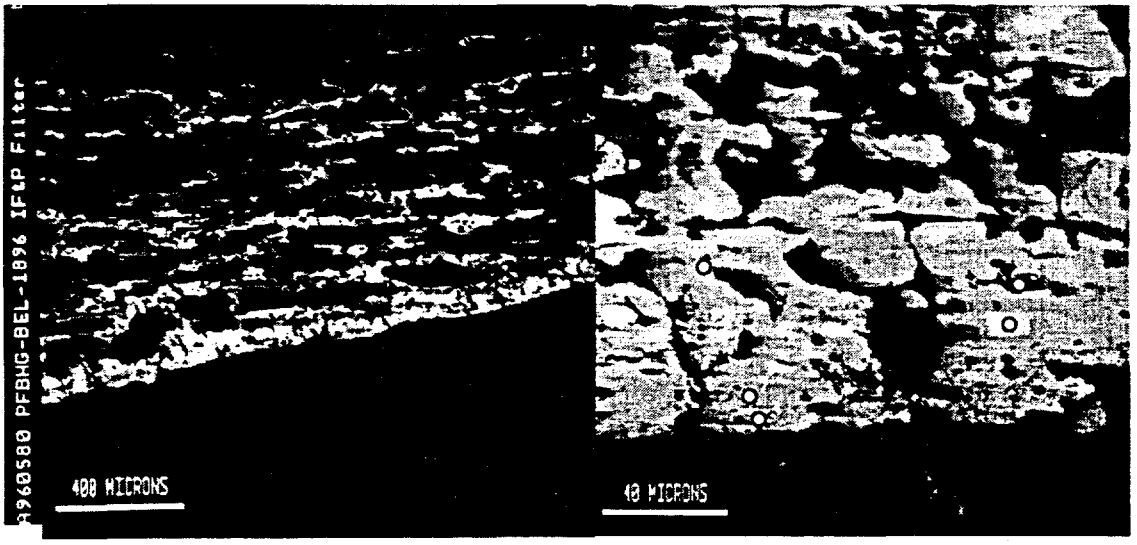

Figure 67. SEM photographs of a section of filter with ash layer taken after Test BEL-1896

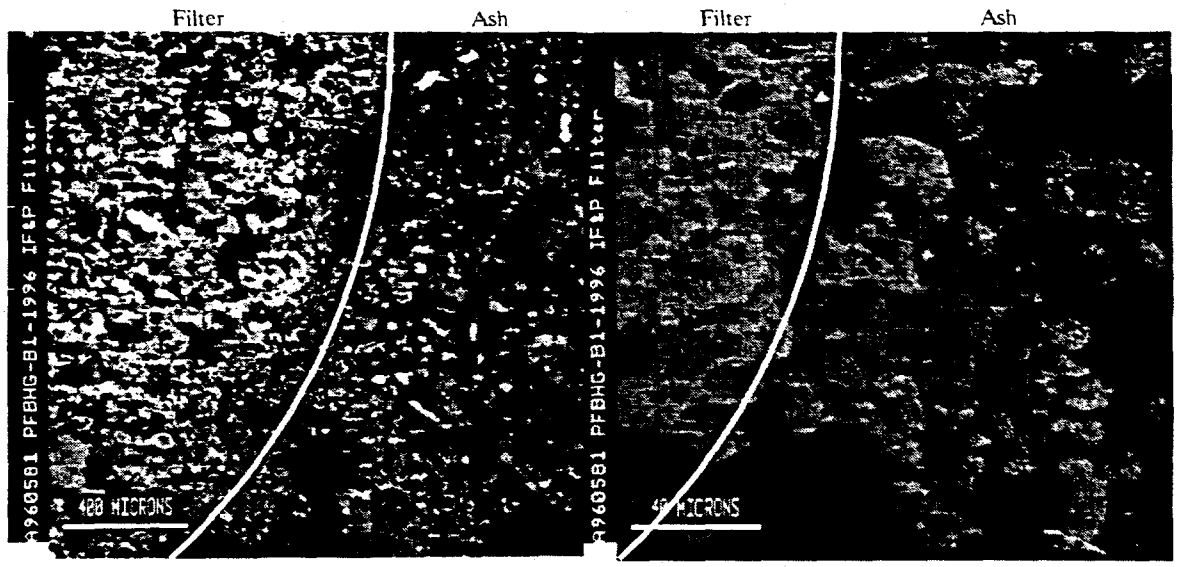

Figure 68. SEM photograph of a piece of filter removed after Test B1-1996

test also appears porous, and there is no evidence of the continuous layer of sodium sulfate noted for the baseline case with the Beulah coal. Elemental maps for a small section of this filter are given in Figure 69. The aluminum and silicon making up this filter are easily seen in these maps. What is interesting to note is the impregnation of sodium, calcium, iron, and sulfur into the interior of this filter. A continued buildup of this sulfated material within the interior of a filter would be expected to eventually cause the filter to fail because of blinding and excessively high pressure drops. The likely source of this material is condensation. A green substance was found in the alkali-sampling probe and the outlet piping of the filter vessel. This condensed material was analyzed and determined to consist mainly of iron and sulfur with some nickel and chromium. The iron, nickel, and chromium may come from the alloys making up the reactor. The only source of the sulfur is the coal. Therefore, in a commercial system, iron may not impregnate the filter as noted during this work, but the sodium, calcium, and sulfur definitely would be available to potentially cause failure of the filter.

Bridging was noted after Test B1-2096 using the Beulah coal and bauxite at an add rate of 3:1. Figure 70 is a photograph of the bridge formed during this run. This material was removed and analyzed with the elemental composition given in Table 37. This material is high in sodium, calcium, and sulfur as

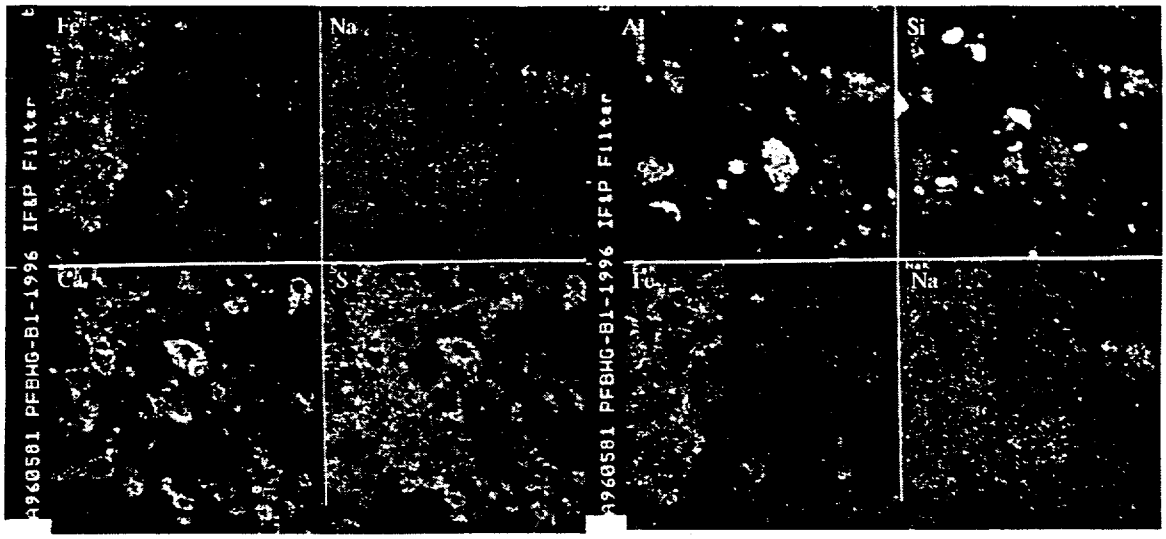

Figure 69. Elemental map of a piece of filter with deposit from Test B1-1996

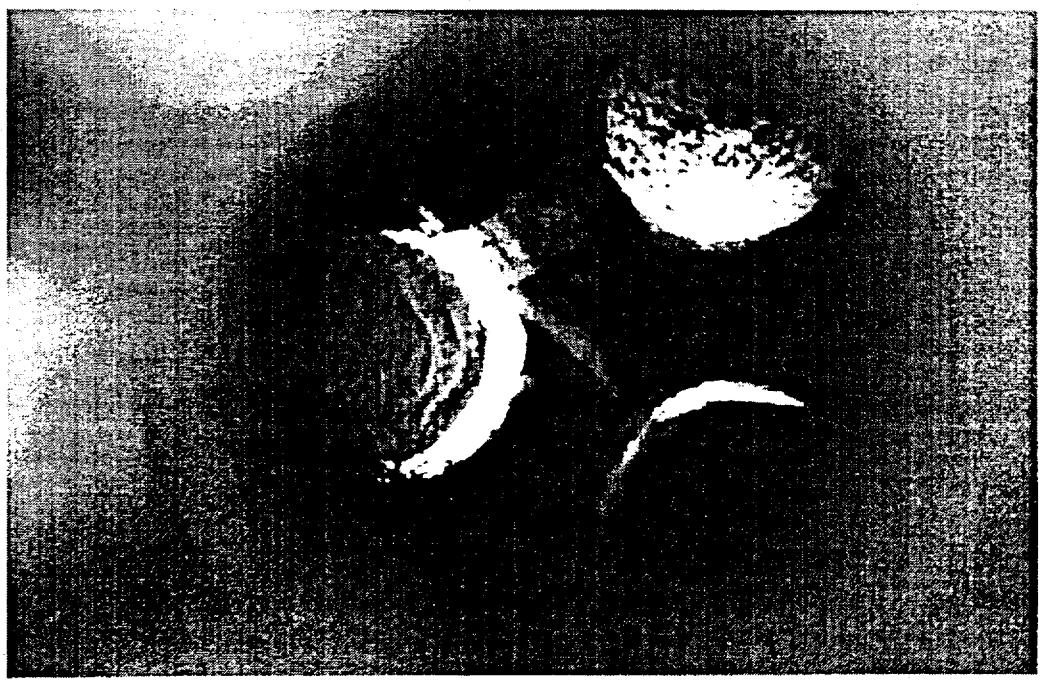

Figure 70. Photograph of an ash bridge formed in the filter vessel during Test B1-2096

Table 37

Analysis of the Bridge and Other Ash Material from Test B1-2096

	Fuel Mix Ash	Cyclone Ash	Filter Vessel Ash	Filter Bridge
Elemental Analysis, mole %, sulfur-free basis				
Si	22.6	29.5	28.6	26.5
Al	13.7	14.7	15.7	11.6
Fe	26.2	9.9	10.5	11.3
Ca	21.8	27.4	26.2	25.6
Mg	9.8	14.5	11.7	9
Na	4.9	3.3	6.2	14.3
S	14.5	6.7	11.2	22.4
Expressed as Percent of Feed				
Si	1	1.31	1.27	1.18
Al	1	1.07	1.14	0.85
Fe	1	0.38	0.4	0.43
Ca	1	1.26	1.21	1.18
Mg	1	1.47	1.19	0.92
Na	1	0.68	1.26	2.91
S	1	0.46	0.77	1.54

seen by the enrichment ratios of 3.74, 1.45, and 1.18, respectively, from the feed material. Its composition is similar to the cyclone ash and filter vessel ash with the exception of the sodium and sulfur. The sodium concentration is almost 2.5 times higher than the ash removed from the filter vessel, and the sulfur is about twice that of the filter vessel ash. Deposits that have been removed from the candles during the cold backpulsing have also been analyzed (see Table 38) and show the same trend: high concentrations of sodium, calcium, and sulfur. This again points to the critical role that sodium plays in bridging and blinding mechanisms. Its role is probably a combination of condensation within the filter vessel due to its slightly lower temperature than the reactor and from fine sodium and calcium sulfate particles that formed as the

result of homogeneous and heterogeneous condensation prior to reaching the filter vessel. These mechanisms of ash formation have been discussed in Section 2.1. Removal of the sodium from the gas using an alkali sorbent is, therefore, a crucial aspect for the operation of the hot-gas filter vessel using fuels with relatively high alkali contents.

Table 38

Elemental Analysis of Candle Deposits from Various PFBR Tests

	B1-1296	BEL-1696	BEL-1896	B1-1996
Expressed as Mole Fraction, sulfur-free basis				
Si	41	28.9	31.3	39.1
Al	10.1	15.8	21.2	12.5
Fe	5.8	9.4	12.1	9.5
Ca	16.4	30.9	22.3	22.6
Mg	5.2	4.3	3	11.3
Na	18.7	7.3	6.9	4.2
S	15.9	24.8	20.7	9.1
Expressed as a Percent of Feed				
Si	1.26	1.07	1.26	0.82
Al	0.62	1.07	1.18	0.71
Fe	0.27	1.28	1.59	0.43
Ca	1.19	0.87	0.62	0.93
Mg	0.78	0.93	0.38	0.61
Na	2.31	2.4	2.27	4.59
S	1.29	1.16	0.97	1.68

CHAPTER 6

CONCLUSIONS AND RECOMMENDATIONS

The work performed as a part of this dissertation consisted of three main efforts: the literature survey, thermogravimetric testing, and bench-scale testing. Conclusions from each of these three efforts are presented. Following the conclusions, recommendations are presented based on the findings of this work.

6.1 Conclusions from Literature Review

- Electricity generating demands are expected to grow at a rate ranging from 1% to 2% per year in the United States, creating a need for over 200 GW of new generating capacity over the next 20 years. PFBC is projected to capture up to 25% of the new market for advanced coal technologies, with much of its market penetration in the area of repowering. Therefore, PFBC is expected to be a major source of new power in the 21st century.
- A number of issues must be resolved for PFBC to capture its projected share of the market. These issues include reducing capital costs and improving reliability and environmental performance. Technical issues related to hot-gas particulate removal, alkali and chlorine control, trace emissions, and the use of advanced cycles must also be resolved for PFBC to reach its full potential.
- The reactions of organically associated mineral matter are of importance in the operating regime of the PFBC. The alkalies, chlorine, and sulfur will vaporize and condense heterogeneously on the surfaces of other ash particles, condense homogeneously to form very fine aerosols, or remain in the vapor phase. These constituents can cause agglomeration and ash deposition, bridging and blinding of hot-gas filters, and corrosion and deposition of turbine blades and, therefore, must be controlled to allow proper operation of the PFBC.

- Measured gas-phase alkali concentrations of 500 to 4000 ppm, depending upon coal type, are high relative to turbine blade specifications of 24 ppb. Therefore, turbine manufacturer specifications for vapor-phase alkali are exceeded even though less than 1% of the total sodium in the fuel is present as vapor. Gas-phase alkali will be higher for those fuels higher in chlorine. The sodium sulfate concentration in the gas phase remains relatively constant because of condensation.
- When sorbents are used in the bubbling fluid bed for adsorption of components from the gas phase, the outlet concentration of the controlled gas will vary inversely with the amount of the sorbent utilized. Therefore, very high sorbent feed rates will be required for high removals of alkali from the gas phase. The capture efficiency will vary directly with sorbent particle size for kinetically limited systems and with the square of particle size for diffusion-controlled systems, assuming there is no elutriation of fines from the bed.
- Aluminosilicates have the most potential for adsorbing alkali under PFBC conditions. Bauxite, kaolinite, and emathlite have been demonstrated to effectively remove alkali vapors when used in packed, moving, and fixed beds.
- Reactions leading to the formation of sodalites have the potential for combined alkali and chlorine removal.
- Alkali metals can be measured either on-line (producing instantaneous alkali values) or off-line (using batch-sampling techniques). The accuracy of on-line methods is still not reliable enough for use in PFBC. Therefore, batch-sampling procedures are recommended even though they only provide average values of alkali metal over a given period of time.

6.2 Conclusions from TGA Screening Tests

- The pTGA at the EERC could not be equipped to feed a continuous and controlled amount of sodium vapor into the pTGA without extensive modifications. Therefore, testing was performed at atmospheric pressure.
- The atmospheric TGA made a good tool for screening sorbents and determining reaction mechanisms. The TGA allows the impact of gas type, temperature, and alkali concentration to

be evaluated and rate data extracted. Samples large enough for analysis by SEM can be generated in the TGA, with these analyses used to help understand the reaction mechanisms.

- Nosean, a sulfur-bearing zeolite, was the favored reaction product when using sorbents for combined alkali, chlorine, and sulfur under the conditions tested. Sodalite, the chlorine-bearing counterpart, would be favored at higher chlorine-to-sulfur ratios and/or higher oxygen partial pressures. Albite reacts with NaCl vapor in an SO_2-bearing gas to capture sodium. The primary mechanism is condensation of Na_2SO_4 on the surface of the albite followed by chemical reaction. The rate of sodium adsorption decreases with decreasing SO_2 concentration in the gas phase because of reductions in the amount of condensed sulfate.
- Albite, quartz, and kaolinite captured sodium by chemical reaction and were kinetically limited. Sodalite and bauxite use physical adsorption as the primary capture method and are diffusion-controlled. After being physically adsorbed, some reaction occurs to permanently bind the alkali.
- The sorbents identified to have commercial potential from the TGA screening tests include albite, kaolinite, and bauxite.

6.3 Conclusions from Bench-Scale Testing

6.3.1 General Observations from the Use of Alkali Sorbents

- The PFBR at the EERC provides a good tool for determining the effectiveness of sorbents in controlling ash chemistry in the PFBC. The impacts of sorbents on bed agglomeration, ash deposition, ash distribution and chemistry, filter blinding and bridging, amount of vapor-phase alkali, and sulfur and nitrogen oxide emissions can be determined.
- The use of bauxite and kaolinite as in-bed sorbents resulted in a decrease in NO_x over the base case without sorbent addition. This may be due to a catalytic effect of the sorbent on the NO_x formation and destruction reactions, similar to those reported for dolomite.

6.3.2 Impacts of Sorbents on Ash Distribution

- Tests with the Beulah coal, which is indicative of fuels with high organically bound sodium, tended to form bed agglomerates, deposit on heat-transfer surfaces, and form loosely bonded

deposits that hung up in the reactor piping. Reduction of the vapor-phase sodium content using bauxite as an in-bed sorbent eliminated these problems.

- All sorbents increased the mass loading of ash to both the cyclone and the filter vessel. The fine sorbents (-30 mesh) caused a disproportional increase in cyclone ash, while the coarse sorbents (-⅛ in.) caused a disproportional increase in filter vessel ash.
- The fine sorbents displayed a higher tendency to form loosely bonded deposits that hung up in the reactor.

6.3.3 Impacts of Sorbents on Vapor-Phase Alkali Concentration

- The vapor-phase alkali concentration is directly related to the quantity of organically bound alkali in the fuel. The vapor-phase sodium concentrations measured from the Beulah, Belle Ayr, and spiked Belle Ayr were approximately proportional to the initial sodium concentration in the starting fuel.
- Kaolinite and bauxite were effective and albite was not effective at reducing the vapor-phase alkali concentration. Kaolinite and bauxite captured similar amounts of sodium at comparable add rates, indicating both were equally effective at alkali capture.
- At a 10:1 sorbent-to-sodium add rate, kaolinite and bauxite reduced the vapor-phase sodium concentration to between 500 and 700 ppb. At a 30:1 add rate, the resulting sodium concentration was 270 ppb. Therefore, it is unlikely that the turbine specifications of 25 to 125 ppb total alkali can be reached using in-bed sorbents.
- In-bed sorbents have a much higher capture efficiency for higher initial alkali concentrations. For example, 90% reduction in sodium from 3600 ppb was realized for tests with the Beulah lignite but only 67% reduction from 1700 ppb using the Belle Ayr coal at the same sorbent add rate.
- The fine sorbents were more effective at reducing vapor-phase sodium concentrations than the coarser sorbents, indicating that the increases in surface area more than offset the shorter bed residence time experienced by the finer sorbents.

6.3.4 Impacts of Sorbents on Ash Deposition

- For fuels high in organically bound sodium (Beulah lignite for example), sodium calcium sulfates form dense, tenacious deposits. When alkali sorbents are utilized to capture sodium, the amount of deposition is reduced, and the form changes to loosely bonded, lightly sintered deposits that could easily be removed by sootblowing.
- The use of albite as a sorbent resulted in no change in deposition characteristics. When kaolinite was used, some reduction in deposition was noted; however, considerable amounts of fines deposited in the reactor piping. Bauxite effectively eliminated deposition at add rates of 10:1 bauxite-to-sodium and greatly reduced the deposition at lower add rates. This indicates that certain sorbents themselves have a propensity for deposition regardless of the vapor-phase sodium concentration, since the kaolinite and bauxite were equally effective at reducing the vapor-phase sodium concentration.
- Bed agglomeration was apparent when utilizing the Beulah lignite. Bauxite effectively controlled agglomeration while albite did not. No evaluation for kaolinite was available from this work.

6.3.5 Impacts of Sorbents on Filter Performance

- The vapor-phase sodium concentration directly impacts bridging of the ceramic filter used for hot-gas particulate removal. Severe filter blinding was noted when the Beulah lignite was used that had a vapor-phase sodium concentration of 3600 ppb. When using the as-received and sodium-spiked Belle Ayr (900 and 1700 ppb vapor-phase sodium), no blinding occurred. Analyses indicate the blinding was caused by condensation and freezing of Na_2SO_4 on the surface of the filter, forming a relatively impervious layer that cannot be removed by backpulsing.
- For the Beulah lignite with a baseline vapor-phase alkali concentration of 3600 ppb, the addition of bauxite at a 10:1 sorbent-to-sodium ratio effectively controlled pressure drop in the filter vessel. An add rate of 3:1 was not effective at controlling pressure drop, while a 5:1 add rate of bauxite was only marginally effective.

- For the sodium-spiked Belle Ayr subbituminous with a baseline vapor-phase alkali concentration of 1700 ppb, the pressure drop in the filter vessel never exceeded 10 in. H_2O for the entire duration of the tests using both the kaolinite and bauxite as sorbents at the 10:1 add rate. The pressure drop without the use of sorbents approached 15 in. H_2O, indicating that the sorbents were effective in reducing filter pressure drop.
- The size of the sorbent utilized had no apparent effect on filter pressure drop at similar add rates.
- Bridging was noted after the test with Beulah coal with bauxite at a 3:1 add rate, which showed only a moderate reduction in vapor-phase sodium concentration. Sodium calcium sulfate was the major component of the bridging material. High sorbent add rates may be effective at eliminating bridges by facilitating high vapor-phase sodium removal, thereby reducing the amount available for homogeneous and heterogeneous condensation to form sticky sulfates.
- During the test program, one of the ceramic filters experienced degradation in the form of spalling from the exterior of the filter. While the filter itself did not fail during the test program, it is speculated that, over time, this spalling would result in a filter failure. The sodium and sulfur appear to be attacking the protective yttrium coating on certain ceramic filters. Yttrium sulfate appears to be the reaction product. The more mobile phases, such as sodium, sulfur, and calcium, were found impregnated deep within the surface of the candle.

The overall conclusion from this work is that in-bed alkali sorbents can effectively reduce the vapor-phase alkali concentration. This reduction is of a magnitude great enough to control ash deposition and agglomeration and filter blinding, but not to a level low enough to meet current turbine manufacturer recommendations for vapor-phase alkali. Bauxite was the best sorbent tested based on its ability to control all of the above-mentioned problems. Kaolinite is less effective because of its tendency to form ash bridges and soft deposits from its fine fraction. Finally, although sodalite and nosean can be formed and result in combined sodium and chlorine or sulfur capture, they do not form at a rate high enough to make them effective sorbents under PFBC conditions.

6.4 Recommendations

Bauxite and kaolinite are both effective in reducing the vapor-phase sodium concentration. The increased loading to the cyclone and filter vessel indicates that they have a limited residence time in the bed. These tests also indicated that the high surface area of finer sorbents enhanced alkali removal. Therefore, alkali capture could be improved by changing the form of the sorbent to keep the high surface area, but increase the size and physical strength to give the sorbent a longer in-bed residence time. This could be accomplished by pelletizing a fine sorbent into pellets of a size approaching the mean size of the bed material. It is recommended that pelletization techniques be examined to determine if they can be utilized for kaolinite and bauxite. If not, other aluminosilicate materials should be researched to find a selection that has a propensity to adsorb alkalies and can form good, strong pellets. Even if these alternative sorbents may not be as effective as bauxite and kaolinite in their raw form, if pelletizing can substantially increase their residence time in the bed, they could prove to be more effective overall.

If bauxite is chosen as a sorbent, consideration should be given to capturing the cyclone and filter ash and recycling the material back to the PFBC. This should improve the overall efficiency of both the bauxite and the dolomite. Pelletizing the sorbent material prior to reintroducing it to the combustor would help stabilize the recycled ash and increase its residence time. The presence of the dolomite in the ash may improve the pelletizing characteristics. This process has been demonstrated for the recycle of fly ash from the circulating FBC of petroleum coke and increased utilization of the limestone from approximately 35% to over 70%.

For future testing on the PFBR to screen alkali sorbents, consideration should be given to sampling from the outlet of the filter vessel in addition to the top of the reactor. This would provide an indication of how much alkali, if any, is captured by the entrained ash and the ash that builds up on the filters. Results of other work have shown that SO_2 is captured on the filters as the flue gas passes through the filter cake. These measurements would be a better indication of the final vapor-phase concentration that the turbine blades would see. Tests at various filter vessel temperatures could provide information to determine how much cooling of flue gas is required to lower the alkali content from the nominal 500 to 700 ppb measured during this work to the 25 to 125 ppb recommended by turbine manufacturers.

Testing should continue to find effective in-bed sorbents for PFBC. If the PFBC is to realize high coal-to-electricity conversion efficiencies, inexpensive methods of capturing alkali are required. In-bed sorbents offer the capability to accomplish this goal.

APPENDIX A

GLOSSARY OF TERMS AND ACRONYMS

Table 39 lists the common acronyms and abbreviations used in this text. Table 40 lists the notations used for equations.

Table 39

Acronyms and Abbreviations

AA	atomic absorption
AASB	analytical alkali sorber bed
ab	albite
AFBC	atmospheric fluidized-bed combustion
ANL	Argonne National Laboratory
APST	alkali and particulate sampling train
atm	atmosphere
B1	Beulah
BEL	Belle Ayr
C	combustion gas
cm	centimeter
COE	cost of electricity
CPC	Combustion Power Company
DOE	Department of Energy
DRI	Data Research Institute
DTA	differential thermal analysis
E	activation energy
EEI	Edison Electric Institute
EERC	Energy & Environmental Research Center
EIA	Energy Information Administration
f	fugacity
FBC	fluidized-bed combustion
FETC	Federal Energy Technology Center
FG	flue gas
FOAM	fiber-optic alkali monitor
FRG	Federal Republic of Germany
FSU	Former Soviet Union
ft	feet
FT-IR	Fourier transform infrared
g	gram
GBF	granular bed filter
GC	gas chromatography
GHSV	gas hourly space velocity
GRI	Gas Research Institute
GW	gigawatt
HAP	hazardous air pollutant
HGCU	hot-gas cleanup
HHV	higher heating value
hr	hour

Continued . . .

Table 39 (continued)

HRSG	heat recovery steam generator
HTHP	high temperature, high pressure
ID	inside diameter
IEA	International Energy Agency
IGCC	integrated gasification combined cycle
in.	inch
ISO	International Organization for Standardization
kg	kilogram
kPa	kilopascals
lb	pound
LHV	lower heating value
LIBS	laser-induced breakdown spectroscopy
LIFS	laser-induced fluorescence spectroscopy
LIPF	laser-induced photo and fluorescence
m	meter
METC	Morgantown Energy Technology Center
mg	milligram
mm	millimeter
MMBtu	million British thermal units
MS	mass spectrometry
MWe	megawatt electricity
NaAc	sodium acetate
ne	nepheline
NERA	National Economic Research Association
NERC	North American Electric Reliability Association
NRC	Nuclear Regulatory Committee, National Research Council
NYU	New York University
OD	outside diameter
OECD	Organization for Economic Cooperation and Development
pc	pulverized coal
PC	personal computer
PFB	pressurized fluidized bed
PFBC	pressurized fluidized-bed combustion(tor)
PFBHG	pressurized fluid-bed reactor with hot gas cleanup
PFBR	pressurized fluid-bed reactor
ppbw	parts per billion by weight
ppm	parts per million
ppmv	parts per million by volume
ppmw	parts per million by weight
psig	pounds per square inch gauge
pTGA	pressurized thermogravimetric analysis
qz	quartz

Continued . . .

Table 39 (continued)

R	universal gas constant
R&D	research and development
scfm	standard cubic feet per minute
Sch	Schedule
sec	second
SEM	scanning electron microscopy
SGV	superficial gas velocity
SRI	Southern Research Institute
STP	standard temperature and pressure
TGA	thermogravimetric analysis
UV	ultraviolet
WEFA	Wharton Economic Forecasting Association
WRI	Western Research Institute
wt	weight

Continued . . .

Table 40

Notation Used for Equations

A	gaseous reactant
A_t	cross-sectional area of the bed
B	solid reactant
C_a	concentration of alkali in the gas phase
C_A^*, C_{Ai}, C_{Ao}, C_{Aex}	concentration of vapor A in gas in equilibrium with solids, in the entering gas stream, at the top of the bed, and at the exit of the FBC
C_{as}, C_s, C_{sf}, C_v	number of active sites, total sites available, used sites, and vacant sites
d_p	particle diameter
D_S	effective diffusivity of gas through the product blanket
e	charge of electron
E(t)	exit age distribution
F_o	feed rate of solids
k, k_a, k_c, k_r	rate constants, for adsorption, for first-order surface reaction, for first-order gas–solid reaction
K	rate of adsorption (change in weight) divided by the alkali concentration
K_a	ratio of the rate constant for adsorption divided by the rate constant for desorption
K_{bc}, K_{ce},	coefficient of gas interchange between bubble and cloud-wake region, and between cloud-wake region and emulsion phase
K_r	rate constant for first-order catalytic reactions
L_m, L_{mf}, L_f	height of fixed bed, bed at minimum fluidizing velocity, and bubbling fluidized bed
M_T	Thiele-type modulus, defined in Eq. 31
N_A, N_B	number of moles of A and B, respectively
Q, Q_i, Q_i^*, Q_o	moisture faction of particles, at initial conditions, at equilibrium conditions, and at exit conditions
R	radius of particle
R_{12}	separation between ions
R_{ads}	rate of adsorption
r_c	radius of unreacted core of reactant solid
t bar	mean residence time of gas or solid in vessel
t	time
T	temperature
u_{mf}, u_o	superficial gas velocity at minimum fluidizing conditions and at operating conditions
V_S	volume of solids in a fluidized-bed reactor
W	mass of solids
$z_{1,2}$	valence of respective ions

APPENDIX B

SUMMARY OF RUN DATA FROM THE PFBR

Data from each of the tests on the bench-scale PFBR are presented in Tables 41 through 51. The tables, generated from the data reduction program for the PFBR, contain the tag number, which refers to the number assigned by the data acquisition system, a description of what each point is, the units, average, and standard deviation. All of the averages are presented with two numbers to the right of the decimal point. This is the convention used in the data reeducation program and does not necessarily reflect the number of significant figures for that point.

Table 41

Run Summary from Test B1-1296

PFBHG-B1-1296 Oct. 16, 1996

Tag	Description	Units	Average	Std. Dev.
AIRFLOW	Air Flow Rate	scfm	12.31	0.402
N FLOW A	Orifice N Flow	scfm	10.44	0.273
FLOW IN	Total Flow In	scfm	22.75	0.607
VELOCITY	Reactor SGV	ft/sec	2.84	0.111
FG SGV	FG SGV	ft/sec	2.93	0.113
EA	Excess Air	%	25.08	3.420
HC13111	Z 1 Heater Temp	°F	1529.09	28.327
HT2PID	Z 1 Heater output	%	50.78	29.818
HC13211	Z 2 Heater Temp	°F	1563.19	27.791
HT3PID	Z 2 Heater output	%	11.24	24.366
HC13311	Z 3 Heater Temp	°F	1525.57	18.941
HT4PID	Z 3 Heater output	%	15.17	28.262
TC11010	Inlet Gas temp	°F	617.61	5.611
TC14001	Reactor Inlet temp	°F	776.49	29.041
TC14002	RT @ 0.25"	°F	1373.86	32.266
TC14003	RT @ 1.75"	°F	1486.26	55.310
TC14004	RT @ 3.50"	°F	1499.86	58.916
TC14005	RT @ 5.00"	°F	1504.79	58.986
TC14006	RT @ 7.00"	°F	1512.45	57.312
TC14007	RT @ 9.00"	°F	1519.92	56.023
TC14008	RT @ 11.00"	°F	1531.91	53.976
TC14009	RT @ 15.00"	°F	1567.42	49.282
TC14010	RT @ 23.00"	°F	1618.24	37.001
TC14011	RT @ 31.00"	°F	1662.03	25.118
TC14012	RT @ 43.25"	°F	1500.59	93.920
TC14028	Cyclone Exit	°F	1509.28	8.241
TC15001	HX FG Out	°F	569.74	12.234
TC18010	Stack Temp	°F	411.16	11.317
ZONE 1	Zone 1 Avg	°F	1504.66	56.975
ZONE 2	Zone 2 Avg	°F	1572.52	46.099
ZONE 3	Zone 3 Avg	°F	1581.31	55.307
T(AVG)	Avg Reactor temp	°F	1540.35	49.556
SO2-A	FG SO_2 - A	ppm	0.00	0.000
SO2-B	FG SO_2 - B	ppm	54.52	70.233
O2-A	FG O_2 - A	%	4.78	0.516
O2-B	FG O_2 - B	%	4.88	0.567
CO2	FG CO_2	%	4.69	0.642
CO	FG CO	ppm	11.24	1.263
NOX	FG NO_x	ppm	68.78	5.174

Continued . . .

Table 41 (continued)

PFBHG-B1-1296				Oct. 16, 1996
Tag	Description	Units	Average	Std. Dev.
N2O	FG N_2O	ppm	23.20	3.600
HC	FG HC	ppm	0.95	0.126
Calculated	S Ret	%	89.52	11.215
S RET	Sulfur Retention	%	94.79	5.579
E-SO2-A	FG SO_2 - A	lb/MMBtu	0.00	0.000
E-NOx	FG NO_x	lb/MMBtu	0.35	0.063
E-N2O	FG N_2O	lb/MMBtu	0.12	0.030
E-CO	FG CO	lb/MMBtu	0.04	0.006
Feedrate	Theor. Coal feed	lb/hr	4.77	0.641
TC16010	HX 1 exit temp	°F	132.13	10.071
TC16020	HX 2 exit temp	°F	0.00	0.000
TC16030	HX 3 exit temp	°F	241.02	5.637
TC12101	Auger HX exit	°F	84.54	5.834
TC17001	Alk. Probe temp	°F	172.87	111.780
TC17002	Alk. Probe temp	°F	313.44	105.985
TC17003	Cyclone Pot temp	°F	114.68	2.575
PT14020	Reactor Static	atm	11.18	0.141
PT14020	Reactor Static	psia	164.26	2.068
PT14021	Reactor dP	in H_2O	19.86	1.294
PT10999	Barometric	psia	14.45	0.011
PT14022	Cyclone dP	in H_2O	7.16	0.465
TC16040	Reactor HX temp	°F	0.00	0.000
R STATIC	Reactor Static	psig	149.81	2.070
HG IN	HG IN	°F	1509.24	8.372
HG TOP	HG TOP	°F	1394.79	2.413
HG UpMid	HG UpMid	°F	1494.77	4.456
HG LoMid	HG LoMid	°F	1519.49	2.244
HG Out	HG Out	°F	966.67	7.151
Htr Top	Htr Top	°F	1031.38	3.492
Htr Btm1	Htr Btm1	°F	971.18	7.095
Htr Btm2	Htr Btm2	°F	946.06	6.053
Fltr1 Up	Fltr1 Up	°F	1188.52	7.937
Fltr1 Lo	Fltr1 Lo	°F	1330.07	11.643
Fltr2 Up	Fltr2 Up	°F	0.00	0.000
Fltr2 Lo	Fltr2 Lo	°F	0.00	0.000
Fltr3 Up	Fltr3 Up	°F	0.00	0.000
Fltr3 Lo	Fltr3 Lo	°F	0.00	0.000
HG Presr	HG Presr	psig	158.11	2.329
HG dP	HG dP	kPa	5.29	5.965
HG dP	HG dP	in H_2O	21.23	23.947
Ash Pot	Ash Pot	°F	109.35	2.231

Table 42

Run Summary from Test B1-1396

PFBHG-B1-1396				Oct. 21, 1996
Tag	Description	Units	Average	Std. Dev.
AIRFLOW	Air Flow Rate	scfm	11.60	1.114
N FLOW A	Orifice N Flow	scfm	11.53	0.951
FLOW IN	Total Flow In	scfm	23.13	1.725
VELOCITY	Reactor SGV	ft/sec	NA	
FG SGV	FG SGV	ft/sec	2.97	0.268
EA	Excess Air	%	23.45	4.774
HC13111	Z 1 Heater Temp	°F	NA	
HT2PID	Z 1 Heater output	%	NA	
HC13211	Z 2 Heater Temp	°F	NA	
HT3PID	Z 2 Heater output	%	NA	
HC13311	Z 3 Heater Temp	°F	NA	
HT4PID	Z 3 Heater output	%	NA	
TC11010	Inlet Gas temp	°F	597.34	9.933
TC14001	Reactor Inlet temp	°F	822.06	36.531
TC14002	RT @ 0.25"	°F	1409.29	90.321
TC14003	RT @ 1.75"	°F	1393.39	128.408
TC14004	RT @ 3.50"	°F	1432.56	135.949
TC14005	RT @ 5.00"	°F	1436.77	135.130
TC14006	RT @ 7.00"	°F	1441.65	137.636
TC14007	RT @ 9.00"	°F	1441.53	138.655
TC14008	RT @ 11.00"	°F	1451.20	143.836
TC14009	RT @ 15.00"	°F	1475.57	150.062
TC14010	RT @ 23.00"	°F	1574.60	119.725
TC14011	RT @ 31.00"	°F	1659.90	92.008
TC14012	RT @ 43.25"	°F	1512.21	84.789
TC14028	Cyclone Exit	°F	1480.54	85.435
TC15001	HX FG Out	°F	488.53	32.463
TC18010	Stack Temp	°F	365.62	14.522
ZONE 1	Zone 1 Avg	°F	1429.18	134.634
ZONE 2	Zone 2 Avg	°F	1500.46	137.552
ZONE 3	Zone 3 Avg	°F	1586.06	87.141
T(AVG)	Avg Reactor temp	°F	1481.94	125.377
SO2-A	FG SO_2 - A	ppm	6.00	3.565
SO2-B	FG SO_2 - B	ppm	75.22	22.733
O2-A	FG O_2 - A	%	4.55	0.702
O2-B	FG O_2 - B	%	4.58	0.613
CO2	FG CO_2	%	3.75	0.837
CO	FG CO	ppm	290.43	247.076

Continued . . .

Table 42 (continued)

PFBHG-B1-1396 Oct. 21, 1996

Tag	Description	Units	Average	Std. Dev.
NOX	FG NO_x	ppm	67.17	6.347
N2O	FG N_2O	ppm	0.10	0.023
HC	FG HC	ppm	2.11	0.426
Calculated	S Ret	%	80.68	3.330
S RET	Sulfur Retention	%	90.37	1.660
E-SO2-A	FG SO_2 - A	lb/MMBtu	0.06	0.044
E-NOx	FG NO_x	lb/MMBtu	0.44	0.085
E-N2O	FG N_2O	lb/MMBtu	0.00	0.000
E-CO	FG CO	lb/MMBtu	1.45	2.012
Feedrate	Theor. Coal feed	lb/hr	3.96	0.951
TC16010	HX 1 exit temp	°F	106.73	5.492
TC16020	HX 2 exit temp	°F	0.00	0.000
TC16030	HX 3 exit temp	°F	174.02	12.279
TC12101	Auger HX exit	°F	74.12	1.506
TC17001	Alk. Probe temp	°F	0.00	0.000
TC17002	Alk. Probe temp	°F	139.77	3.517
TC17003	Cyclone Pot temp	°F	101.51	4.306
PT14020	Reactor Static	atm	10.83	0.538
PT14020	Reactor Static	psia	159.18	7.905
PT14021	Reactor dP	in H_2O	8.00	2.574
PT10999	Barometric	psia	14.46	0.009
PT14022	Cyclone dP	in H_2O	10.20	1.508
TC16040	Reactor HX temp	°F	204.06	16.282
R STATIC	Reactor Static	psig	144.72	7.906
HG IN	HG IN	°F	1480.70	84.945
HG TOP	HG TOP	°F	1320.96	28.708
HG UpMid	HG UpMid	°F	1427.40	34.666
HG LoMid	HG LoMid	°F	1455.42	34.581
HG Out	HG Out	°F	1200.00	0.000
Htr Top	Htr Top	°F	NA	
Htr Btm1	Htr Btm1	°F	NA	
Htr Btm2	Htr Btm2	°F	NA	
Fltr1 Up	Fltr1 Up	°F	NA	
Fltr1 Lo	Fltr1 Lo	°F	NA	
Fltr2 Up	Fltr2 Up	°F	NA	
Fltr2 Lo	Fltr2 Lo	°F	NA	
Fltr3 Up	Fltr3 Up	°F	NA	
Fltr3 Lo	Fltr3 Lo	°F	NA	
HG Presr	HG Presr	psig	143.20	9.002
HG dP	HG dP	kPa	3.41	2.981
HG dP	HG dP	in H_2O	13.71	11.967
Ash Pot	Ash Pot	°F	NA	

Table 43

Run Summary from Test BEL-1496

PFBHG-BEL-1496				Oct. 23, 1996
Tag	Description	Units	Average	Std. Dev.
AIRFLOW	Air Flow Rate	scfm	13.00	0.159
N FLOW A	Orifice N Flow	scfm	10.00	0.109
FLOW IN	Total Flow In	scfm	23.00	0.253
VELOCITY	Reactor SGV	ft/sec	2.90	0.069
FG SGV	FG SGV	ft/sec	3.01	0.071
EA	Excess Air	%	25.53	1.444
HC13111	Z 1 Heater Temp	°F	1546.33	9.517
HT2PID	Z 1 Heater output	%	58.27	23.756
HC13211	Z 2 Heater Temp	°F	1627.54	28.748
HT3PID	Z 2 Heater output	%	3.59	14.938
HC13311	Z 3 Heater Temp	°F	1595.03	30.107
HT4PID	Z 3 Heater output	%	0.00	0.000
TC11010	Inlet Gas temp	°F	609.13	4.721
TC14001	Reactor Inlet temp	°F	800.89	13.134
TC14002	RT @ 0.25"	°F	1403.62	12.448
TC14003	RT @ 1.75"	°F	1505.74	39.162
TC14004	RT @ 3.50"	°F	1517.33	38.127
TC14005	RT @ 5.00"	°F	1524.25	36.139
TC14006	RT @ 7.00"	°F	1535.70	34.449
TC14007	RT @ 9.00"	°F	1543.38	34.277
TC14008	RT @ 11.00"	°F	1560.82	33.653
TC14009	RT @ 15.00"	°F	1595.99	32.949
TC14010	RT @ 23.00"	°F	1677.42	25.834
TC14011	RT @ 31.00"	°F	1767.75	31.513
TC14012	RT @ 43.25"	°F	1618.14	31.233
TC14028	Cyclone Exit	°F	1554.11	25.348
TC15001	HX FG Out	°F	691.93	27.147
TC18010	Stack Temp	°F	481.21	18.188
ZONE 1	Zone 1 Avg	°F	1525.28	35.497
ZONE 2	Zone 2 Avg	°F	1611.41	29.909
ZONE 3	Zone 3 Avg	°F	1692.95	30.002
T(AVG)	Avg Reactor temp	°F	1584.65	29.614
SO2-A	FG SO_2 - A	ppm	0.00	0.000
SO2-B	FG SO_2 - B	ppm	16.18	15.138
O2-A	FG O_2 - A	%	4.84	0.213
O2-B	FG O_2 - B	%	4.88	0.275
CO2	FG CO_2	%	5.01	0.228
CO	FG CO	ppm	0.00	0.000
NOX	FG NO_x	ppm	77.10	7.773
N2O	FG N_2O	ppm	0.53	0.111

Continued . . .

Table 43 (continued)

PFBHG-BEL-1496 Oct. 23, 1996

Tag	Description	Units	Average	Std. Dev.
HC	FG HC	ppm	17.28	1.963
Calculated	S Ret	%	86.24	12.761
S RET	Sulfur Retention	%	86.48	12.540
E-SO2-A	FG SO_2 - A	lb/MMBtu	0.07	0.630
E-NOx	FG NO_x	lb/MMBtu	0.35	0.044
E-N2O	FG N_2O	lb/MMBtu	0.00	0.001
E-CO	FG CO	lb/MMBtu	0.00	0.000
Feedrate	Theor. Coal feed	lb/hr	3.93	0.240
TC16010	HX 1 exit temp	°F	215.14	8.888
TC16020	HX 2 exit temp	°F	0.00	0.000
TC16030	HX 3 exit temp	°F	243.97	20.274
TC12101	Auger HX exit	°F	80.03	1.703
TC17001	Alk. Probe temp	°F	148.07	43.388
TC17002	Alk. Probe temp	°F	303.61	169.241
TC17003	Cyclone Pot temp	°F	97.80	5.765
PT14020	Reactor Static	atm	11.20	0.076
PT14020	Reactor Static	psia	164.54	1.118
PT14021	Reactor dP	in H_2O	10.82	0.444
PT10999	Barometric	psia	14.41	0.026
PT14022	Cyclone dP	in H_2O	7.19	0.235
TC16040	Reactor HX temp	°F	294.25	15.020
R STATIC	Reactor Static	psig	150.13	1.118
HG IN	HG IN	°F	1553.98	25.324
HG TOP	HG TOP	°F	1404.46	27.174
HG UpMid	HG UpMid	°F	1500.75	29.926
HG LoMid	HG LoMid	°F	1525.42	27.266
HG Out	HG Out	°F	936.64	39.536
Htr Top	Htr Top	°F	1004.26	7.971
Htr Btm1	Htr Btm1	°F	795.78	15.027
Htr Btm2	Htr Btm2	°F	950.31	16.841
Fltr1 Up	Fltr1 Up	°F	1147.08	59.297
Fltr1 Lo	Fltr1 Lo	°F	1313.16	31.857
Fltr2 Up	Fltr2 Up	°F	0.00	0.000
Fltr2 Lo	Fltr2 Lo	°F	0.00	0.000
Fltr3 Up	Fltr3 Up	°F	0.00	0.000
Fltr3 Lo	Fltr3 Lo	°F	0.00	0.000
HG Presr	HG Presr	psig	154.39	3.427
HG dP	HG dP	kPa	1.65	0.211
HG dP	HG dP	in H_2O	6.61	0.846
Ash Pot	Ash Pot	°F	88.23	4.648

Table 44

Run Summary from Test BEL-1596

PFBHG-BEL-1596				Oct. 25, 1996
Tag	Description	Units	Average	Std. Dev.
AIRFLOW	Air Flow Rate	scfm	13.00	0.143
N FLOW A	Orifice N Flow	scfm	10.00	0.097
FLOW IN	Total Flow In	scfm	23.00	0.231
VELOCITY	Reactor SGV	ft/sec	2.93	0.056
FG SGV	FG SGV	ft/sec	3.04	0.057
EA	Excess Air	%	23.88	1.854
HC13111	Z 1 Heater Temp	°F	1546.06	30.534
HT2PID	Z 1 Heater output	%	14.81	26.306
HC13211	Z 2 Heater Temp	°F	1615.54	14.931
HT3PID	Z 2 Heater output	%	0.72	7.023
HC13311	Z 3 Heater Temp	°F	1588.52	20.258
HT4PID	Z 3 Heater output	%	0.00	0.000
TC11010	Inlet Gas temp	°F	605.05	4.731
TC14001	Reactor Inlet temp	°F	777.46	22.258
TC14002	RT @ 0.25"	°F	1394.36	34.083
TC14003	RT @ 1.75"	°F	1520.91	38.198
TC14004	RT @ 3.50"	°F	1537.44	30.673
TC14005	RT @ 5.00"	°F	1546.49	26.186
TC14006	RT @ 7.00"	°F	1561.22	23.816
TC14007	RT @ 9.00"	°F	1569.59	23.769
TC14008	RT @ 11.00"	°F	1588.09	23.545
TC14009	RT @ 15.00"	°F	1627.51	24.109
TC14010	RT @ 23.00"	°F	1676.31	18.373
TC14011	RT @ 31.00"	°F	1737.23	21.579
TC14012	RT @ 43.25"	°F	1609.42	35.069
TC14028	Cyclone Exit	°F	1569.16	14.575
TC15001	HX FG Out	°F	724.85	16.844
TC18010	Stack Temp	°F	511.51	14.857
ZONE 1	Zone 1 Avg	°F	1547.13	26.219
ZONE 2	Zone 2 Avg	°F	1630.64	20.966
ZONE 3	Zone 3 Avg	°F	1673.33	26.196
T(AVG)	Avg Reactor temp	°F	1597.42	18.798
SO2-A	FG SO_2 - A	ppm	397.71	246.218
SO2-B	FG SO_2 - B	ppm	470.48	117.513
O2-A	FG O_2 - A	%	4.60	0.280
O2-B	FG O_2 - B	%	4.81	0.309
CO2	FG CO_2	%	4.85	0.266
CO	FG CO	ppm	0.02	0.173

Continued . . .

Table 44 (continued)

PFBHG-BEL-1596 Oct. 25, 1996

Tag	Description	Units	Average	Std. Dev.
NOX	FG NO_x	ppm	172.48	72.095
N2O	FG N_2O	ppm	3.68	7.638
HC	FG HC	ppm	1.02	0.062
Calculated	S Ret	%	57.56	25.440
S RET	Sulfur Retention	%	48.49	12.603
E-SO2-A	FG SO_2 - A	lb/MMBtu	2.53	1.519
E-NOx	FG NO_x	lb/MMBtu	0.81	0.366
E-N2O	FG N_2O	lb/MMBtu	0.02	0.035
E-CO	FG CO	lb/MMBtu	0.00	0.001
Feedrate	Theor. Coal feed	lb/hr	3.80	0.202
TC16010	HX 1 exit temp	°F	221.47	11.227
TC16020	HX 2 exit temp	°F	0.00	0.000
TC16030	HX 3 exit temp	°F	263.47	9.142
TC12101	Auger HX exit	°F	79.40	1.863
TC17001	Alk. Probe temp	°F	42.80	73.808
TC17002	Alk. Probe temp	°F	176.98	18.958
TC17003	Cyclone Pot temp	°F	96.87	1.694
PT14020	Reactor Static	atm	11.19	0.110
PT14020	Reactor Static	psia	164.38	1.610
PT14021	Reactor dP	in H_2O	1.53	2.617
PT10999	Barometric	psia	14.40	0.016
PT14022	Cyclone dP	in H_2O	6.09	1.228
TC16040	Reactor HX temp	°F	310.61	7.385
R STATIC	Reactor Static	psig	149.98	1.610
HG IN	HG IN	°F	1569.09	14.629
HG TOP	HG TOP	°F	1405.99	17.110
HG UpMid	HG UpMid	°F	1509.31	12.156
HG LoMid	HG LoMid	°F	1528.97	12.709
HG Out	HG Out	°F	969.79	24.117
Htr Top	Htr Top	°F	1022.37	8.590
Htr Btm1	Htr Btm1	°F	781.34	20.845
Htr Btm2	Htr Btm2	°F	938.40	12.589
Fltr1 Up	Fltr1 Up	°F	1171.38	34.656
Fltr1 Lo	Fltr1 Lo	°F	1322.79	15.414
Fltr2 Up	Fltr2 Up	°F	0.00	0.000
Fltr2 Lo	Fltr2 Lo	°F	0.00	0.000
Fltr3 Up	Fltr3 Up	°F	0.00	0.000
Fltr3 Lo	Fltr3 Lo	°F	0.00	0.000
HG Presr	HG Presr	psig	152.88	2.354
HG dP	HG dP	kPa	2.16	0.469
HG dP	HG dP	in H_2O	8.66	1.883
Ash Pot	Ash Pot	°F	90.32	2.993

Table 45

Run Summary from Test BEL-1696

PFBHG-BEL-1696				Oct. 28, 1996
Tag	Description	Units	Average	Std. Dev.
AIRFLOW	Air Flow Rate	scfm	12.52	0.237
N FLOW A	Orifice N Flow	scfm	9.95	0.225
FLOW IN	Total Flow In	scfm	22.47	0.290
VELOCITY	Reactor SGV	ft/sec	2.90	0.090
FG SGV	FG SGV	ft/sec	3.03	0.093
EA	Excess Air	%	25.23	2.768
HC13111	Z 1 Heater Temp	°F	1559.17	8.227
HT2PID	Z 1 Heater output	%	3.25	12.938
HC13211	Z 2 Heater Temp	°F	1584.17	15.381
HT3PID	Z 2 Heater output	%	0.13	1.881
HC13311	Z 3 Heater Temp	°F	1550.12	14.748
HT4PID	Z 3 Heater output	%	0.00	0.000
TC11010	Inlet Gas temp	°F	615.75	6.241
TC14001	Reactor Inlet temp	°F	794.60	8.665
TC14002	RT @ 0.25"	°F	1407.74	8.108
TC14003	RT @ 1.75"	°F	1548.51	28.030
TC14004	RT @ 3.50"	°F	1561.12	27.202
TC14005	RT @ 5.00"	°F	1564.11	26.529
TC14006	RT @ 7.00"	°F	1568.22	25.139
TC14007	RT @ 9.00"	°F	1570.38	24.424
TC14008	RT @ 11.00"	°F	1580.27	24.163
TC14009	RT @ 15.00"	°F	1602.05	24.567
TC14010	RT @ 23.00"	°F	1643.27	20.126
TC14011	RT @ 31.00"	°F	1701.66	22.443
TC14012	RT @ 43.25"	°F	1562.28	31.001
TC14028	Cyclone Exit	°F	1537.71	20.103
TC15001	HX FG Out	°F	674.76	44.482
TC18010	Stack Temp	°F	473.85	31.506
ZONE 1	Zone 1 Avg	°F	1562.47	25.606
ZONE 2	Zone 2 Avg	°F	1608.53	22.022
ZONE 3	Zone 3 Avg	°F	1631.97	24.706
T(AVG)	Avg Reactor temp	°F	1590.19	22.050
SO2-A	FG SO_2 - A	ppm	382.20	152.139
SO2-B	FG SO_2 - B	ppm	348.16	197.361
O2-A	FG O_2 - A	%	4.80	0.435
O2-B	FG O_2 - B	%	7.59	6.499
CO2	FG CO_2	%	4.81	0.434
CO	FG CO	ppm	8.14	24.947

Continued . . .

Table 45 (continued)

PFBHG-BEL-1696 Oct. 28, 1996

Tag	Description	Units	Average	Std. Dev.
NOX	FG NO_x	ppm	60.75	9.626
N2O	FG N_2O	ppm	0.10	0.020
HC	FG HC	ppm	13.99	17.028
Calculated	S Ret	%	58.35	14.926
S RET	Sulfur Retention	%	19.83	33.702
E-SO2-A	FG SO_2 - A	lb/MMBtu	2.49	0.891
E-NOx	FG NO_x	lb/MMBtu	0.29	0.049
E-N2O	FG N_2O	lb/MMBtu	0.00	0.000
E-CO	FG CO	lb/MMBtu	0.02	0.071
Feedrate	Theor. Coal feed	lb/hr	3.72	0.340
TC16010	HX 1 exit temp	°F	213.51	20.158
TC16020	HX 2 exit temp	°F	0.00	0.000
TC16030	HX 3 exit temp	°F	241.14	18.407
TC12101	Auger HX exit	°F	77.94	1.153
TC17001	Alk. Probe temp	°F	64.08	123.450
TC17002	Alk. Probe temp	°F	246.43	64.815
TC17003	Cyclone Pot temp	°F	111.56	4.909
PT14020	Reactor Static	atm	11.13	0.242
PT14020	Reactor Static	psia	163.64	3.557
PT14021	Reactor dP	in H_2O	10.60	0.531
PT10999	Barometric	psia	14.54	0.030
PT14022	Cyclone dP	in H_2O	6.87	1.014
TC16040	Reactor HX temp	°F	284.90	25.196
R STATIC	Reactor Static	psig	149.10	3.562
HG IN	HG IN	°F	1537.76	20.076
HG TOP	HG TOP	°F	1359.48	50.022
HG UpMid	HG UpMid	°F	1470.67	38.394
HG LoMid	HG LoMid	°F	1491.65	34.678
HG Out	HG Out	°F	909.64	63.184
Htr Top	Htr Top	°F	988.73	43.039
Htr Btm1	Htr Btm1	°F	780.57	26.597
Htr Btm2	Htr Btm2	°F	942.24	22.264
Fltr1 Up	Fltr1 Up	°F	1103.51	90.671
Fltr1 Lo	Fltr1 Lo	°F	1287.02	42.501
Fltr2 Up	Fltr2 Up	°F	0.00	0.000
Fltr2 Lo	Fltr2 Lo	°F	0.00	0.000
Fltr3 Up	Fltr3 Up	°F	0.00	0.000
Fltr3 Lo	Fltr3 Lo	°F	0.00	0.000
HG Presr	HG Presr	psig	151.96	7.001
HG dP	HG dP	kPa	1.50	0.244
HG dP	HG dP	in H_2O	6.01	0.978
Ash Pot	Ash Pot	°F	94.53	11.204

Table 46

Run Summary from Test BEL-1796

PFBHG-BEL-1796				Oct. 30, 1996
Tag	Description	Units	Average	Std. Dev.
AIRFLOW	Air Flow Rate	scfm	12.74	0.126
N FLOW A	Orifice N Flow	scfm	9.49	0.087
FLOW IN	Total Flow In	scfm	22.24	0.201
VELOCITY	Reactor SGV	ft/sec	2.85	0.073
FG SGV	FG SGV	ft/sec	2.97	0.076
EA	Excess Air	%	25.94	2.636
HC13111	Z 1 Heater Temp	°F	1529.84	21.335
HT2PID	Z 1 Heater output	%	41.46	31.386
HC13211	Z 2 Heater Temp	°F	1612.44	16.288
HT3PID	Z 2 Heater output	%	0.38	4.791
HC13311	Z 3 Heater Temp	°F	1559.01	11.804
HT4PID	Z 3 Heater output	%	0.00	0.000
TC11010	Inlet Gas temp	°F	621.96	5.914
TC14001	Reactor Inlet temp	°F	778.66	19.950
TC14002	RT @ 0.25"	°F	1378.21	21.816
TC14003	RT @ 1.75"	°F	1526.25	38.113
TC14004	RT @ 3.50"	°F	1544.14	33.729
TC14005	RT @ 5.00"	°F	1553.40	28.605
TC14006	RT @ 7.00"	°F	1564.00	26.418
TC14007	RT @ 9.00"	°F	1570.34	26.096
TC14008	RT @ 11.00"	°F	1582.63	25.524
TC14009	RT @ 15.00"	°F	1613.56	25.307
TC14010	RT @ 23.00"	°F	1672.37	20.151
TC14011	RT @ 31.00"	°F	1729.13	24.005
TC14012	RT @ 43.25"	°F	1588.74	33.261
TC14028	Cyclone Exit	°F	1527.51	20.467
TC15001	HX FG Out	°F	544.35	30.796
TC18010	Stack Temp	°F	395.15	17.560
ZONE 1	Zone 1 Avg	°F	1551.63	28.731
ZONE 2	Zone 2 Avg	°F	1622.85	22.585
ZONE 3	Zone 3 Avg	°F	1658.93	26.608
T(AVG)	Avg Reactor temp	°F	1594.46	23.314
SO2-A	FG SO_2 - A	ppm	424.34	119.962
SO2-B	FG SO_2 - B	ppm	440.55	102.654
O2-A	FG O_2 - A	%	4.89	0.419
O2-B	FG O_2 - B	%	5.14	0.511
CO2	FG CO_2	%	5.02	0.427
CO	FG CO	ppm	31.00	17.697

Continued . . .

Table 46 (continued)

PFBHG-BEL-1796 Oct. 30, 1996

Tag	Description	Units	Average	Std. Dev.
NOX	FG NO_x	ppm	40.71	5.802
N2O	FG N_2O	ppm	16.99	2.660
HC	FG HC	ppm	1.31	0.577
Calculated	S Ret	%	55.87	9.432
S RET	Sulfur Retention	%	0.00	0.000
E-SO2-A	FG SO_2 - A	lb/MMBtu	2.63	0.562
E-NOx	FG NO_x	lb/MMBtu	0.19	0.034
E-N2O	FG N_2O	lb/MMBtu	0.07	0.014
E-CO	FG CO	lb/MMBtu	0.08	0.033
Feedrate	Theor. Coal feed	lb/hr	3.84	0.336
TC16010	HX 1 exit temp	°F	106.86	4.437
TC16020	HX 2 exit temp	°F	0.00	0.000
TC16030	HX 3 exit temp	°F	229.10	13.057
TC12101	Auger HX exit	°F	74.61	1.625
TC17001	Alk. Probe temp	°F	35.40	67.848
TC17002	Alk. Probe temp	°F	236.14	42.482
TC17003	Cyclone Pot temp	°F	108.07	3.765
PT14020	Reactor Static	atm	11.17	0.181
PT14020	Reactor Static	psia	164.13	2.667
PT14021	Reactor dP	in H_2O	11.04	0.467
PT10999	Barometric	psia	14.47	0.020
PT14022	Cyclone dP	in H_2O	7.93	0.560
TC16040	Reactor HX temp	°F	231.54	15.683
R STATIC	Reactor Static	psig	149.66	2.669
HG IN	HG IN	°F	1527.55	20.350
HG TOP	HG TOP	°F	1360.53	39.420
HG UpMid	HG UpMid	°F	1482.41	34.952
HG LoMid	HG LoMid	°F	1509.22	31.217
HG Out	HG Out	°F	931.26	55.647
Htr Top	Htr Top	°F	1001.98	28.480
Htr Btm1	Htr Btm1	°F	731.64	46.340
Htr Btm2	Htr Btm2	°F	951.63	17.346
Fltr1 Up	Fltr1 Up	°F	1127.88	83.522
Fltr1 Lo	Fltr1 Lo	°F	1308.03	41.165
Fltr2 Up	Fltr2 Up	°F	0.00	0.000
Fltr2 Lo	Fltr2 Lo	°F	0.00	0.000
Fltr3 Up	Fltr3 Up	°F	0.00	0.000
Fltr3 Lo	Fltr3 Lo	°F	0.00	0.000
HG Presr	HG Presr	psig	155.92	5.260
HG dP	HG dP	kPa	1.09	0.252
HG dP	HG dP	in H_2O	4.39	1.011
Ash Pot	Ash Pot	°F	95.54	8.006

Table 47

Run Summary from Test BEL-1896

PFBHG-BEL-1896				Nov. 1, 1996
Tag	Description	Units	Average	Std. Dev.
AIRFLOW	Air Flow Rate	scfm	12.24	0.227
N FLOW A	Orifice N Flow	scfm	10.26	0.202
FLOW IN	Total Flow In	scfm	22.51	0.252
VELOCITY	Reactor SGV	ft/sec	2.88	0.047
FG SGV	FG SGV	ft/sec	3.00	0.048
EA	Excess Air	%	24.56	2.567
HC13111	Z 1 Heater Temp	°F	1490.30	27.900
HT2PID	Z 1 Heater output	%	34.33	30.580
HC13211	Z 2 Heater Temp	°F	1563.29	13.092
HT3PID	Z 2 Heater output	%	0.75	6.943
HC13311	Z 3 Heater Temp	°F	1512.23	12.385
HT4PID	Z 3 Heater output	%	1.71	8.888
TC11010	Inlet Gas temp	°F	613.17	4.733
TC14001	Reactor Inlet temp	°F	743.19	20.463
TC14002	RT @ 0.25"	°F	1332.10	31.011
TC14003	RT @ 1.75"	°F	1539.44	20.175
TC14004	RT @ 3.50"	°F	1553.22	19.725
TC14005	RT @ 5.00"	°F	1556.10	19.118
TC14006	RT @ 7.00"	°F	1560.79	17.312
TC14007	RT @ 9.00"	°F	1566.44	16.879
TC14008	RT @ 11.00"	°F	1573.72	17.096
TC14009	RT @ 15.00"	°F	1591.55	18.840
TC14010	RT @ 23.00"	°F	1620.03	17.765
TC14011	RT @ 31.00"	°F	1658.23	21.859
TC14012	RT @ 43.25"	°F	1534.73	28.241
TC14028	Cyclone Exit	°F	1484.60	27.186
TC15001	HX FG Out	°F	577.62	17.587
TC18010	Stack Temp	°F	416.12	13.591
ZONE 1	Zone 1 Avg	°F	1555.20	17.490
ZONE 2	Zone 2 Avg	°F	1595.10	17.215
ZONE 3	Zone 3 Avg	°F	1596.48	23.772
T(AVG)	Avg Reactor temp	°F	1575.43	15.144
SO2-A	FG SO_2 - A	ppm	299.16	164.734
SO2-B	FG SO_2 - B	ppm	381.33	138.649
O2-A	FG O_2 - A	%	4.70	0.384
O2-B	FG O_2 - B	%	4.80	0.386
CO2	FG CO_2	%	4.77	0.331
CO	FG CO	ppm	17.90	7.884

Continued . . .

Table 47 (continued)

PFBHG-BEL-1896 Nov. 1, 1996

Tag	Description	Units	Average	Std. Dev.
NOX	FG NO_x	ppm	53.50	6.191
N2O	FG N_2O	ppm	16.54	1.107
HC	FG HC	ppm	0.89	0.050
Calculated	S Ret	%	67.69	16.520
S RET	Sulfur Retention	%	49.98	22.067
E-SO2-A	FG SO_2 - A	lb/MMBtu	1.93	0.986
E-NOx	FG NO_x	lb/MMBtu	0.26	0.036
E-N2O	FG N_2O	lb/MMBtu	0.08	0.008
E-CO	FG CO	lb/MMBtu	0.05	0.022
Feedrate	Theor. Coal feed	lb/hr	3.69	0.259
TC16010	HX 1 exit temp	°F	106.91	3.014
TC16020	HX 2 exit temp	°F	0.00	0.000
TC16030	HX 3 exit temp	°F	233.41	6.998
TC12101	Auger HX exit	°F	76.62	0.690
TC17001	Alk. Probe temp	°F	0.00	0.000
TC17002	Alk. Probe temp	°F	244.59	40.218
TC17003	Cyclone Pot temp	°F	108.18	3.670
PT14020	Reactor Static	atm	11.20	0.082
PT14020	Reactor Static	psia	164.60	1.199
PT14021	Reactor dP	in H_2O	10.91	4.034
PT10999	Barometric	psia	14.58	0.017
PT14022	Cyclone dP	in H_2O	6.49	1.117
TC16040	Reactor HX temp	°F	240.38	8.832
R STATIC	Reactor Static	psig	150.03	1.200
HG IN	HG IN	°F	1484.63	27.191
HG TOP	HG TOP	°F	1360.69	17.684
HG UpMid	HG UpMid	°F	1482.02	17.156
HG LoMid	HG LoMid	°F	1498.71	14.630
HG Out	HG Out	°F	948.14	32.228
Htr Top	Htr Top	°F	1006.86	9.549
Htr Btm1	Htr Btm1	°F	763.74	22.412
Htr Btm2	Htr Btm2	°F	938.45	12.716
Fltr1 Up	Fltr1 Up	°F	1154.27	47.650
Fltr1 Lo	Fltr1 Lo	°F	1303.37	20.861
Fltr2 Up	Fltr2 Up	°F	0.00	0.000
Fltr2 Lo	Fltr2 Lo	°F	0.00	0.000
Fltr3 Up	Fltr3 Up	°F	0.00	0.000
Fltr3 Lo	Fltr3 Lo	°F	0.00	0.000
HG Presr	HG Presr	psig	154.74	3.113
HG dP	HG dP	kPa	1.38	0.157
HG dP	HG dP	in H_2O	5.55	0.632
Ash Pot	Ash Pot	°F	96.06	8.385

Table 48

Run Summary from Test B1-1996

PFBHG-B1-1996				Nov. 5, 1996
Tag	Description	Units	Average	Std. Dev.
AIRFLOW	Air Flow Rate	scfm	12.53	0.212
N FLOW A	Orifice N Flow	scfm	10.52	0.162
FLOW IN	Total Flow In	scfm	23.05	0.359
VELOCITY	Reactor SGV	ft/sec	2.95	0.058
FG SGV	FG SGV	ft/sec	3.08	0.056
EA	Excess Air	%	24.13	2.300
HC13111	Z 1 Heater Temp	°F	1523.77	30.202
HT2PID	Z 1 Heater output	%	36.53	32.056
HC13211	Z 2 Heater Temp	°F	1582.36	17.123
HT3PID	Z 2 Heater output	%	0.00	0.000
HC13311	Z 3 Heater Temp	°F	1501.50	9.945
HT4PID	Z 3 Heater output	%	4.21	12.382
TC11010	Inlet Gas temp	°F	605.85	7.368
TC14001	Reactor Inlet temp	°F	739.17	24.038
TC14002	RT @ 0.25"	°F	1356.82	32.233
TC14003	RT @ 1.75"	°F	1525.76	27.148
TC14004	RT @ 3.50"	°F	1552.92	25.469
TC14005	RT @ 5.00"	°F	1557.24	23.709
TC14006	RT @ 7.00"	°F	1566.65	22.133
TC14007	RT @ 9.00"	°F	1572.96	22.242
TC14008	RT @ 11.00"	°F	1587.58	20.597
TC14009	RT @ 15.00"	°F	1618.68	19.872
TC14010	RT @ 23.00"	°F	1643.57	20.152
TC14011	RT @ 31.00"	°F	1641.58	18.636
TC14012	RT @ 43.25"	°F	1510.54	13.777
TC14028	Cyclone Exit	°F	1470.07	10.152
TC15001	HX FG Out	°F	549.85	11.658
TC18010	Stack Temp	°F	403.42	8.513
ZONE 1	Zone 1 Avg	°F	1555.11	22.402
ZONE 2	Zone 2 Avg	°F	1616.61	19.549
ZONE 3	Zone 3 Avg	°F	1576.06	14.495
T(AVG)	Avg Reactor temp	°F	1577.75	18.051
SO2-A	FG SO_2 - A	ppm	2.03	9.332
SO2-B	FG SO_2 - B	ppm	3.63	8.924
O2-A	FG O_2 - A	%	4.62	0.350
O2-B	FG O_2 - B	%	4.97	0.453
CO2	FG CO_2	%	5.25	0.442
CO	FG CO	ppm	11.02	4.207

Continued . . .

Table 48 (continued)

PFBHG-B1-1996				Nov. 5, 1996
Tag	Description	Units	Average	Std. Dev.
NOX	FG NO_x	ppm	75.87	18.944
N2O	FG N_2O	ppm	0.10	0.019
HC	FG HC	ppm	1.40	0.272
Calculated	S Ret	%	99.61	1.870
S RET	Sulfur Retention	%	99.67	0.835
E-SO2-A	FG SO_2 - A	lb/MMBtu	0.01	0.063
E-NOx	FG NO_x	lb/MMBtu	0.34	0.095
E-N2O	FG N_2O	lb/MMBtu	0.00	0.000
E-CO	FG CO	lb/MMBtu	0.03	0.012
Feedrate	Theor. Coal feed	lb/hr	5.47	0.446
TC16010	HX 1 exit temp	°F	106.58	2.811
TC16020	HX 2 exit temp	°F	0.00	0.000
TC16030	HX 3 exit temp	°F	226.37	7.240
TC12101	Auger HX exit	°F	73.44	0.703
TC17001	Alk. Probe temp	°F	0.08	0.880
TC17002	Alk. Probe temp	°F	261.17	29.982
TC17003	Cyclone Pot temp	°F	106.79	1.968
PT14020	Reactor Static	atm	11.18	0.089
PT14020	Reactor Static	psia	164.35	1.308
PT14021	Reactor dP	in H_2O	16.56	8.964
PT10999	Barometric	psia	14.51	0.014
PT14022	Cyclone dP	in H_2O	4.95	0.329
TC16040	Reactor HX temp	°F	233.42	7.814
R STATIC	Reactor Static	psig	149.84	1.309
HG IN	HG IN	°F	1470.08	10.154
HG TOP	HG TOP	°F	1318.88	27.101
HG UpMid	HG UpMid	°F	1455.51	7.632
HG LoMid	HG LoMid	°F	1466.61	4.752
HG Out	HG Out	°F	928.50	26.889
Htr Top	Htr Top	°F	1004.91	13.055
Htr Btm1	Htr Btm1	°F	762.97	19.482
Htr Btm2	Htr Btm2	°F	950.02	11.237
Fltr1 Up	Fltr1 Up	°F	1115.76	43.434
Fltr1 Lo	Fltr1 Lo	°F	1255.86	13.884
Fltr2 Up	Fltr2 Up	°F	0.00	0.000
Fltr2 Lo	Fltr2 Lo	°F	0.00	0.000
Fltr3 Up	Fltr3 Up	°F	0.00	0.000
Fltr3 Lo	Fltr3 Lo	°F	0.00	0.000
HG Presr	HG Presr	psig	156.37	2.925
HG dP	HG dP	kPa	1.59	0.237
HG dP	HG dP	in H_2O	6.38	0.953
Ash Pot	Ash Pot	°F	124.81	21.792

Table 49

Run Summary from Test B1-2096

PFBHG-B1-2096				Nov. 7, 1996
Tag	Description	Units	Average	Std. Dev.
AIRFLOW	Air Flow Rate	scfm	11.99	0.254
N FLOW A	Orifice N Flow	scfm	10.48	0.232
FLOW IN	Total Flow In	scfm	22.47	0.479
VELOCITY	Reactor SGV	ft/sec	2.85	0.111
FG SGV	FG SGV	ft/sec	2.99	0.115
EA	Excess Air	%	23.89	1.858
HC13111	Z 1 Heater Temp	°F	1507.11	77.315
HT2PID	Z 1 Heater output	%	49.03	29.486
HC13211	Z 2 Heater Temp	°F	1561.86	24.183
HT3PID	Z 2 Heater output	%	7.08	20.863
HC13311	Z 3 Heater Temp	°F	1495.79	12.887
HT4PID	Z 3 Heater output	%	7.03	18.581
TC11010	Inlet Gas temp	°F	614.46	5.913
TC14001	Reactor Inlet temp	°F	763.24	39.033
TC14002	RT @ 0.25"	°F	1355.70	74.167
TC14003	RT @ 1.75"	°F	1513.61	62.320
TC14004	RT @ 3.50"	°F	1527.41	56.107
TC14005	RT @ 5.00"	°F	1532.00	54.994
TC14006	RT @ 7.00"	°F	1540.26	50.614
TC14007	RT @ 9.00"	°F	1548.51	47.501
TC14008	RT @ 11.00"	°F	1562.24	43.657
TC14009	RT @ 15.00"	°F	1596.64	37.893
TC14010	RT @ 23.00"	°F	1623.67	30.776
TC14011	RT @ 31.00"	°F	1633.50	18.139
TC14012	RT @ 43.25"	°F	1513.21	18.808
TC14028	Cyclone Exit	°F	1472.67	5.438
TC15001	HX FG Out	°F	521.99	26.976
TC18010	Stack Temp	°F	385.62	17.229
ZONE 1	Zone 1 Avg	°F	1532.36	53.606
ZONE 2	Zone 2 Avg	°F	1594.18	36.764
ZONE 3	Zone 3 Avg	°F	1573.35	15.277
T(AVG)	Avg Reactor temp	°F	1559.10	38.995
SO2-A	FG SO_2 - A	ppm	0.01	0.163
SO2-B	FG SO_2 - B	ppm	8.23	3.700
O2-A	FG O_2 - A	%	4.61	0.294
O2-B	FG O_2 - B	%	4.65	0.347
CO2	FG CO_2	%	4.86	0.341
CO	FG CO	ppm	15.70	1.657

Continued . . .

Table 49 (continued)

PFBHG-B1-2096				Nov. 7, 1996
Tag	Description	Units	Average	Std. Dev.
NOX	FG NO_x	ppm	58.47	8.476
N2O	FG N_2O	ppm	0.10	0.019
HC	FG HC	ppm	0.00	0.000
Calculated	S Ret	%	98.35	0.737
S RET	Sulfur Retention	%	99.18	0.367
E-SO2-A	FG SO_2 - A	lb/MMBtu	0.00	0.001
E-NOx	FG NO_x	lb/MMBtu	0.29	0.042
E-N2O	FG N_2O	lb/MMBtu	0.00	0.000
E-CO	FG CO	lb/MMBtu	0.05	0.005
Feedrate	Theor. Coal feed	lb/hr	4.97	0.358
TC16010	HX 1 exit temp	°F	102.07	2.008
TC16020	HX 2 exit temp	°F	0.00	0.000
TC16030	HX 3 exit temp	°F	218.78	11.536
TC12101	Auger HX exit	°F	72.79	2.023
TC17001	Alk. Probe temp	°F	909.80	1069.379
TC17002	Alk. Probe temp	°F	263.36	32.310
TC17003	Cyclone Pot temp	°F	107.96	3.662
PT14020	Reactor Static	atm	11.18	0.100
PT14020	Reactor Static	psia	164.30	1.468
PT14021	Reactor dP	in H_2O	20.85	2.366
PT10999	Barometric	psia	14.41	0.016
PT14022	Cyclone dP	in H_2O	6.99	0.864
TC16040	Reactor HX temp	°F	222.64	15.737
R STATIC	Reactor Static	psig	149.90	1.469
HG IN	HG IN	°F	1472.57	5.492
HG TOP	HG TOP	°F	1357.66	34.928
HG UpMid	HG UpMid	°F	1463.57	27.714
HG LoMid	HG LoMid	°F	1480.34	24.680
HG Out	HG Out	°F	905.85	47.622
Htr Top	Htr Top	°F	991.62	40.291
Htr Btm1	Htr Btm1	°F	838.97	17.120
Htr Btm2	Htr Btm2	°F	940.95	19.107
Fltr1 Up	Fltr1 Up	°F	1088.93	70.792
Fltr1 Lo	Fltr1 Lo	°F	1253.22	41.849
Fltr2 Up	Fltr2 Up	°F	0.00	0.000
Fltr2 Lo	Fltr2 Lo	°F	0.00	0.000
Fltr3 Up	Fltr3 Up	°F	0.00	0.000
Fltr3 Lo	Fltr3 Lo	°F	0.00	0.000
HG Presr	HG Presr	psig	154.01	4.011
HG dP	HG dP	kPa	2.98	1.007
HG dP	HG dP	in H_2O	11.95	4.043
Ash Pot	Ash Pot	°F	93.92	11.157

Table 50

Run Summary from Test B1-2196

PFBH-B1-2196				Nov. 27, 1996
Tag	Description	Units	Average	Std. Dev.
AIRFLOW	Air Flow Rate	scfm	12.80	0.246
N FLOW A	Orifice N Flow	scfm	10.18	0.206
FLOW IN	Total Flow In	scfm	22.98	0.395
VELOCITY	Reactor SGV	ft/sec	2.91	0.109
FG SGV	FG SGV	ft/sec	3.04	0.113
EA	Excess Air	%	26.07	3.633
HC13111	Z 1 Heater Temp	°F	1518.29	39.796
HT2PID	Z 1 Heater output	%	43.13	34.418
HC13211	Z 2 Heater Temp	°F	1604.38	25.872
HT3PID	Z 2 Heater output	%	0.63	6.374
HC13311	Z 3 Heater Temp	°F	1506.45	27.532
HT4PID	Z 3 Heater output	%	4.27	15.190
TC11010	Inlet Gas temp	°F	605.54	10.162
TC14001	Reactor Inlet temp	°F	747.12	30.888
TC14002	RT @ 0.25"	°F	1343.93	42.699
TC14003	RT @ 1.75"	°F	1513.50	56.817
TC14004	RT @ 3.50"	°F	1535.23	57.557
TC14005	RT @ 5.00"	°F	1536.64	59.343
TC14006	RT @ 7.00"	°F	1543.62	59.744
TC14007	RT @ 9.00"	°F	1552.32	59.332
TC14008	RT @ 11.00"	°F	1567.84	55.177
TC14009	RT @ 15.00"	°F	1623.65	38.887
TC14010	RT @ 23.00"	°F	1666.64	35.964
TC14011	RT @ 31.00"	°F	1670.81	32.930
TC14012	RT @ 43.25"	°F	1530.75	41.667
TC14028	Cyclone Exit	°F	1348.70	14.774
TC15001	HX FG Out	°F	672.97	51.605
TC18010	Stack Temp	°F	469.26	38.943
ZONE 1	Zone 1 Avg	°F	1536.26	57.802
ZONE 2	Zone 2 Avg	°F	1619.38	28.923
ZONE 3	Zone 3 Avg	°F	1600.78	35.541
T(AVG)	Avg Reactor temp	°F	1574.10	38.575
SO2-A	FG SO_2 - A	ppm	15.59	36.633
SO2-B	FG SO_2 - B	ppm	25.33	141.800
O2-A	FG O_2 - A	%	4.90	0.485
O2-B	FG O_2 - B	%	4.87	0.477
CO2	FG CO_2	%	5.02	0.622
CO	FG CO	ppm	25.17	175.529

Continued . . .

Table 50 (continued)

PFBH-B1-2196 Nov. 27, 1996

Tag	Description	Units	Average	Std. Dev.
NOX	FG NO_x	ppm	107.99	22.844
N2O	FG N_2O	ppm	0.10	0.016
HC	FG HC	ppm	6.52	15.232
Calculated	S Ret	%	95.00	23.768
S RET	Sulfur Retention	%	97.55	14.025
E-SO2-A	FG SO_2 - A	lb/MMBtu	0.16	0.742
E-NOx	FG NO_x	lb/MMBtu	0.52	0.141
E-N2O	FG N_2O	lb/MMBtu	0.00	0.000
E-CO	FG CO	lb/MMBtu	0.17	1.240
Feedrate	Theor. Coal feed	lb/hr	5.23	0.645
TC16010	HX 1 exit temp	°F	227.28	44.813
TC16020	HX 2 exit temp	°F	0.00	0.000
TC16030	HX 3 exit temp	°F	245.87	25.388
TC12101	Auger HX exit	°F	71.36	1.346
TC17001	Alk. Probe temp	°F	0.00	0.000
TC17002	Alk. Probe temp	°F	235.30	22.433
TC17003	Cyclone Pot temp	°F	113.22	15.695
PT14020	Reactor Static	atm	11.22	0.110
PT14020	Reactor Static	psia	164.90	1.622
PT14021	Reactor dP	in H_2O	15.70	3.849
PT10999	Barometric	psia	14.69	0.022
PT14022	Cyclone dP	in H_2O	5.26	1.928
TC16040	Reactor HX temp	°F	284.53	34.971
R STATIC	Reactor Static	psig	150.21	1.626
HG IN	HG IN	°F	1348.78	14.741
HG TOP	HG TOP	°F	133.61	6.892
HG UpMid	HG UpMid	°F	1452.84	37.797
HG LoMid	HG LoMid	°F	1471.39	33.226
HG Out	HG Out	°F	895.72	62.223
Htr Top	Htr Top	°F	977.40	45.386
Htr Btm1	Htr Btm1	°F	856.57	34.117
Htr Btm2	Htr Btm2	°F	968.09	26.554
Fltr1 Up	Fltr1 Up	°F	1065.55	82.267
Fltr1 Lo	Fltr1 Lo	°F	1256.80	42.813
Fltr2 Up	Fltr2 Up	°F	0.00	0.000
Fltr2 Lo	Fltr2 Lo	°F	0.00	0.000
Fltr3 Up	Fltr3 Up	°F	0.00	0.000
Fltr3 Lo	Fltr3 Lo	°F	0.00	0.000
HG Presr	HG Presr	psig	153.39	2.970
HG dP	HG dP	kPa	3.18	1.592
HG dP	HG dP	in H_2O	12.76	6.393
Ash Pot	Ash Pot	°F	116.98	34.511

Table 51

Run Summary from Test B1-2296

PFBHG-B1-2296				Dec. 4, 5, 1996
Tag	Description	Units	Average	Std. Dev.
AIRFLOW	Air Flow Rate	scfm	12.25	0.389
N FLOW A	Orifice N Flow	scfm	10.22	0.337
FLOW IN	Total Flow In	scfm	22.48	0.715
VELOCITY	Reactor SGV	ft/sec	2.88	0.122
FG SGV	FG SGV	ft/sec	3.02	0.124
EA	Excess Air	%	25.15	1.469
HC13111	Z 1 Heater Temp	°F	1528.35	31.540
HT2PID	Z 1 Heater output	%	33.48	32.390
HC13211	Z 2 Heater Temp	°F	1582.19	14.226
HT3PID	Z 2 Heater output	%	0.51	5.526
HC13311	Z 3 Heater Temp	°F	1501.02	12.695
HT4PID	Z 3 Heater output	%	2.18	10.799
TC11010	Inlet Gas temp	°F	615.13	7.029
TC14001	Reactor Inlet temp	°F	773.39	29.255
TC14002	RT @ 0.25"	°F	1355.07	30.682
TC14003	RT @ 1.75"	°F	1534.01	39.322
TC14004	RT @ 3.50"	°F	1551.62	33.000
TC14005	RT @ 5.00"	°F	1555.58	31.809
TC14006	RT @ 7.00"	°F	1563.07	28.149
TC14007	RT @ 9.00"	°F	1568.74	25.429
TC14008	RT @ 11.00"	°F	1582.89	23.064
TC14009	RT @ 15.00"	°F	1616.40	23.583
TC14010	RT @ 23.00"	°F	1640.11	20.156
TC14011	RT @ 31.00"	°F	1647.78	16.692
TC14012	RT @ 43.25"	°F	1520.66	18.825
TC14028	Cyclone Exit	°F	1331.58	12.498
TC15001	HX FG Out	°F	535.39	46.588
TC18010	Stack Temp	°F	396.37	30.188
ZONE 1	Zone 1 Avg	°F	1554.61	30.007
ZONE 2	Zone 2 Avg	°F	1613.13	21.278
ZONE 3	Zone 3 Avg	°F	1584.22	15.817
T(AVG)	Avg Reactor temp	°F	1578.09	21.133
SO2-A	FG SO_2 - A	ppm	1.16	12.789
SO2-B	FG SO_2 - B	ppm	25.01	20.986
O2-A	FG O_2 - A	%	4.78	0.223
O2-B	FG O_2 - B	%	5.10	0.273
CO2	FG CO_2	%	5.07	0.274
CO	FG CO	ppm	4.59	2.367
NOX	FG NO_x	ppm	60.86	9.956
N2O	FG N_2O	ppm	0.11	0.021

Continued . . .

Table 51 (continued)

PFBHG-B1-2296				Dec. 4, 5, 1996
Tag	Description	Units	Average	Std. Dev.
HC	FG HC	ppm	1.05	0.392
Calculated	S Ret	%	99.81	2.053
S RET	Sulfur Retention	%	97.64	1.759
E-SO2-A	FG SO_2 - A	lb/MMBtu	0.01	0.069
E-NOx	FG NO_x	lb/MMBtu	0.28	0.043
E-N2O	FG N_2O	lb/MMBtu	0.00	0.000
E-CO	FG CO	lb/MMBtu	0.01	0.007
Feedrate	Theor. Coal feed	lb/hr	5.19	0.325
TC16010	HX 1 exit temp	°F	108.57	7.266
TC16020	HX 2 exit temp	°F	0.00	0.000
TC16030	HX 3 exit temp	°F	218.82	22.093
TC12101	Auger HX exit	°F	71.62	1.151
TC17001	Alk. Probe temp	°F	150.17	150.149
TC17002	Alk. Probe temp	°F	220.00	59.997
TC17003	Cyclone Pot temp	°F	120.71	10.565
PT14020	Reactor Static	atm	11.19	0.135
PT14020	Reactor Static	psia	164.42	1.988
PT14021	Reactor dP	in H_2O	21.76	1.795
PT10999	Barometric	psia	14.35	0.095
PT14022	Cyclone dP	in H_2O	6.78	0.732
TC16040	Reactor HX temp	°F	228.36	24.083
R STATIC	Reactor Static	psig	150.07	1.984
HG IN	HG IN	°F	1331.64	12.483
HG TOP	HG TOP	°F	1302.67	68.353
HG UpMid	HG UpMid	°F	1445.06	45.718
HG LoMid	HG LoMid	°F	1467.80	40.399
HG Out	HG Out	°F	916.93	71.266
Htr Top	Htr Top	°F	992.65	51.199
Htr Btm1	Htr Btm1	°F	988.01	23.019
Htr Btm2	Htr Btm2	°F	959.70	23.186
Fltr1 Up	Fltr1 Up	°F	1103.77	96.947
Fltr1 Lo	Fltr1 Lo	°F	1262.39	62.565
Fltr2 Up	Fltr2 Up	°F	0.00	0.000
Fltr2 Lo	Fltr2 Lo	°F	0.00	0.000
Fltr3 Up	Fltr3 Up	°F	0.00	0.000
Fltr3 Lo	Fltr3 Lo	°F	0.00	0.000
HG Presr	HG Presr	psig	157.50	5.034
HG dP	HG dP	kPa	5.02	2.167
HG dP	HG dP	in H_2O	20.15	8.700
Ash Pot	Ash Pot	°F	100.31	9.869

APPENDIX C

THERMOGRAMS FROM SORBENT-SCREENING TESTS

Thermograms from the TGA testing used to investigate the sodalite reactions and to screen the conventional sorbents are presented in this appendix. Table 52 shows the test conditions for each test. The thermograms are presented as Figures 71 through 87.

Table 52

Matrix for TGA Testing

			Carrier Gas Used at Each Temperature					
Test	Sorbent	NaCl	700°C	733°C	766°C	800°C	800°C	850°C
1	Albite	Yes	-	-	-	-	-	N_2
2	Albite	No	-	-	-	-	-	N_2
3	Albite	Yes	C[1]	C	C	C	N_2	-
4	Albite	No	C	C	C	C	N_2	-
5	Albite + quartz	Yes	C	C	C	C	N_2	-
6	Albite + quartz	Yes	N_2	N_2	N_2	N_2	-	-
7	Sodalite	Yes	C	C	C	C	N_2	-
8	Sodalite	No	C	C	C	C	N_2	-
9	Sodalite	Yes	N_2	N_2		N_2	C	-
10	Nepheline	Yes	C	C	C	C	N_2	-
11	$AlO(OH)_3$	Yes	C	C	C	C	N_2	-
12	Kaolinite	Yes	C	C	C	C	N_2	-
13	Bauxite	Yes	N_2	N_2	N_2	N_2	C	-
14	Bauxite	Yes	-	-	-	-	C	-
15	Zeolite	Yes	N_2	N_2	N_2	N_2	C	-
16	Sodalite	No	N_2	N_2	N_2	N_2	C	-
17	Albite	Yes	C	C	C	C	N_2	

[1] Combustion gas

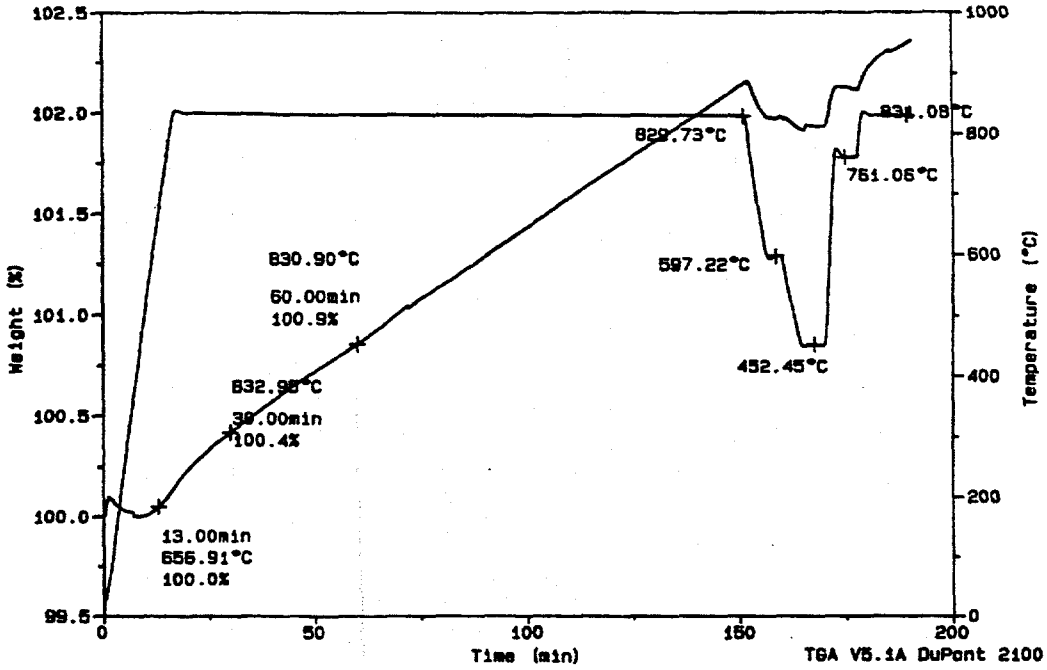

Figure 71. Thermogram from Test 1, albite with NaCl and nitrogen as the initial gas

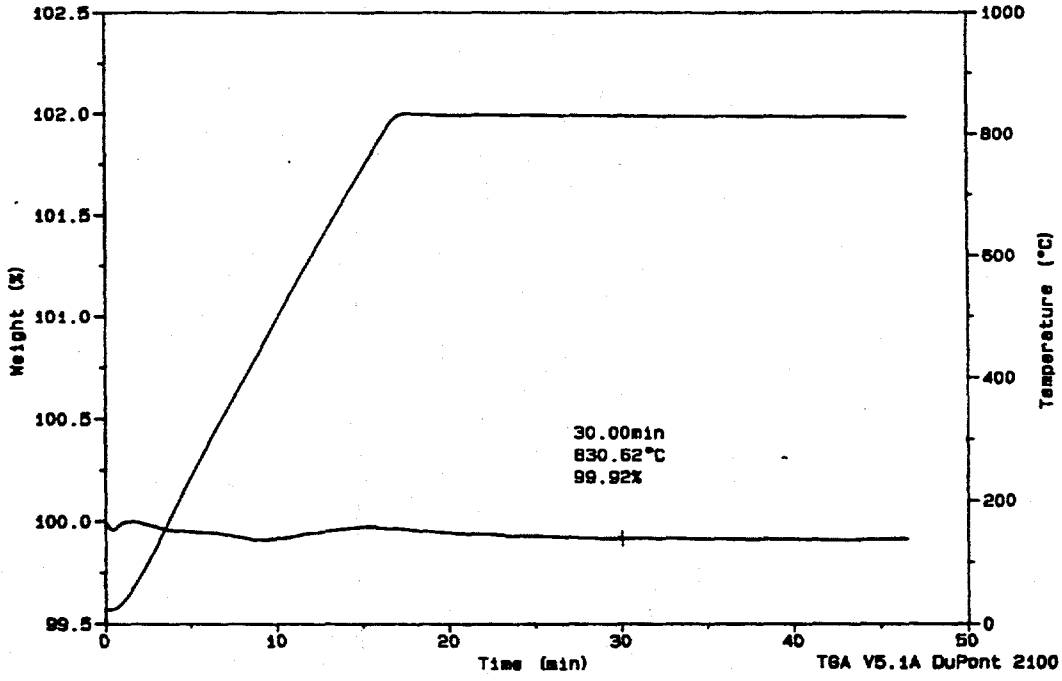

Figure 72. Thermogram from Test 2, albite without NaCl and nitrogen as the initial gas

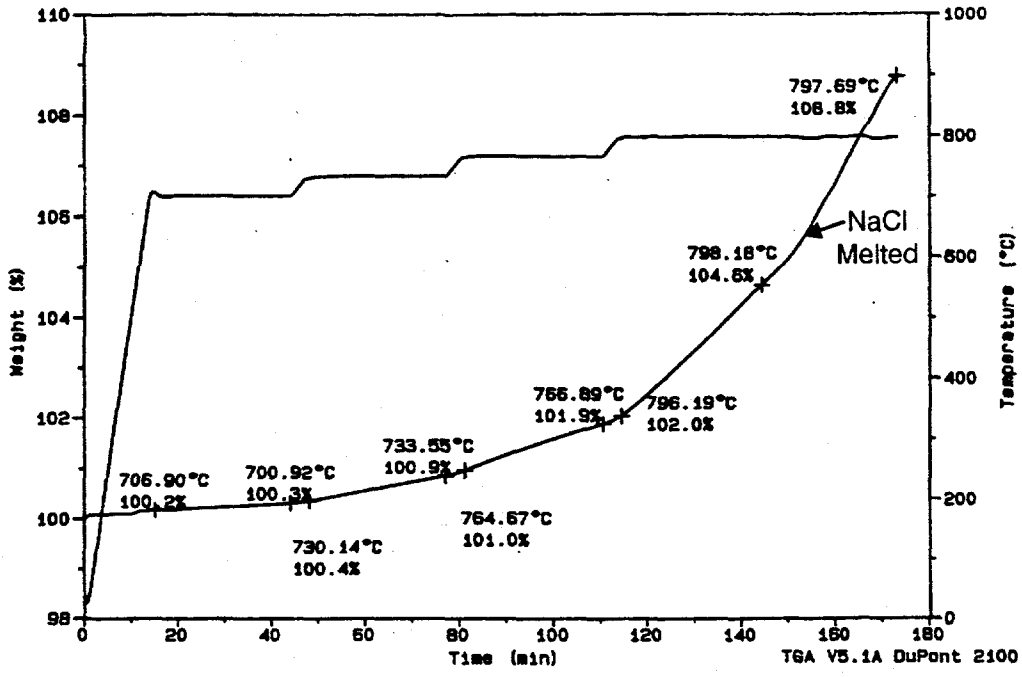

Figure 73. Thermogram from Test 3, albite with NaCl and combustion gas as the initial gas

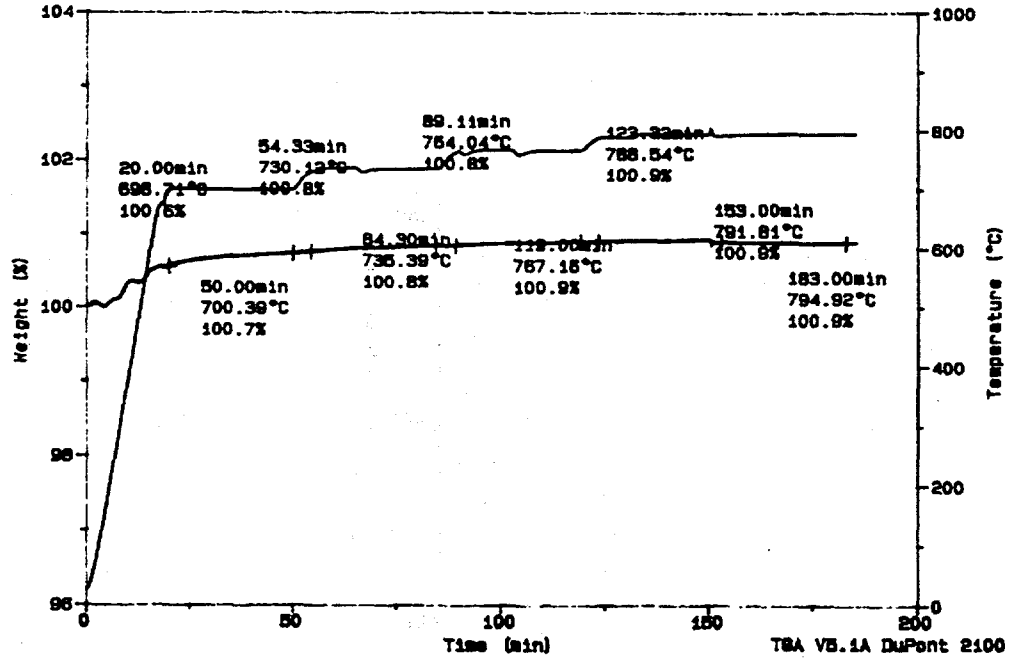

Figure 74. Thermogram from Test 4, albite without NaCl and combustion gas as the initial gas

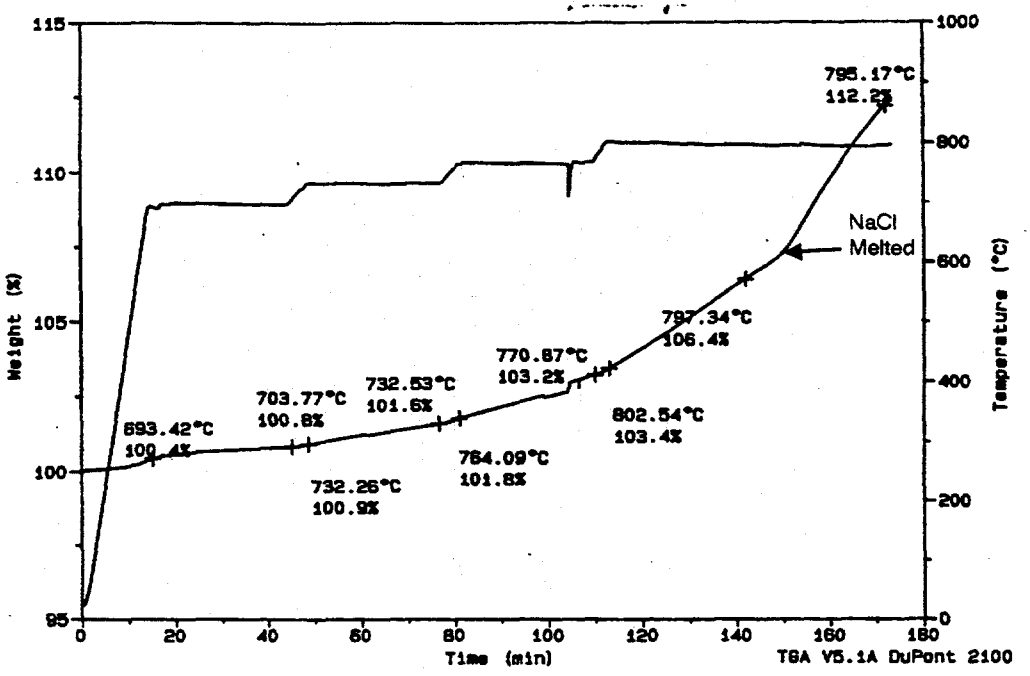

Figure 75. Thermogram from Test 5, albite and quartz with NaCl and combustion gas as the initial gas

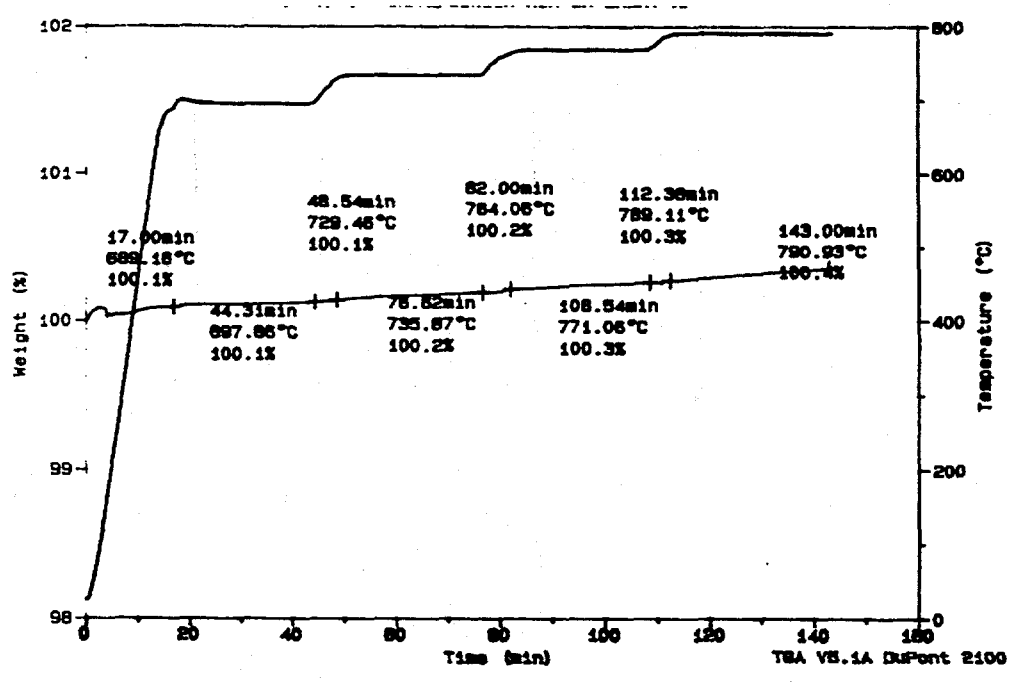

Figure 76. Thermogram from Test 6, albite and quartz with NaCl and nitrogen as the initial gas

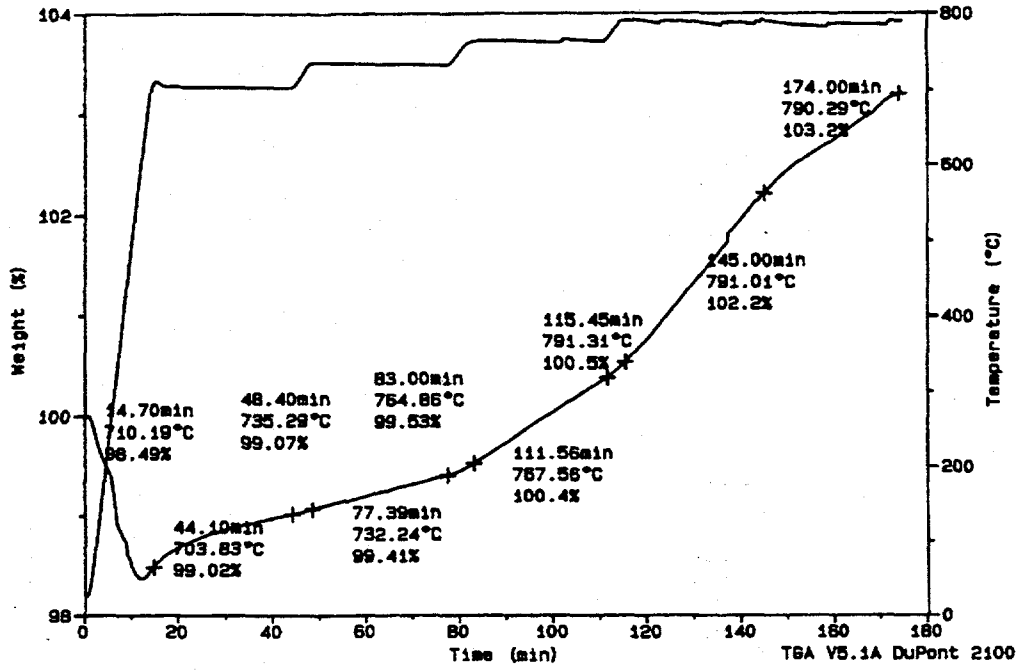

Figure 77. Thermogram from Test 7, sodalite with NaCl and combustion gas as the initial gas

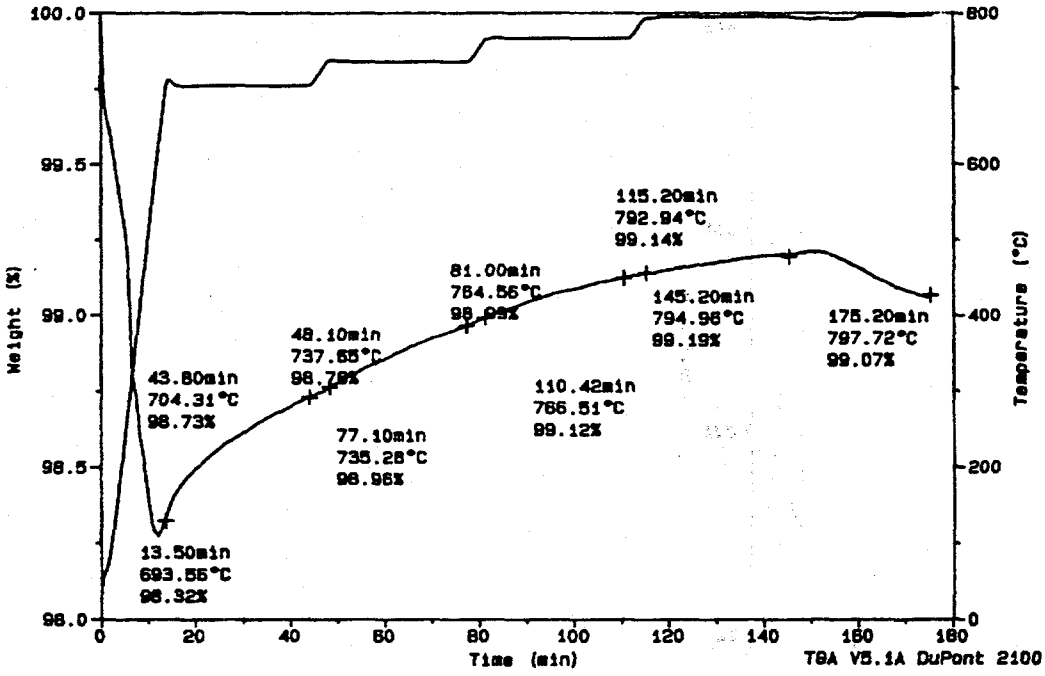

Figure 78. Thermogram from Test 8, sodalite without NaCl and combustion gas as the initial gas

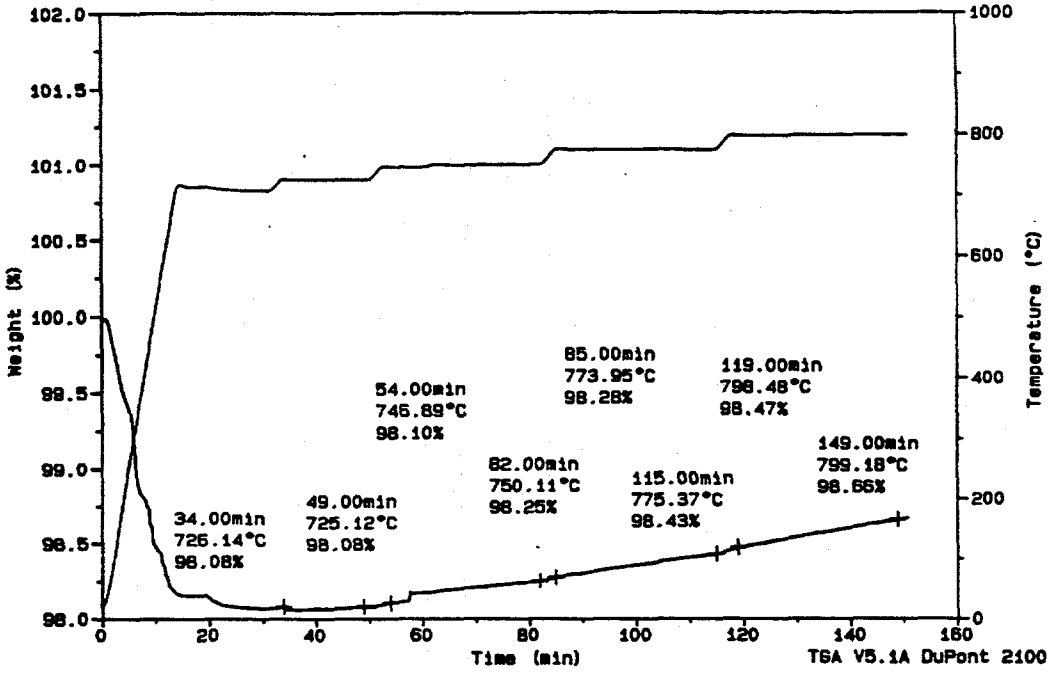

Figure 79. Thermogram from Test 9, sodalite with NaCl and nitrogen as the initial gas

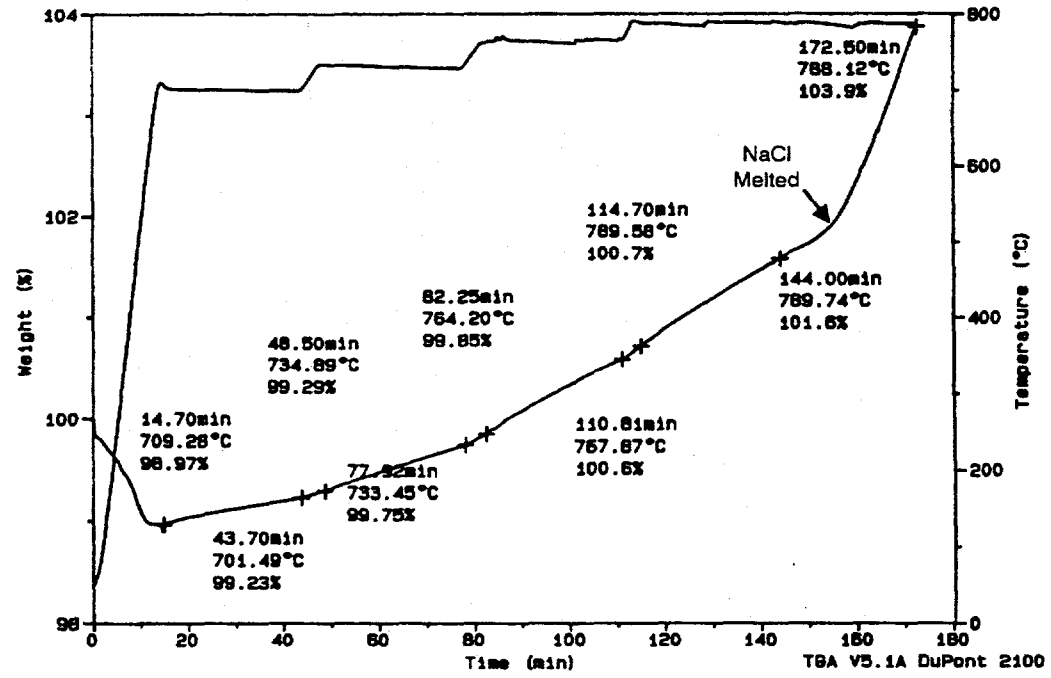

Figure 80. Thermogram from Test 10, nepheline with NaCl and combustion gas as the initial gas

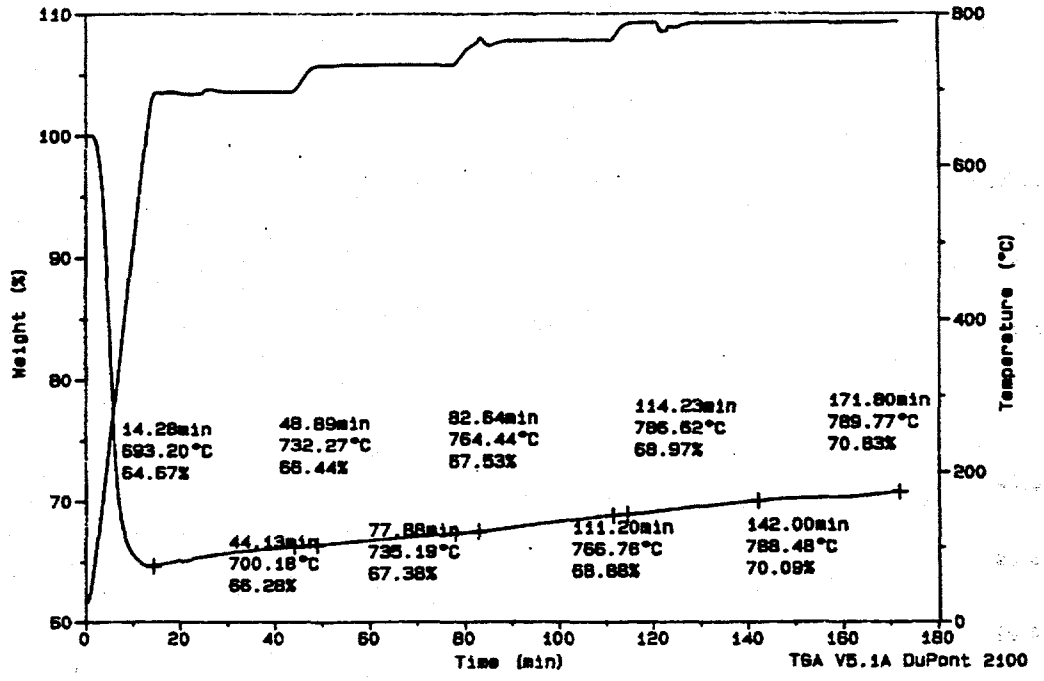

Figure 81. Thermogram from Test 11, $AlO(OH)_3$ with NaCl and combustion gas as the initial gas

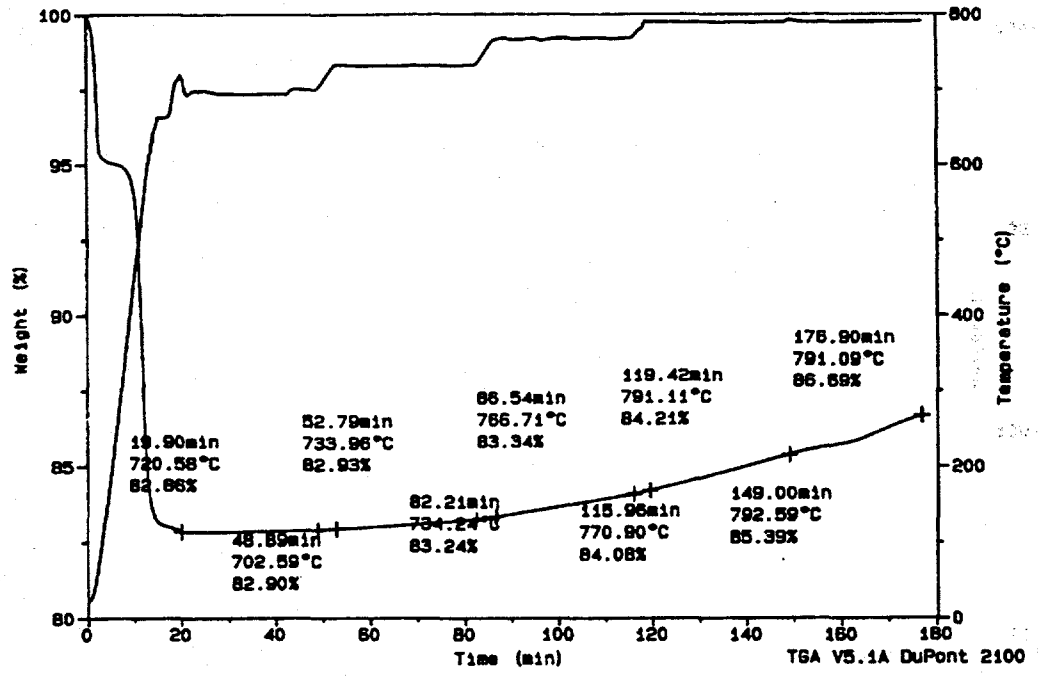

Figure 82. Thermogram from Test 12, kaolinite with NaCl and combustion gas as the initial gas

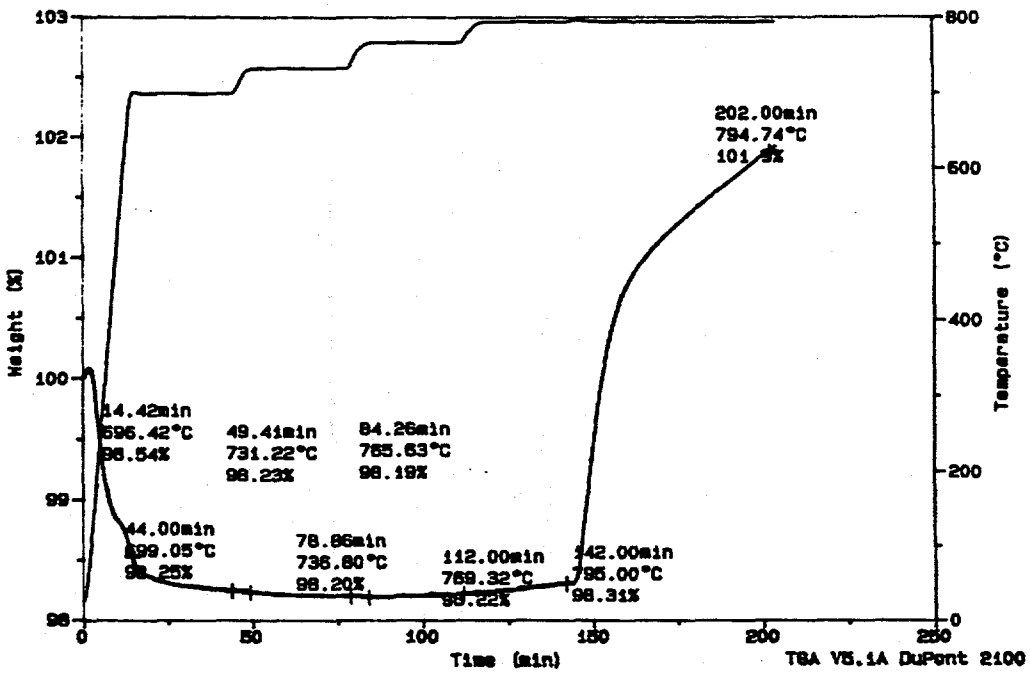

Figure 83. Thermogram from Test 13, activated bauxite with NaCl and nitrogen as the initial gas

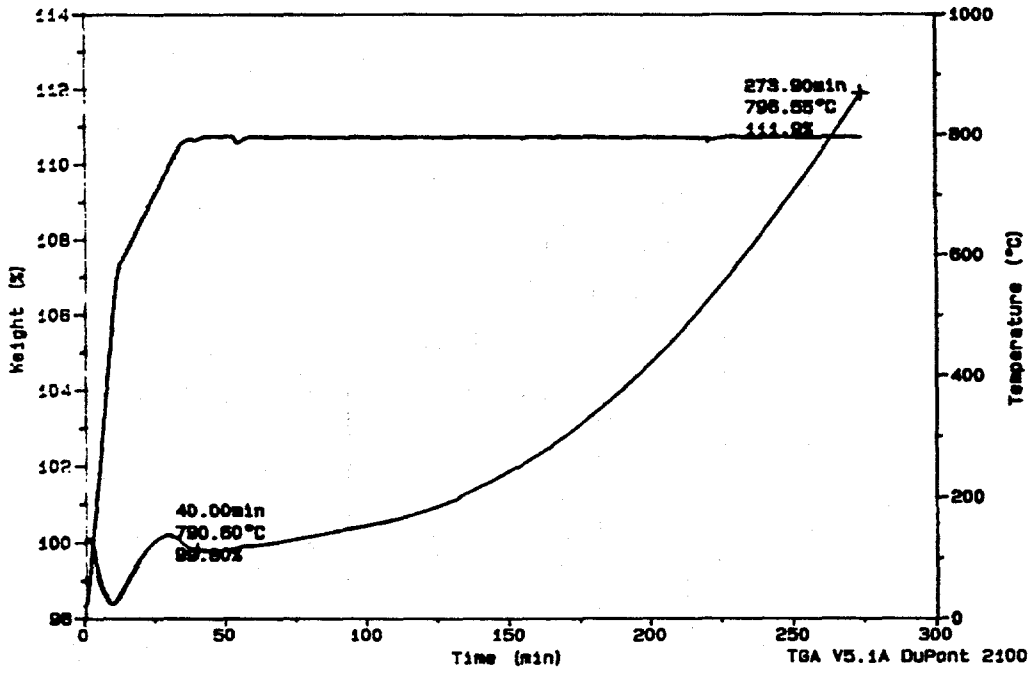

Figure 84. Thermogram from Test 14, activated bauxite with NaCl and combustion gas as the initial gas

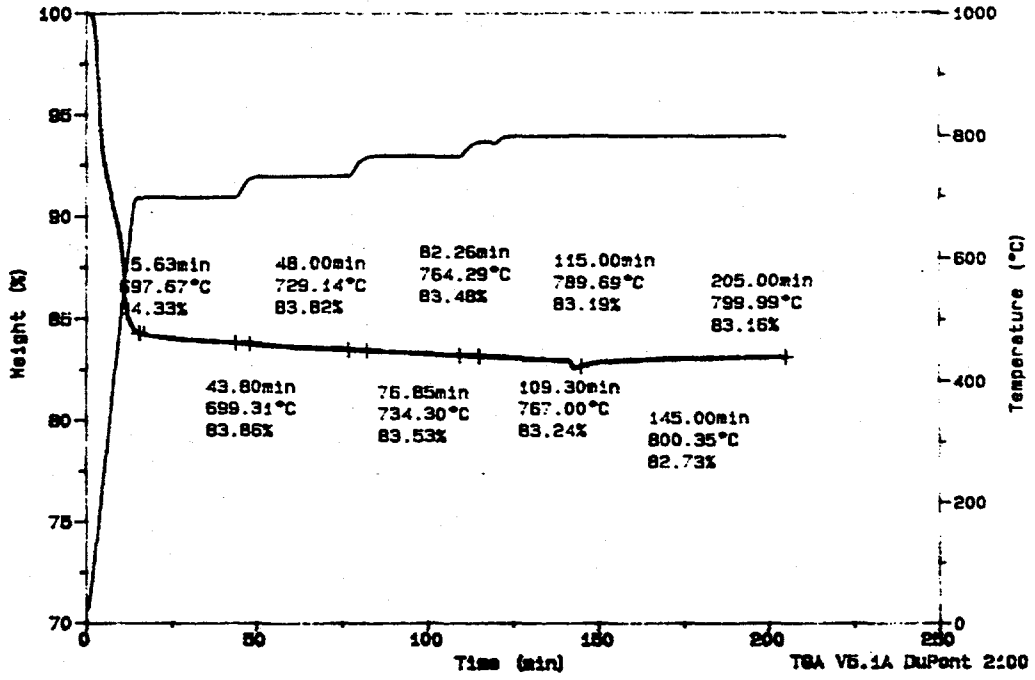

Figure 85. Thermogram from Test 15, zeolite with NaCl and nitrogen as the initial gas

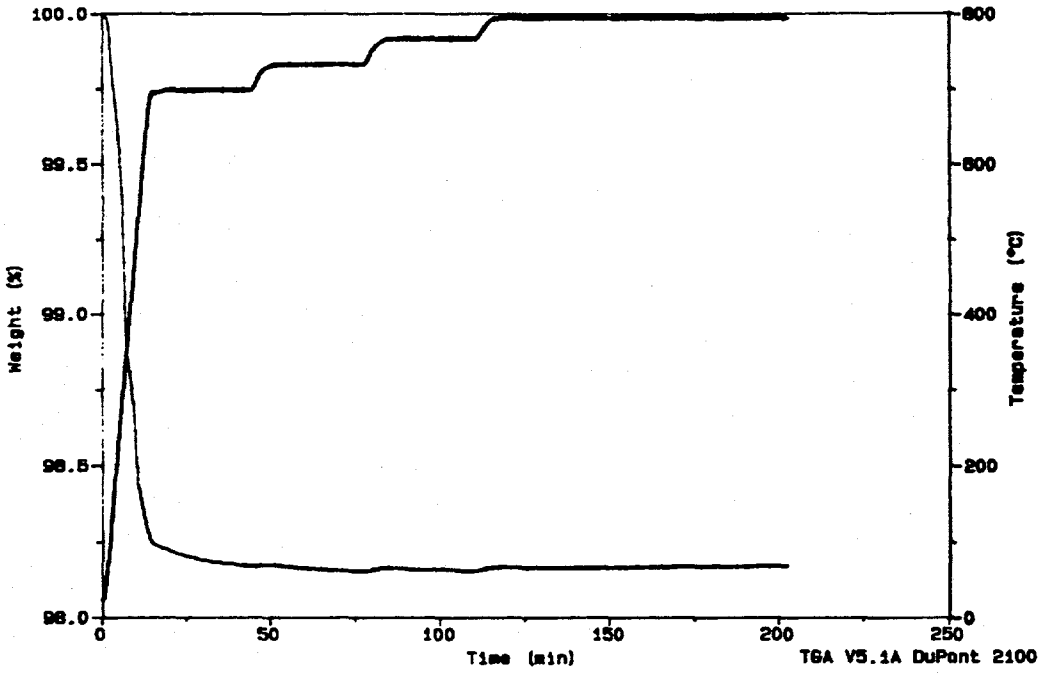

Figure 86. Thermogram from Test 16, sodalite without NaCl and nitrogen as the initial gas

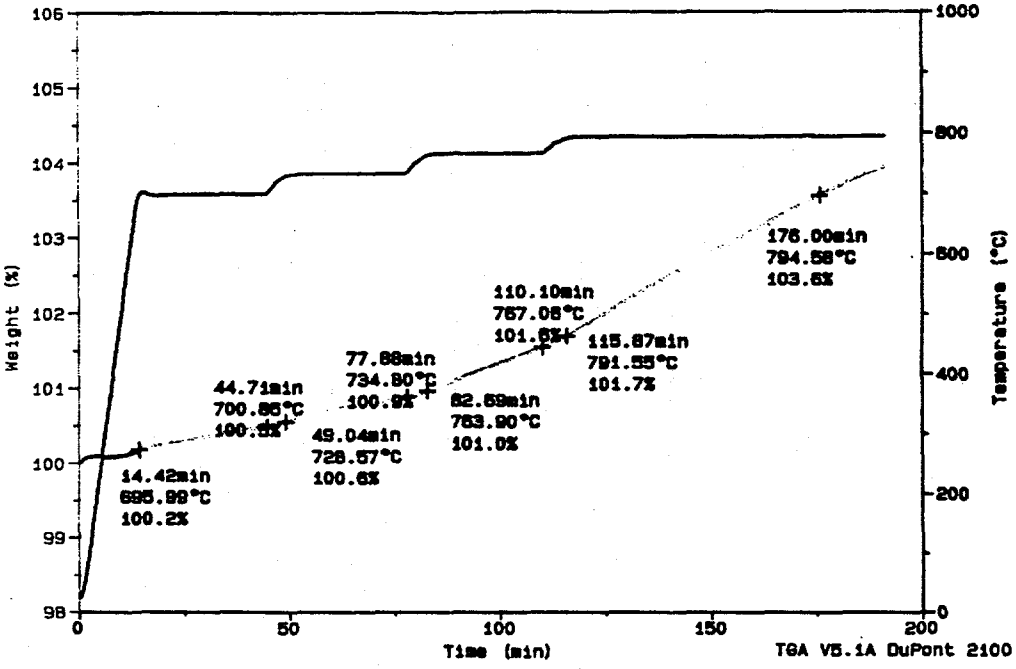

Figure 87. Thermogram from Test 17, albite with NaCl and combustion gas as the initial gas

REFERENCES

Abbasian, J.; Rehmal, A. "H_2S Removal from Fuel Gas During Coal Gasification," *In* Proceedings of the 199th ACS National Meeting; Boston, MA, April 22–27, 1990; Vol. 35, No. 1, pp 196–206.

Abdulally, I. "Foster Wheeler Energy International," Personal communication, May 21, 1996.

Alliance to Save Energy. "An Alternative Energy Future," American Gas Association and Solar Energy Industries Association: Washington, DC, 1992.

Bachovchin, D.M; Alvin, MA. "A Study of High-Temperature Removal of Alkali in a Pressurized Gasification System," *In* Proceedings of the Gas Stream Cleanup Papers from DOE–METC-Sponsored Contractors' Review Meetings in 1987; DOE/METC-87/6082, Oct. 1987.

Bachovchin, D.M.; Alvin, M.A.; DeZubay, E.A.; Mulik, P.R. "A Study of High-Temperature Removal of Alkali in a Pressurized Gasification System," final report DOE/FETC/20050-2226; Oct. 1986.

Brdar, R.D. "Advanced Coal-Fired Power Systems," Presented at the 1996 Hot-Gas Cleanup Contractors Review Meeting, Morgantown, WV, July 16, 1996.

Benson, S.A.; Abrahamson, H.A.; Zygarlicke, C.J.; Mills, M.E. "Combustion Inorganic Transformations," final technical report for April 1988–June 1989; Contract No. DE-FC21-86MC10637, 1989.

Benson, S.A.; Holm, P.A. "Comparison of Inorganic Constituents in Three Low-Rank Coals," *Industrial and Engineering Chemistry Product Research and Development* **1985**, *24*, 145–149.

Benson, S.A.; Hurley, J.P. "Distribution of Inorganics," quarterly report for Contract DOE/FE/60181-1531; 1983.

Benson, S.A.; Hurley, J.P.; Steadman, E.N. "Distribution of Inorganics," quarterly report for Contract DOE/FE/60181-1574, 1984a.

Benson, S.A.; Hurley, J.P.; Steadman, E.N. "Distribution of Inorganics," quarterly report for Contract DOE/FE/60181-1642, 1984b.

Bergerson, C.G.; Risbud, S.H. *Introduction to Phase Equilibria in Ceramics*; The American Ceramic Society, Inc.: Columbus, Ohio, 1984.

Boteler; D.C.; Boley, C.C. "Partial Devolatilization of Coal in Two Entrained-Bed Carbonizers," v.s. Bureau of Mines, RI-7843, 1973.

Boley, C.C.; Fegley, M.M. "Design and Operation of Two Refractory-Lined, Internally Heated, Entrained-Bed Carbonizers," GFERC/RI-77/1, p 38, 1977.

Calvert, S. et al. "The A.P.T. Dry Plate Scrubber for Alkali Vapor Control," *In* Proceedings of the 2nd Annual Contractors' Meeting on Contaminant Control; Morgantown, WV, Feb. 3–5, 1981.

Cramer, H. *VGB Kraftwerks Technik* **1986**, 66, 750–753.

Coal and Synfuels Technology **1993**, *14* (47), 47.

Cuenca, M.A.; Anthony, E.J., Eds. *Pressurized Fluidized Bed Combustion*; Blackie Academic & Professional: London, 1995.

Dellefield, R.J.; Reed, M.E. "U.S. Department of Energy Perspective on PFBC," U.S. Department of Energy Morgantown Energy Technology Center report; 1992.

Energy Information Administration, U.S. Department of Energy. *Annual Energy Outlook;* DOE/EIA-0383(94), Washington, DC, 1994.

Energy Information Administration, U.S. Department of Energy. *International Energy Annual 1993*; DOE/EIA-0219(93), Washington, DC, May 1995.

Energy Information Administration, U.S. Department of Energy. *Supplement to the Annual Energy Outlook 1994*; DOE/EIA-0554(94), Washington, DC, 1994.

Energy Information Administration, U.S. Department of Energy. *World Energy Project Systems;* Washington, DC, 1996.

Energy Information Administration, U.S. Department of Energy. *1992 Annual Energy Outlook;* DOE/EIA-0383 (92), Washington, DC, 1992.

Erickson, G. *Chemica Scripta* **1978**, *8*, 100–103.

Erickson, T.A.; Ludlow, D.K.; Benson, S.A. "Interaction of Sodium, Sulfur, and Silica during Coal Combustion," *Energy & Fuels* **1991**, 5 (4), 539–547.

Erickson, T.A.; Ludlow, D.K.; Benson, S.A. "Fly Ash Development from Sodium, Sulphur, and Silica During Coal Combustion," *Fuel* **1992**, 71, 15–18.

Fantom, I.R. "Measurements and Control of Alkali Metal Vapors in Coal-Derived Fuel Gas," *In* Proceedings of the 2nd Int. Symp. on Gas Cleaning at High Temperatures; Blackie Academic and Professional, pp 541–555, 1993.

Fogler, H.S. *The Elements of Chemical Kinetics and Reactor Calculations*; Prentice-Hall Inc., Englewood Cliffs, NJ, 1974.

Gas Research Institute. *Baseline Projection of U.S. Energy Supply and Demand*; Chicago, 1994.

Gilberti, D.F. et al. "Hot Gas Cleanup Using Porous Ceramic Cross-Flow Filters," *In* Proceedings of the 3rd Annual Contractors' Meeting on Contaminant Control; Morgantown, WV, Feb. 17–19, 1982.

Golan, L.P. et al. "Demonstration of the Feasibility of a Magnetic Stabilized Bed for the Removal of Particulates and Alkali," *In* Proceeding of the 3rd Annual Contractors' Meeting on Contaminant Control; Morgantown, WV, Feb. 17–19, 1982.

Goldback, G.; Haas, J. "Combustion Power Company, Inc.," Personal communication, June 17, 1991.

Greene, F.T.; O'Donnell, J.E. "Investigation of the Mechanisms of Ash Deposit Formation from Low-Rank Coal Combustion," report for Contract DOE/FC/10287-2416; 1987.

Guha, M.; McCall, G. "Predicting the Market Penetration of the Next Generation of Coal-Fired Technologies," *Power-Gen 1990*.

Helbe, J.J.; Srinivasacher, S.; Boni, A.A.; Charon, O; Modestino, A. "Measurement and Modeling of Vapor-Phase Sodium Chloride Formed During Pulverized Coal Combustion," CST90-05-23, 1990.

Hurley, J.P. "A Pilot-Scale Study of the Formation of Ash During Pulverized Low-Rank Coal Combustion," Ph.D. Thesis, The Pennsylvania State University, 1990.

Hurley, J.P.; Steadman, E.N.; Kleesattel, D.R. "Distribution of Inorganics," final report for Contract DOE/FE/60181; 1986.

31th IEA FBC Meeting, Nov. 2–4, 1995, Aix-en-Provence, France.

International Energy Agency. *Annual Report 1992–1993*; Organization for Economic Cooperation and Development: Paris, 1993.

Ishida, M.; Wen, C.Y., *AIChE J.* **1968**, 14, 311.

Jackson, P.J. *Ash Deposits and Corrosion Due to Impurities in Combustion Gases*; Bryers, R.W., Ed.; Hemisphere Publishing: Washington, DC, 1978; pp 147–161.

Jannson, S.; Pillai, K.; Malm, H. "PFBC—The Leading Clean Coal Technology for the Future," New Electricity 21 Conference, May 1992.

Jansson, S.A. "Status of PFBC," *In* Proceedings of the Institute of Energy's 5th International Fluid Combustion Conference: FBC Technology and the Environmental Challenge; London, December 1991; Adam Hilger: Bristol, UK, 1991, pp 19–30.

Karner, F.R.; Hurley, J.P.; Beckwith, DC; Kleesattel, D.R.; Roaldson, R.R.; Steadman, E.N.; Zygarlicke, C.J. "Distribution of Inorganics," quarterly report for Contract DOE/FE/60181–1845, 1984.

Kimura, S.J. *Chem. Eng. Japan* **1981**, 14, 190.

Kimura, S.; Tone, S., Otake, T. *J. Chem. Eng. Japan* **1982**, 15, 73.

Kingery, W.D.; Bowen, H.K.; Uhlmann, D.R. *Introduction to Ceramics*; John Wiley & Sons, Inc.; New York, 1976.

Krishnan, G.N.; Wood, B.J.; Korens, N.; Anderson, G.L. "High-Temperature Coal Gas Chloride Cleanup for Molten Carbonate Fuel Cell Applications," *In* Proceedings of 6th Annual Contractors' Review Meeting on Contaminant Control in Coal-Derived Gas Streams; DOE/METC-86/6042, (DE86001088), July 1986, pp 48–57.

Kunii, D.; Levenspiel, O. *Fluidization Engineering*; Butterworth-Heinemann; Stoneham, MA, 1991.

Laatikaninen, J.; Nieminen, M.; Hippinen, I. "Release of Sodium and Potassium in PFB Combustion of Peat and Coal," *In* Proceedings of the 1993 International Fluidized-Bed Combustion Conference; 1993, pp 1369–1374.

Lee, S.H.D.; Carls, E.L. "Bench-Scale Tests of Alkali Vapor Removal from PFBC Exhaust Using a Fixed Bed of Activated Bauxite Sorbent," Presented at the 1988 METC Heat Engines Contractors Review Meeting, Morgantown, WV, 1988.

Lee, S.H.D.; Carls, E.L. "Measurement of Alkali Metal Vapors and Their Removal from a Pressurized Fluidized-Bed Combustor Process Stream," Annual Report ANL/FE-88-4, Oct. 1986–Sept. 1987, 37 p.

Lee, S.H.D.; Johnson, I. "Removal of Gaseous Alkali Metal Compounds from Hot Flue Gas by Particulate Sorbents,"*Transactions of the ASME: Journal of Engineering for Power* **1980**, *102*, 397–402.

Lee, S.H.D.; Myles, K.M. "Alkali Measurement in PFBC and Its Control by a Granular Bed of Activated Bauxite," *In* Proceedings of the 10th International Fluidized Bed Conference; May 1989, pp 793–801.

Lee, S.H.D.; Myles, K.M. "Alkali Metal Vapor Removal from a Pressurized Fluidized-Bed Combustor Process Stream," annual report for the period October 1985 – September 1986; ANL/FE-88-3, DE88-013966, March 1988.

Lee, S.H.D.; Swift, W.M. "A Fixed Granular-Bed Sorber for Measurement and Control of Alkali Vapors in PFBC," *In* Proceedings of the 1991 International Fluidized Bed Combustion Conference; 1991, pp 1095–1103.

Lee, S.H.D.; Teats, F.G.;Swift, W.M.; Banerjee, D.D. "Alkali-Vapor Emission from PFBC of Illinois Coals," Short Communication, *Combust. Sci. and Tech.* **1992**, *86*, 327–336.

Lee, S.H.D.; Teats, F.G.; Swift, W.M.; Banerjee, D.D. "Measurement of Alkali-Vapor Emission from Pressurized Fluidized-Bed Combustion of Illinois Coals," *In* Proceedings of the 1993 International Fluidized Bed Combustion Conference; 1993, pp 1359–1368.

Levenspiel, O. *Chemical Reaction Engineering*, 2nd ed.; Wiley, New York, 1972.

Lippert, T.E.; Alvin, M.A.; Bachovchin, D.M.; Haldipur, G.B.; Newby, R.A.; Smeltzer, E.E. "Development and Commercialization of Hot-Gas Filtration Systems," Presented at the 11th International Conference on Fluidized-Bed Combustion, Montreal, Canada, 1991.

Longwall, J.P.; Rubin, E.S.; Wilson, J. "Coal: Energy for the Future," *Prog. Energy Combust. Sci.* **1995**, *21*, 269–360.

Makovich, L.; Smalley, G. *Electric World* **1993**, *207* (11), 17–24.

Mann, M.D. "Investigation of Tidd PFBC Agglomeration Chemical Characterization," EERC Publication No. 94-EERC-01-1, 1994.

Mann, M.D.; Swanson, M.L.; Yagla, S. "Characterization of Alkali and Sulfur Sorbents for Pressurized Fluidized-Bed Combustion," *In* Proceedings of the 13th International Fluidized Bed Conference; Orlando, FL, May 1995.

Manzoori, A.R. "Role of the Inoganic Matter in Agglomeration and Defluidization During the Circulating Fluid Bed Combustion of Low-Rank Coals," Ph.D. thesis, The University of Adelaide, 1990.

McLaughlin, J. "The Removal of Volatile Alkali Salt Vapours from Hot Coal-Derived Gases," Ph.D. thesis, Guildford, UK, Department of Chemical and Process Engineering, University of Surrey, Nov. 1990, 214p.

Miller, R.N.; Given, P.H. "A Geochemical Study of the Inorganic Constituents of Some Low-Rank Coals," report for Contract DOE/FE-2494-TR-1; 1979.

Minchener, A.J.; Clark, R.C.; Dawes, S.G. "The British Coal Topping Cycle Development Programme," *In* Proceedings of the 11th International Conference on Fluidized-Bed Combustion; ASME 1991, pp 115–118.

Mojtahedi, W.; Backman, R. "Release of Alkali Metals in Pressurized Fluidized-Bed Combustion and Gasification of Peat," Technical Research Center of Finland, Publication 53, 1989.

Mojtahedi, W.; Nieminen, M.; Hulkkonen, S.; Jahkola, A. "Partitioning of Trace Elements in Pressurized Fluidized-Bed Combustion," *Fuel Processing and Technology* **1990**, 26, 83–97.

Morgan, M.E. "Inorganic Constituents in American Lignites," Master's Thesis, The Pennsylvania State University, 1980.

Mulik, P.R. "High-Temperature Removal of Alkali Vapors in Hot Gas Cleaning Systems," *In* Proceedings of the 3rd Annual Contractors' Review Meeting on Contaminant Control; Morgantown, WV, Feb. 1982.

Mulik, P.A.; Alvin, M.A.; Bachovchin, D.M. "Simultaneous High-Temperature Removal of Alkali and Particulates in a Pressurized Gasification System," DOE-MC-1632-8, 1983.

National Research Council. "Policy Implications of Greenhouse Warming," Committee on Science, Engineering, and Public Policy National Academy of Science Press: Washington, DC, 1992.

NCB Coal Utilization Research Laboratory. "20 Atmosphere Rig PFBC Test Results: Tests 10 and 12 – Investigations into the Use of Limestone as a Sorbent," DOE/MC/14129-1463 (DE83015869); Aug. 1983.

Neville, M.; Quann, R.J.; Haynes, B.S.; Sarofim, A.F. "Vaporization and Condensation of Mineral Matter During Pulverized Coal Combustion," *In* Proceedings of the 18th Symposium (International) on Combustion; The Combustion Institute, 1981, pp 1267–1274.

O'Gorman, J.V.; Walker, P.L. "Thermal Behavior of Mineral Fractions Separated from Selected American Coals," *Fuel* **1973**, *52*, 71–79.

Oldenberg, R.C. "Optical Detection of Corrosive Compounds," *In* Proceedings of the Advanced Research and Technology Development Direct Utilization, Instrumentation, and Diagnostics Contractors' Review Meeting; DOE/FETC-89/6108 (DE90000424), Oct. 1989; Vol. 1, pp 87–99.

Park, J.Y.; Levenspiel, O. *Chem. Eng. Sci.* **1975**, 30, 1207

Pintsch, S.; Gudenau, H.W. "Alkaline Hot Gas Cleaning in Combined Cycle Processes, Part 1: State of the Art as in Literature," *VGB Kraftwerkstechnik* **1991a**, *1*, 40–45.

Pintsch, S.; Gudenau, H.W. "Alkaline Hot Gas Cleaning in Gas Turbine and Steam Turbine Processes, Part 2: Thermodynamic Calculations," *VGB Kraftwerkstechnik* **1991b**, *3*, 199–205.

Pitrolo, A.A.; Bechtel, T.F. "Simplied IGCC: Coal's 'Adam Smith' Response to a Changing World," *In* Proceedings of the 7th Annual EPRI Contractors' Conference on Coal Gasification; EPRI AP-6006-SR, 1988.

Punjak, W.A.; Uberoi, M.; Shadman, F. "High-Temperature Adsorption of Alkali Vapors on Solid Sorbents," *AIChE Journal* **1989**, *35* (7).